

# Application of trace-element compositions of detrital apatite to explore for porphyry deposits in central British Columbia



Alexei S. Rukhlov<sup>1,a</sup>, Alain Plouffe<sup>2</sup>, Travis Ferbey<sup>1</sup>, Mao Mao<sup>1</sup>, and Jody Spence<sup>3</sup>

<sup>1</sup> British Columbia Geological Survey, Ministry of Energy and Mines, Victoria, BC, V8W 9N3

<sup>2</sup> Geological Survey of Canada, 601 Booth Street, Ottawa, ON, K1A 0E8

<sup>3</sup> School of Earth and Ocean Sciences, University of Victoria, Victoria, BC, V8P 5C2

<sup>a</sup> corresponding author: Alexei.Rukhlov@gov.bc.ca

Recommended citation: Rukhlov, A.S., Plouffe, A., Ferbey, T., Mao, M., and Spence, J., 2016. Application of trace-element compositions of detrital apatite to explore for porphyry deposits in central British Columbia. In: Geological Fieldwork 2015, British Columbia Ministry of Energy and Mines, British Columbia Geological Survey Paper 2016-1, pp. 145-179.

## Abstract

Apatite grains recovered from tills (14 samples) at the Highland Valley, Gibraltar, Mount Polley, and Woodjam porphyry deposits, and mineralized bedrock (2 samples) at the Woodjam Southeast Zone were analysed by electron microprobe and laser ablation-inductively coupled plasma mass spectrometry. The Cl/F and Cl/OH ratios of these grains, assuming molar (F + OH + Cl) = 1, are similar to those of apatites from producing porphyry deposits elsewhere (e.g., Yerrington, Nevada; Bingham, Utah; Henderson, Colorado). Most apatite grains in till from Mount Polley have higher SO<sub>3</sub>, SiO<sub>2</sub>, Na<sub>2</sub>O, Sr, Mg, V, Ba, Zr, Mo, Nb contents and (La/Sm)<sub>CN</sub>, and lower Mn, Y, and ΣHREE (total heavy rare earth elements) contents relative to those from the Highland Valley, Gibraltar and Woodjam deposits. Only apatite grains from till overlying the contact between the Takomkane batholith and Nicola Group volcano-sedimentary rocks at Woodjam show higher As abundances (121–1191 ppm) than those from Mount Polley (mostly 5.5–158 ppm As), perhaps reflecting a sedimentary source. Apatite grains in till from Mount Polley show weak negative Ce anomalies (Ce/Ce\*; mostly 0.89–1.03) and moderate to weak negative Eu anomalies (Eu/Eu\*; mostly 0.50–0.99). In contrast, those from the Highland Valley, Gibraltar and Woodjam deposits show weak positive Ce anomalies (Ce/Ce\* mostly between 1.00 and 1.24) and strong negative Eu anomalies (Eu/Eu\* mostly between 0.11 and 0.47). Most apatite grains from tills at Woodjam and a few from other deposits indicate variable degrees of depletion in minor and trace elements and LREEs (light rare earth elements), with highly variable (Ce/Yb)<sub>CN</sub> (<0.01–47), (La/Sm)<sub>CN</sub> (0.06–6.0), (Gd/Yb)<sub>CN</sub> (0.01–39), Ce/Ce\* (0.23–3.8) and elevated Eu/Eu\* (up to 1.5), probably reflecting metasomatic alteration of primary apatite. The systematic differences in abundances of redox-sensitive SO<sub>3</sub>, Mn, V, As, Ce and Eu between apatite grains from Mount Polley and other porphyry deposits are consistent with a more oxidized alkalic porphyry Cu-Au compared to more reduced calc-alkaline porphyry Cu±Mo±Au systems. Although apatite crystallization temperature is needed to quantify the oxidation state of these porphyry deposits, average Mn contents of the pristine apatite grains yield log *f*O<sub>2</sub> values of -11.2 ± 0.5 for Mount Polley, -12.8 ± 0.6 for Woodjam Southeast Zone, -14.1 ± 0.7 for Gibraltar, and -16.3 ± 1.0 for Highland Valley, using an empirical apatite oxybarometer for a given range of temperatures (920–660°C) and compositions (andesitic to rhyolitic). The strong negative Eu anomalies, coupled with higher Mn and lower Mg and Sr contents, of apatite grains at the Highland Valley, Gibraltar and Woodjam deposits also indicate more fractionated, felsic magmas, lacking significant Fe-Mg minerals, compared to the Mount Polley alkalic porphyry Cu-Au system. Classification of the examined apatite grains using discriminant functions correctly identifies the porphyry deposits in all four study areas. Unlike detrital apatite grains at other deposits, those from tills at Woodjam mostly show barren-rock affinity or evidence of metasomatic depletion in most minor and trace elements, suggesting derivation mainly from a higher-level, propylitic alteration zone rather than from mineralized rocks such as at the Woodjam Southeast Zone. Our results show that apatite trace-element chemistry is diagnostic of specific porphyry deposits and their relative oxidation states and thus can be used as an exploration tool for these deposits.

**Keywords:** Apatite, trace-element compositions, LA-ICP-MS, EMPA, porphyry Cu-Mo, alkalic porphyry Cu-Au, till, indicator mineral, mineral exploration, Gibraltar, Highland Valley Copper, Mount Polley, Woodjam

## 1. Introduction

The Quesnel and Stikine magmatic arc terranes (Late Triassic-Early Jurassic) of the Canadian Cordillera in British Columbia are highly prospective for porphyry Cu±Mo±Au deposits (e.g., Sutherland Brown, 1976; Dawson et al., 1991; Schroeter, 1995; Logan, 2013). However, exploring for these deposits is challenged by glacial deposits that drape much of the Interior Plateau (Ward et al., 2009). In 2010, the Geological Survey of Canada (GSC) launched a five year program (Targeted Geoscience Initiative-4, or TGI-4) to develop

methods for targeting buried mineral deposits. As part of this program, the British Columbia Geological Survey and the Geological Survey of Canada conducted till surveys near four porphyry copper deposits in the Interior Plateau: the Highland Valley Copper and Gibraltar mines (calc-alkaline porphyry Cu-Mo); the Mount Polley mine (alkalic porphyry Cu-Au-Ag); and the Woodjam developed prospect (alkalic Cu-Au to calc-alkaline porphyry Cu-Mo; Fig. 1; Anderson et al., 2012a, b, c; Plouffe et al., 2012, 2013a, b, 2014; Ferbey and Plouffe, 2014; Ferbey et al., 2014; Hashmi et al., 2014, 2015; Plouffe

and Ferbey, 2015a, d). The objective of these surveys was to develop mineral exploration methods using till geochemistry and mineralogy tied to studies of ice-flow history and glacial dispersion.

Apatite,  $\text{Ca}_5[\text{PO}_4]_3(\text{F}, \text{OH}, \text{Cl})$ , is an accessory mineral in porphyry  $\text{Cu}\pm\text{Mo}\pm\text{Au}$  deposits, and apatite textures, optical properties, and chemical compositions are diagnostic of these deposits (e.g., Carson and Jambor, 1974; Williams and Cesbron, 1977; Belousova et al., 2002; Bath et al., 2006; Liaghat and Tosdal, 2008; Bouzari et al., 2010, 2011a, b, 2015; Celis et al., 2013, 2014; Mao et al., 2015). Most studies have focused on apatite from rock samples and, so far, little research has been done on detrital apatite grains recovered from till. Nonetheless, till sampling near porphyry and IOCG deposits has shown that apatite can survive glacial transport and post-glacial weathering (Kelley et al., 2011; Normandeau et al., 2014; Hashmi et al., 2015). Furthermore, apatite appears to be more abundant in tills deposited down paleo-ice-flow direction from mineralized zones and thus holds potential as a porphyry indicator mineral (PIM). Given that detrital apatite grains in tills can be derived from multiple sources, apatite trace-element compositions provide criteria to discriminate between porphyry systems and other bedrock sources (Mao et al., 2015).

This study builds on the work of Mao et al. (2015), who proposed a discrimination approach of using trace-element compositions of apatite from many types of ore deposits, including virtually all types of metallic deposits in British Columbia. Here we test the effectiveness of the method to explore for porphyry deposits by analyzing trace-element compositions of apatite grains recovered from till and bedrock samples from the four TGI-4 study areas (Fig. 1). Elsewhere (Rukhlov et al., 2016) we provide full appendices of the new analytical data by electron microprobe (EMPA) and laser ablation – inductively coupled plasma mass spectrometry (LA-ICP-MS). Our results demonstrate that trace-element compositions of detrital apatite grains identify the porphyry deposits in all four study areas and thus confirm the findings of Mao et al. (2015) that detrital apatite chemistry provides a robust tool for mineral exploration.

## 2. Physiography and glacial history

The four study areas (Fig. 1) are in the Interior Plateau (Holland, 1976). At the onset of the most recent Late Wisconsinan glacial event (Fraser glaciation; Clague, 1989), local valley glaciers formed in mountainous areas of the Interior Plateau (Clague, 1989; Plouffe, 2000). As glaciation proceeded, most of the ice sheet built up from the coalescence of valley and piedmont glaciers flowing into the Interior Plateau from the Coast (west) and Cariboo (east) mountains (Tipper, 1971a, b). Eventually, ice was sufficiently thick to flow outward from the Interior Plateau, independent of topography.

At Highland Valley (Fig. 2), ice-flow indicators suggest a single phase of ice movement from a divide at about  $52^\circ$  north, with flow generally to the south to southeast (Plouffe and Ferbey, 2015b). Glacial striations and clast lithology in the till

indicate that ice flowing from the Coast or Cariboo mountains did not reach the area during the build up to the Fraser Glaciation maximum. Farther north, the first glaciers to advance over the Gibraltar (Fig. 3), Mount Polley (Fig. 4), and Woodjam (Fig. 5) areas moved west to southwest from the Cariboo Mountains (Plouffe and Ferbey, 2015d). Glacial striations and landforms indicate a second phase of flow, directed north to northwest, likely from an ice divide near  $52^\circ$  north during the glacial maximum (Ferbey et al., 2013). Evidence for a third phase, to the south-southeast, is preserved at Gibraltar. Although the origin and timing of this movement remain unclear, it could be related to an early ice flow out of an unnamed mountain ridge marked with cirques and arêtes north of the deposit (Plouffe and Ferbey, 2015c). Multiple ice-flow movements in these three areas imply multiple detrital transport histories (Plouffe and Ferbey, 2015d).

The Cordilleran ice sheet left a glacial sediment cover of variable thickness. In addition to multiple transport paths, this variation needs to be considered when interpreting till geochemistry and mineralogy. Although mineralization at Gibraltar, Mount Polley and Highland Valley is generally covered by glacial deposits 2-10 metres thick, local mineralized outcrops were exposed before mining in each case (Rotherham et al., 1972; Casselman et al., 1995; Byrne et al., 2013; Rees, 2013). Any mineralized zone that was protected from glacial erosion by a cover of pre-glacial sediment or non-mineralized rock will not yield a geochemical or mineralogical signal in Late Wisconsinan till (Plouffe et al., 2012; Plouffe and Ferbey, 2015d). For example, at Woodjam, the Southeast Zone is covered by more than 200 m of unconsolidated sediments, probably in part pre-glacial (J.W. Morton, pers. comm. 2014; see profiles in del Real et al., 2014). Similarly, unconsolidated sediments form a 40-100 m thick blanket over the Three Firs prospect at Woodjam, which is also partly covered by up to 20 m of Cenozoic basaltic flows of the Chilcotin Group (Bissig et al., 2013; see Figure 6 in Vandekerckhove et al., 2014).

## 3. Geology and porphyry mineralization

The four porphyry deposits in this study are hosted by the Late Triassic to Early Jurassic alkaline (alkalic porphyry  $\text{Cu-Au}$ ) and calc-alkaline (porphyry  $\text{Cu-Mo}\pm\text{Au}$ ) intrusions of the Quesnel terrane. Three of these deposits (Highland Valley, Gibraltar, and Mount Polley) are producing open-pit mines, and the Woodjam is a developed prospect. The following briefly summarizes the geology of the deposits.

### 3.1. Highland Valley

The Guichon Creek batholith (Late Triassic) hosts at least five economic porphyry  $\text{Cu-Mo}$  deposits comprising the Highland Valley porphyry district, about 54 km southwest of Kamloops (Fig. 2; McMillan, 1985, 2005; Casselman et al., 1995; McMillan et al., 2009; Byrne et al., 2013). The batholith cuts volcanic and sedimentary rocks of the Nicola Group (Late Triassic) and is made up of a core of granodiorite to quartz monzonite that is rimmed by older diorite to quartz diorite (McMillan, 1985;

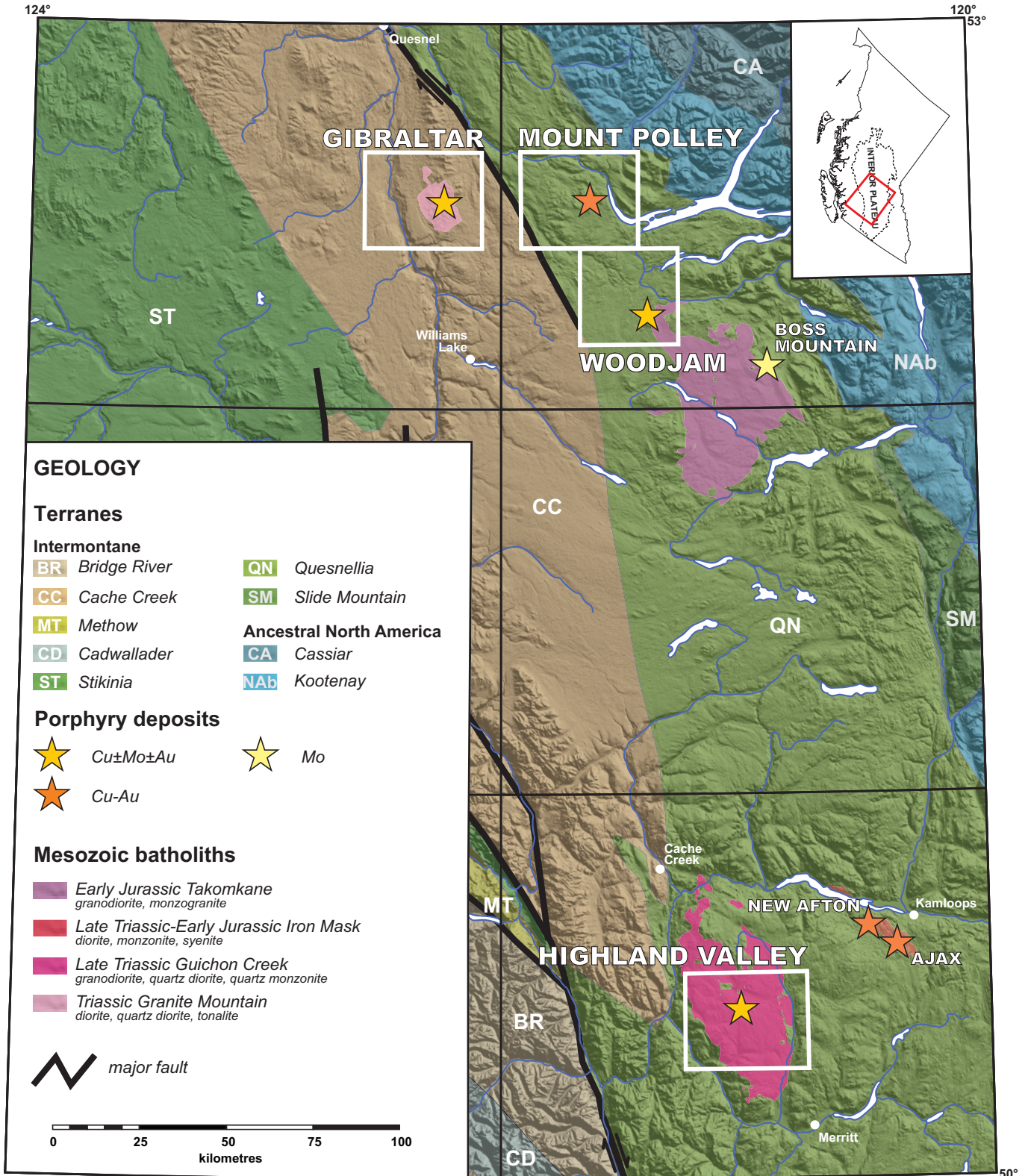


**Fig. 1.** Terranes (after Nelson et al., 2013), Mesozoic batholiths (after Massey et al., 2005; Logan et al., 2010), major porphyry deposits, and locations of Highland Valley, Gibraltar, Mount Polley, and Woodjam study areas in south-central British Columbia.

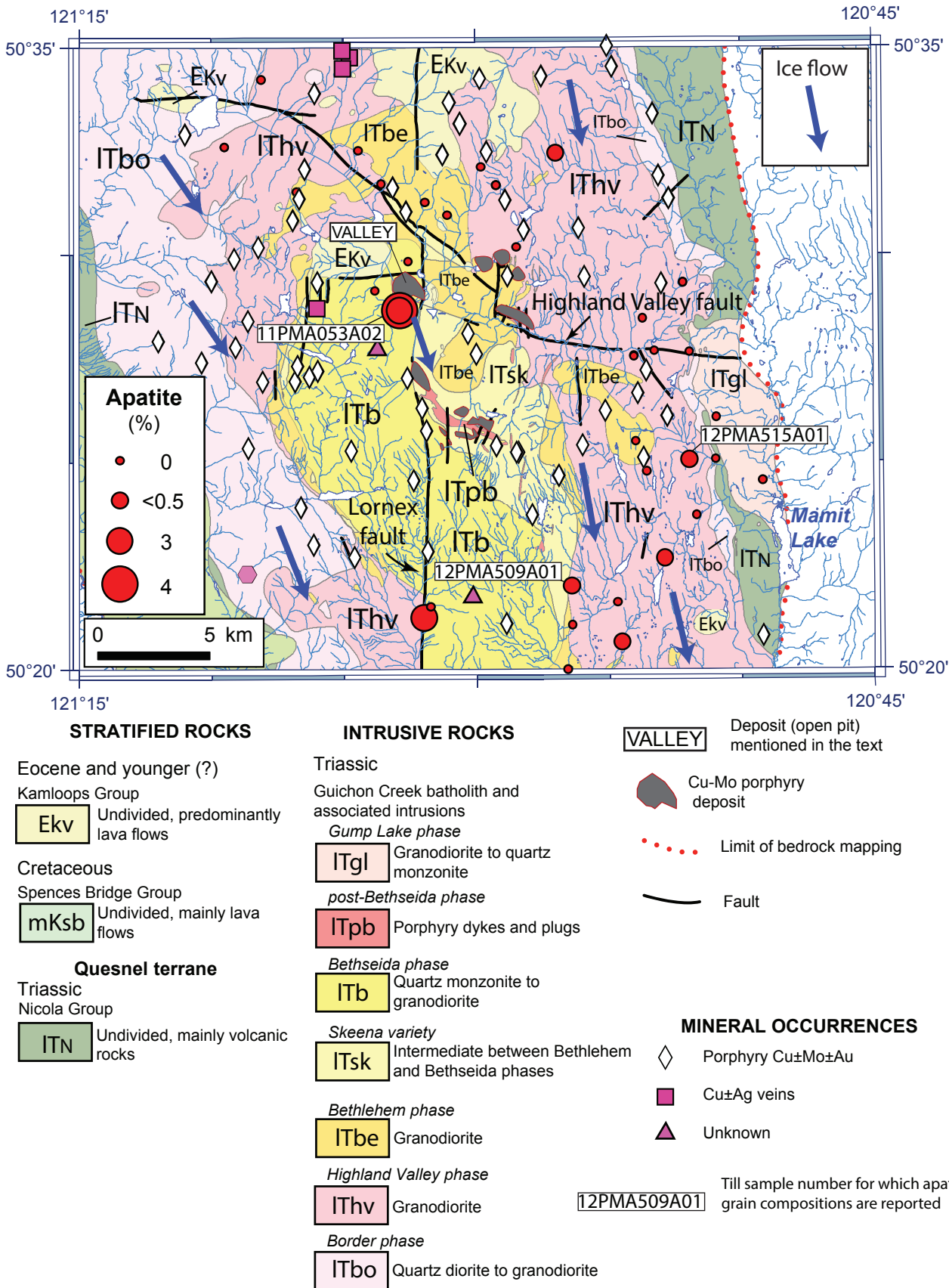
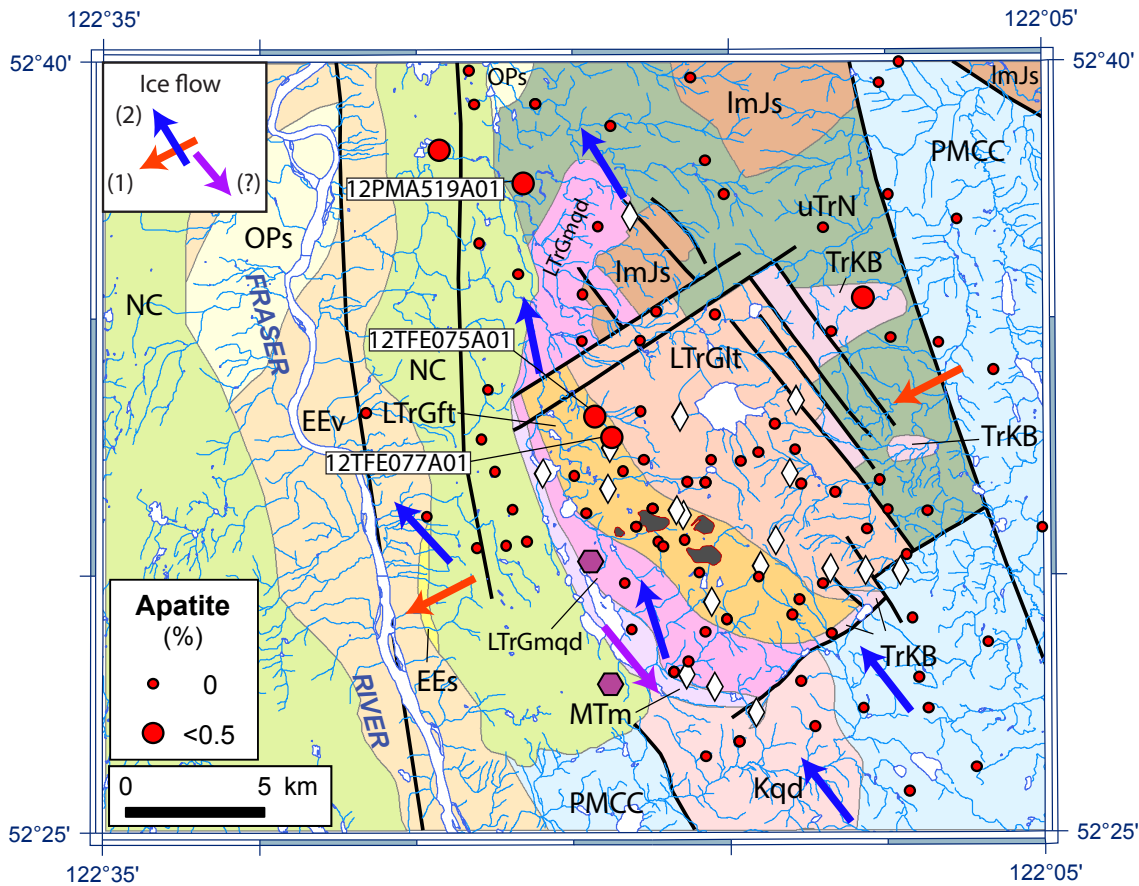


Fig. 2. Geology, sample locations, generalized ice-flow directions, mineral occurrences and apatite content of till (0.25–0.50 mm, >3.2 g·cm<sup>-3</sup>, >1.0 A fraction), Highland Valley calc-alkaline porphyry Cu-Mo district. Geology after McMillan (1985) and McMillan et al. (2009).



**STRATIFIED ROCKS**

- Neogene
  - Chilcotin Group
    - NC** Basaltic volcanic rocks with lesser sedimentary rocks
- Oligocene to Pliocene
  - OPs** Conglomerate
- Eocene to Oligocene
  - Endako Group
    - EEv** Basaltic volcanic rocks with lesser sedimentary rocks
    - EEs** Sedimentary rocks
- Quesnel terrane**
  - Lower - Middle Jurassic
    - Ashcroft Formation
      - ImJs** Polymictic volcanic and plutonic-clast conglomerate
  - Upper Triassic and Lower Jurassic
    - Nicola Group
      - uTrN** Volcanic sandstone-siltstone
- Cache Creek terrane**
  - Carboniferous - Lower Jurassic
    - Cache Creek Complex
      - PMCC** Undivided marine sedimentary and volcanic rocks

**METAMORPHIC ROCKS**

- Eocene ?
  - MTm** Chlorite-sericite-quartz-feldspar schist

**INTRUSIVE ROCKS**

- Triassic? Jurassic? Cretaceous?
  - Burgess Creek stock (Border phase)**
    - TrKB** Quartz diorite, tonalite

- Middle Cretaceous
  - Sheridan stock (ca. 108 Ma)**

- Kqd** Quartz diorite, quartz monzonite, granodiorite, granite

- Late Triassic
  - Granite Mountain batholith (ca. 215 Ma)**

- LTrGmqd** Melanocratic quartz diorite
- LTrGft** Foliated tonalite (Mine phase)
- LTrGlt** Leucocratic tonalite, trondhjemite (Granite Mountain phase)

- Cu-Mo porphyry deposit

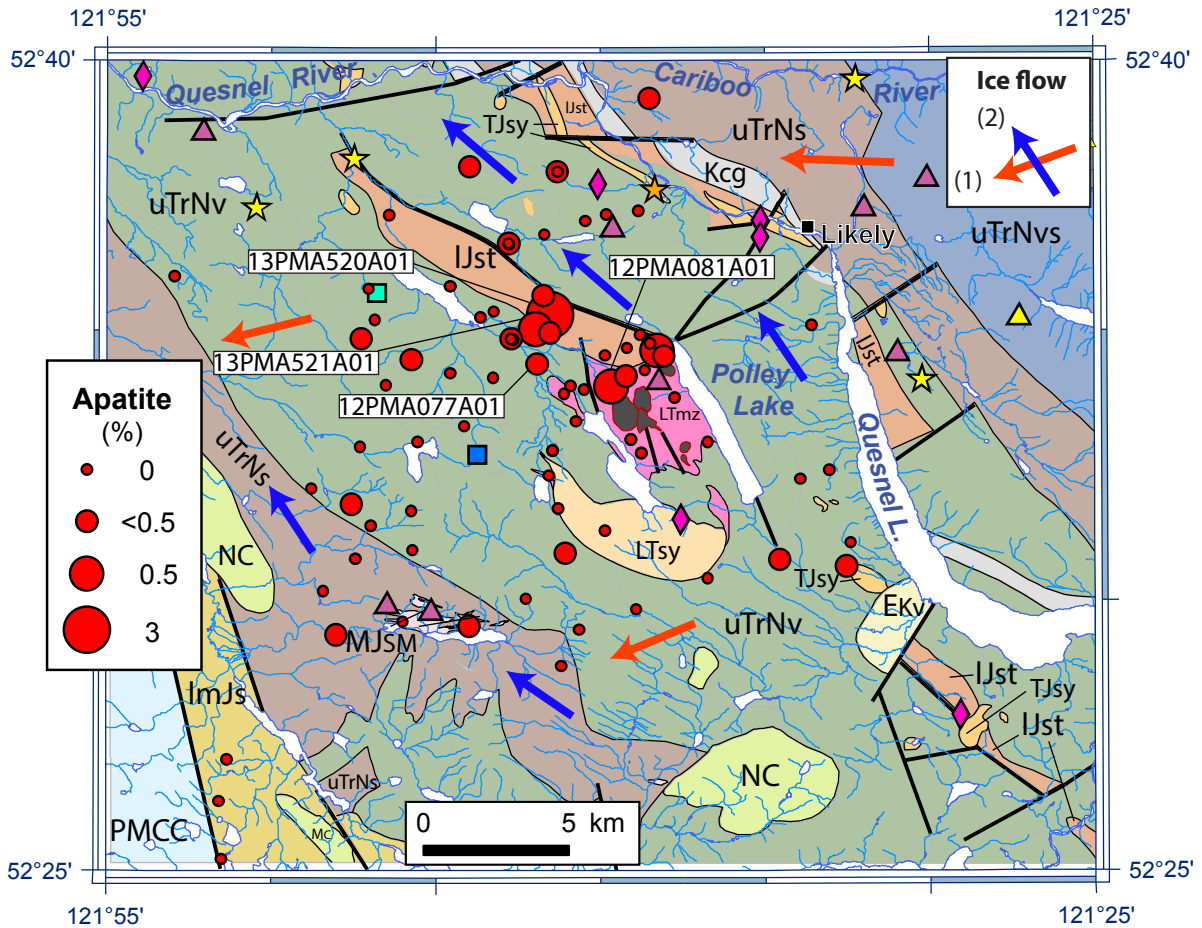
- Fault

**MINERAL OCCURRENCES**

- Porphyry Cu±Mo±Au
- Cu-Mo setting unknown

**12PMA519A01** Till sample number for which apatite grain compositions are reported

**Fig. 3.** Geology, sample locations, generalized ice-flow directions, mineral occurrences and apatite content of till (0.25–0.50 mm, >3.2 g·cm<sup>-3</sup>, >1.0 A fraction), Gibraltar calc-alkaline porphyry Cu-Mo mine area. Geology after Ash et al. (1999a) and Schiarizza (2014).



**STRATIFIED ROCKS**

- Quaternary to Neogene  
Chilcotin Group
- NC** Basaltic volcanic rocks
- Paleogene  
Kamloops Group
- EKv** Calc-alkaline volcanic rocks
- Cretaceous  
Bowron River Coal Beds
- Kcg** Undivided sedimentary rocks
- Quesnel terrane**  
Middle to Upper Triassic  
Nicola Group
- uTrNv** Basaltic, volcanic and volcaniclastic rocks
- uTrNs** Undivided sedimentary rocks
- uTrNvs** Transitional mixed volcanic and sedimentary rocks
- Lower to Middle Jurassic
- ImJs** Undivided sedimentary rocks
- IJst** Argillite, greywacke, wacke, conglomerate, turbidites

**Cache Creek terrane**

- Permian to Triassic  
Cache Creek Complex
- PMCC** Siltstone, ribbon chert, limestone, ultramafite, basalt and gabbro

**Slide Mountain terrane**

- Carboniferous to Permian  
Crooked Amphibolite
- uPzC** Serpentine ultramafic rocks

**INTRUSIVE ROCKS**

- Middle Jurassic  
**Ste. Marie plutonic rocks**
- MJSM** Quartz diorite, quartz monzonite, granodiorite, granite
- Late Triassic to Early Jurassic
- TJsy** Syenitic to monzonitic intrusive rocks
- LTsy** Syenitic intrusive rocks
- Mount Polley intrusive complex**
- LTmz** Syenitic to monzodioritic intrusive rocks

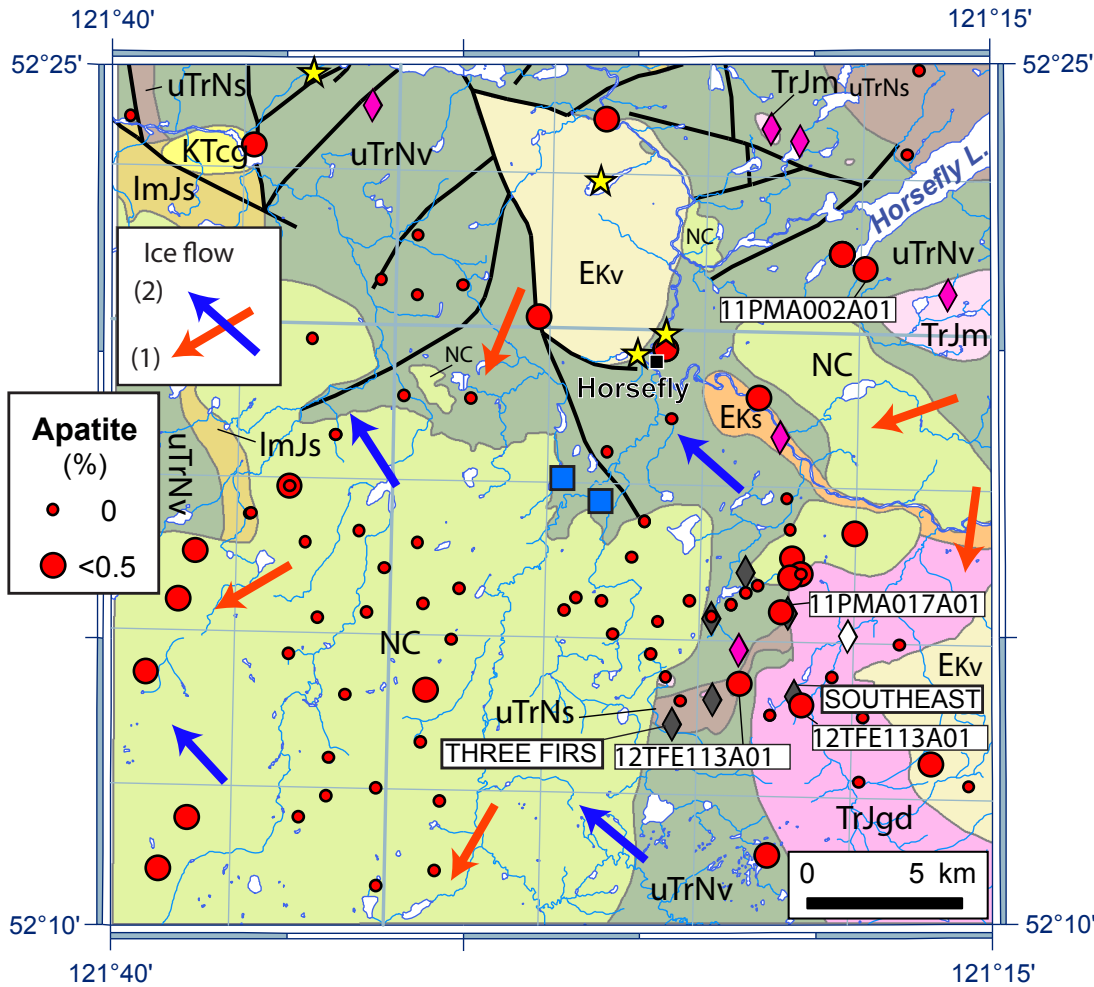
- Cu-Au porphyry deposit
- Fault

**MINERAL OCCURRENCES**

- Porphyry Cu-Au
- Au-quartz veins
- Surficial gold placers
- Buried-channel gold placers
- Sediment-hosted Cu
- Volcanic redbed Cu
- Unknown

**13PMA520A01** Till sample number for which apatite grain compositions are reported

**Fig. 4.** Geology, sample locations, generalized ice-flow directions, mineral occurrences and apatite content of till (0.25–0.50 mm, >3.2 g·cm<sup>-3</sup>, >1.0 A fraction; after Hashmi et al., 2015), Mount Polley alkalic porphyry Cu-Au mine area. Geology after Logan et al. (2007a, 2010).



**STRATIFIED ROCKS**

Oligocene - Pliocene  
Chilcotin Group

**NC** Basaltic volcanic rocks

Eocene  
Kamloops Group  
**EKs** Shale, siltstone and sandstone  
**Ekv** Andesite, trachyandesite

Tertiary - Cretaceous  
**KTcg** Undivided sedimentary rocks

**Quesnel terrane**  
Jurassic  
**ImJs** Undivided sedimentary rocks

Triassic  
Nicola Group  
**uTrNv** Undivided volcanic rocks  
**uTrNs** Undivided sedimentary rocks

**INTRUSIVE ROCKS**

Triassic to Jurassic  
**TrJm** Syenitic to monzonitic intrusive rocks

Takomkane batholith  
**TrJgd** Granodioritic intrusive rocks

**MINERAL OCCURRENCES**

- ★ Gold placer
- Volcanic redbed Cu
- ◆ Alkalic porphyry Cu-Au
- ◇ Porphyry Cu±Mo±Au
- ◆ **THREE FIRS** Woodjam porphyry Cu-Mo±Au main mineralized zone with name mentioned in text
- **11PMA002A01** Till sample number for which apatite grain compositions are reported

**Fig. 5.** Geology, sample locations, generalized ice-flow directions, mineral occurrences and apatite content of till (0.25–0.50 mm, >3.2 g·cm<sup>-3</sup>, >1.0 A fraction), Woodjam high-K, calc-alkaline porphyry Cu-Mo±Au developed prospect area. Geology after Logan et al. (2007b, 2010) and Schiarizza et al. (2009a, b).

Casselman et al., 1995). A total of 1615.16 million tonnes of ore grading 0.40% Cu and 0.010% Mo have been processed from the Highland Valley deposits, with reserves (as of December 2012) estimated to be 697 million tonnes grading 0.29% Cu and 0.008% Mo (Byrne et al., 2013). The major deposits are at the intersection of the Lornex and Highland Valley faults (Fig. 2; Casselman et al., 1995). The main ore minerals include chalcopyrite, bornite and molybdenite. Regional hydrothermal vein alteration, with green sericite, chlorite and epidote, is prominent at Highland Valley, extending approximately 10 km to the northwest, north and southeast from the intersection of the Lornex and Highland Valley faults (see Figure 14 in Casselman et al., 1995). Sedimentary and volcanic rocks of the Kamloops Group (Eocene) locally overlie the northern part of the intrusion. Apatite has been reported as an accessory mineral in both K-silicate and muscovite alteration zones, and in fresh Guichon batholith intrusive rocks (Casselman et al., 1995; Bouzari et al., 2011b).

### 3.2. Gibraltar

The Granite Mountain batholith (Late Triassic) hosts the Gibraltar calc-alkaline porphyry Cu-Mo deposit, approximately 50 km north of Williams Lake, and comprises an intrusive complex made up of diorite to quartz diorite, tonalite, and trondhjemite (Fig. 3; Drummond et al., 1973, 1976; Bysouth et al., 1995; Ash et al., 1999a, b; Ash and Riveros, 2001; Schiarizza, 2014, 2015). Most of the mineralization is hosted by foliated tonalite (Mine phase) in the core of the intrusion (van Straaten et al., 2013). Supergene ore was mined from two of the pits in the initial phases of mining (Rotherham et al., 1972). Combining the past production and the current resources, the Gibraltar deposit comprises 1.22 billion tonnes of ore with a Cu grade of 0.317% and an estimated Mo grade of 0.010% (van Straaten et al., 2013). The predominant ore minerals include chalcopyrite and molybdenite, and chalcocite in the supergene zones (Ash et al., 1999b).

Sutherland Brown (1974), Drummond et al. (1976), and Bysouth et al. (1995) originally assigned host rocks of the Granite Mountain batholith to the Cache Creek oceanic terrane (Late Paleozoic to Early Mesozoic), unlike other porphyry deposits in southern British Columbia, which are in the Quesnel terrane. However, part of the batholith and the mineralization underwent ductile deformation and were metamorphosed to greenschist grade, which raised questions as to whether the mineralization is a porphyry style (e.g., Sutherland Brown, 1974; Ash et al., 1999b). Recently, Schiarizza (2014, 2015) found that the Granite Mountain batholith cuts the Nicola Group, the defining stratigraphic unit of Quesnel terrane, and concluded that it occupies a panel of Quesnel terrane that was juxtaposed against Cache Creek rocks along later faults. Ductile strain features in the ore bodies imply that mineralization was before or during deformation (van Straaten et al., 2013). Apatite was reported in the tonalite of the Mine phase (Ash and Riveros, 2001).

### 3.3. Mount Polley

The Mount Polley intrusive complex (Late Triassic), made up of diorite, monzodiorite, monzonite, and plagioclase porphyry, hosts the Mount Polley alkalic porphyry Cu-Au deposit, approximately 45 km east of the Gibraltar mine (Fig. 4). The complex cuts sedimentary and volcanic rocks of the Nicola Group (Middle to Late Triassic; Hodgson et al., 1976; Logan et al., 2007a, b, 2010). Production includes 452 million pounds of Cu, 0.695 million ounces of Au, and 2.2 million ounces of Ag from 80 million tonnes of ore (Rees, 2013). The reserves (as of January 2013) were estimated to be 93 million tonnes grading 0.297% Cu, 0.299 g/t Au, and 0.620 g/t Ag (Rees, 2013). Three Cu-Au mineralized zones are present at Mount Polley, one in the core of the intrusion, a second in the southeast sector, and a third, higher-grade zone, in the northeast sector. Part of the mineralization is spatially associated with hydrothermal breccias cemented by magnetite and disseminated chalcopyrite. The main ore minerals include chalcopyrite and bornite. Gold forms inclusions in pyrite and chalcopyrite (Fraser et al., 1995; Pass, 2010). Apatite is present in both the calc-potassic alteration zone ('alteration zone III' of Rees, 2013) and fresh monzonite (Bouzari et al., 2011b). Celis et al. (2014) also reported ubiquitous subhedral to anhedral apatite grains (0.5 mm) in intrusive rocks and alteration zones.

### 3.4. Woodjam

Satellite intrusions about 1.5 km north of the Takomkane batholith (Late Triassic to Early Jurassic) host six porphyry-style mineralized zones comprising the Woodjam developed prospect, about 45 km east of Williams Lake and 35 km southeast of the Mount Polley mine (Fig. 5; Logan et al., 2007a, b, 2010; Schiarizza et al., 2009a, b; Schroeter, 2009). The intrusive rocks vary from monzodiorite to quartz monzonite (Schroeter, 2009). The batholith cuts sedimentary and volcanic rocks of the Nicola Group (Late Triassic). Mineralization in the camp is mainly of the high-K, calc-alkaline porphyry Cu-Mo±Au variety (Vandekerckhove et al., 2014) similar to that at Red Chris (Rees et al., 2015) and Kemess South (Duuring et al., 2009). Texturally variable quartz monzonite intrusions host the Southeast Zone deposit and display alteration and mineralization typical of calc-alkaline porphyry deposits, although other mineralized zones such as the Deerhorn prospect may have some alkalic porphyry features (del Real et al., 2014). Epidote-chlorite-pyrite, illite and hematite overprint both pervasive K-feldspar-biotite-magnetite alteration assemblage in the centre of the Southeast Zone and albite±epidote assemblage along its margins. The latter also occurs near the contact between the Takomkane batholith and rocks of the Nicola Group (del Real et al., 2014). Inferred resources for three of the mineralized zones are 221.7 million tonnes of ore with grades ranging from 0.22 to 0.31% Cu and from 0.26 to 0.49 g/t Au (Sherlock et al., 2013; Sherlock and Trueman, 2013; del Real et al., 2014). Ore minerals include chalcopyrite with minor bornite, and small amount of molybdenite and native copper. Gold is mainly related to chalcopyrite and bornite and is only

visible microscopically (Sherlock et al., 2013; see Figure 19 in Vandekerckhove et al., 2014). A large portion of the Woodjam area is underlain by volcanic and subordinate sedimentary rocks of the Kamloops (Eocene) and Chilcotin (Oligocene to Pliocene) groups (Fig. 5). Potassic, propylitic, and tourmaline alteration styles are present at Woodjam, but apatite has not been reported in any of the alteration zones or fresh intrusive rocks.

#### 4. Samples

We examined 147 apatite grains recovered from 14 till samples and 2 mineralized bedrock samples at Highland Valley, Gibraltar, Mount Polley, and Woodjam (Table 1). From each area, three to four till samples were selected, mainly down-ice from known mineralization (for details of the till sampling, see Plouffe and Ferbey, 2015d). Figures 2–5 show the percentage of apatite in the 0.25–0.50 mm,  $>3.2 \text{ g}\cdot\text{cm}^{-3}$ ,  $>1.0 \text{ A}$  (non-magnetic) fraction of till samples, determined, along with other porphyry indicator minerals (e.g., visible gold, chalcocopyrite, epidote), as part of the TGI-4 studies (Plouffe et al., 2013a; Plouffe and Ferbey, 2015a, d). These mineralogical data guided our selection of till samples for this study.

The two rock samples from the Woodjam Southeast Zone (Table 1) are mineralized quartz monzonites from Gold Fields Limited's diamond-drill hole SE11-27. Sample 258404 is from the 115.8 to 117.0 m depth interval; sample 258405 is from the interval 117.0 to 119.0 m. Based on a binocular microscope description of the rock fragments (2–6 mm; S.A. Averill, pers. comm. 2014), the rocks are massive and porphyritic to equigranular. The porphyritic varieties contain 15–30% euhedral, albite-twinned plagioclase and 5% biotite phenocrysts (1–2 mm) in a fine-grained (0.15–0.50 mm) granophyric groundmass made up of 65% alkali feldspar (perthite), 30% quartz, 0–5% biotite, 0–1% magnetite, and 0–0.2% pyrrhotite. The equigranular quartz monzonite is medium grained (1–2 mm) and consists of 40% euhedral, fresh and commonly albite-twinned plagioclase, 35% interstitial, anhedral, perthitic alkali feldspar, 20% quartz, and 5% biotite. The rocks are stained by hematite and contain 1–2% chalcocopyrite along hairline fractures, and lining or filling fractured quartz veinlets (1–5 mm wide). Biotite is mostly altered to chlorite, and calcite (1%) fills younger, unmineralized fractures. Other accessory minerals, in the heavy mineral concentrates (HMC), include apatite  $>$  pyrite  $>$  chalcocite  $>$  molybdenite  $>$  titanite  $\approx$  rutile. Bornite (0.10–0.25 mm) and visible gold (15–125  $\mu\text{m}$ ) were identified in the panned fraction of heavy mineral concentrates.

We also examined thin sections from five rock samples from the Gibraltar mine (not listed in Table 1) to determine if apatite separation would be feasible. Although rare apatite is in four of these, we failed in our attempt to recover apatite grains from two Gibraltar mine samples (mineralized, sheared tonalite, sample SVA75-7-14.6, and massive quartz diorite, sample GSC-2). Based on a binocular microscope description of hand specimens (S.A. Averill, pers. comm. 2014) and petrographic examinations, the sheared tonalite is a medium-grained (2–

mm), augen schist made up of pervasively sericitized and saussuritized plagioclase (40%), quartz (30%), and retrograde chlorite after biotite (30%) with trace leucoxene after primary titanite. Chlorite forms folded wisps and locally continuous seams separating quartz and feldspar augen. Chalcocopyrite (1%) and trace amounts of molybdenite, pyrite, and rutile are restricted to the chlorite $\pm$ quartz $\pm$ albite veins or seams and are similarly foliated and folded, possibly suggesting that mineralization was before deformation. Carbonate and epidote are also common. Rare euhedral to subhedral apatite (0.10–0.28 mm by 0.08–0.14 mm) forms clusters in chlorite $\pm$ quartz $\pm$ albite veins, with traces of chalcocopyrite and rutile, and along feldspar-quartz boundaries. The massive quartz diorite is an equigranular, medium-grained (1–2 mm) rock made up of euhedral, pervasively sericitized and saussuritized plagioclase (70%), chlorite (20%), and quartz (10%), with traces of titanite, pyrite, sphalerite, chalcocopyrite, and covellite. Traces of supergene azurite and malachite coat fractures. Rare, mostly euhedral apatite (0.10–0.26 mm by 0.04–0.12 mm) occurs along quartz-chlorite and plagioclase-epidote-chlorite boundaries. Zircon is an accessory mineral in both rocks.

#### 5. Methods

##### 5.1. Sample preparation

Apatite separation and identification were completed at Overburden Drilling Management Ltd. (Ottawa, ON) following the protocol adopted at the Geological Survey of Canada (Plouffe et al., 2013c). Blind quality controls, including blank samples from a weathered granite (to monitor laboratory cross-contamination), field duplicate samples (to test sampling site variability), and spiked samples (to evaluate the reproducibility of the heavy mineral separation and the identification of indicator minerals) were inserted. Till samples (~10 kg) were processed to recover heavy minerals ( $>2.8 \text{ g}\cdot\text{cm}^{-3}$  fraction) as follows. First, the samples were wet sieved to the  $<2 \text{ mm}$  fraction and concentrated by gravity on a shaking table. Shaking table concentrates were then separated with methylene iodide diluted with acetone into 2.8–3.2  $\text{g}\cdot\text{cm}^{-3}$  and  $>3.2 \text{ g}\cdot\text{cm}^{-3}$  fractions. Next, ferromagnetic minerals were removed with a hand magnet before re-sieving into three size fractions (0.25–0.50 mm, 0.5–1.0 mm, and 1–2 mm). The 0.25–0.50 mm fraction was processed on a Carpc High-Intensity Lift electro-magnetic separator (model MLH) set at 0.6, 0.8 and 1.0 A. Apatite grains (Fig. 6) were hand-picked from the 0.25–0.50 mm,  $>3.2 \text{ g}\cdot\text{cm}^{-3}$ ,  $>1.0 \text{ A}$  fraction under a binocular microscope. Apatite contents in this fraction of the till and rock samples vary from trace ( $<0.5\%$ ) to 3% (Table 1, Fig. 6). No apatite grains were observed in the 0.5–2.0 mm fraction of the till samples, nor was apatite found in the finer (0.18–0.25 mm) and 2.8–3.2  $\text{g}\cdot\text{cm}^{-3}$  fractions of the two rock samples from Gibraltar. Because apatite has a density that varies from 3.17 to 3.23  $\text{g}\cdot\text{cm}^{-3}$  (Berry et al., 1983), it is typically recovered from the 2.96–3.32  $\text{g}\cdot\text{cm}^{-3}$  fraction (Mao et al., 2015), but we analyzed only grains recovered from the  $>3.2 \text{ g}\cdot\text{cm}^{-3}$  fraction, a separation adopted in other apatite studies (Normandeau et

**Table 1.** Summary of estimated apatite contents in till and bedrock samples, recovered apatite grains, and the analyses performed on apatite grains.

N	Sample <sup>1</sup>	Northing <sup>2</sup>	Eastings <sup>2</sup>	Type	Apatite <sup>3</sup> %	Grains picked	EDS checked	Grains used	EMPA	LA-ICP-MS	Area	Main deposit type
1	12PMA519A01	5830965	543370	Till	<0.5 (8)	8	8	8	7	5	Gibraltar	Calc-alkaline porphyry Cu-Mo
2	12TFE075A01	5822574	546002	Till	<0.5 (~30)	25	15	10	10	8		
3	12TFE077A01	5821831	546631	Till	<0.5 (~50)	27	7	10	10	10		
4	11PMA053A02	5593549	638475	Till	3 (~600)	30	5	10	10	10	Highland Valley	Calc-alkaline porphyry Cu-Mo
5	12PMA509A01	5581422	646465	Till	<0.5 (16)	16	16	10	6	6		
6	12PMA515A01	5587223	651586	Till	<0.5 (5)	5	5	5	5	5		
7	12PMA077A01	5825591	588194	Till	<0.5 (~30)	23	23	10	9	9	Mount Polley	Alkalic porphyry Cu-Au
8	12PMA081A01	5824874	590751	Till	0.5 (~150)	33	3	10	10	10		
9	13PMA520A01	5827291	588619	Till	0.5 (~100)	27	17	10	10	10		
10	13PMA521A01	5826794	588125	Till	0.5 (~100)	25	25	10	10	10	Woodjam	High-K, calc-alkaline porphyry Cu-Mo±Au
11	11PMA002A01	5802049	615155	Till	<0.5 (~30)	20	20	10	9	7		
12	11PMA017A01	5790909	612652	Till	<0.5 (~40)	25	25	10	10	10		
13	12TFE113A01	5787923	613380	Till	<0.5 (~30)	21	6	10	10	9		
14	12TFE116A01	5788577	611357	Till	<0.5 (10)	10	10	10	10	8	Woodjam (Southeast Zone)	High-K, calc-alkaline porphyry Cu-Mo±Au
15	258404	5788122	613121	Rock <sup>4</sup>	<0.5 (~50)	22	7	11	11	11		
16	258405	5788122	613122	Rock <sup>4</sup>	1 (~200)	27	7	10	10	10		
17	MAD standard			Fragments of large crystal				10	10	26*	First Mine Discovery, Madagascar	Pegmatite
18	DUR standard			Fragments of large crystal				7	7	26	Cerro de Mercado, Durango	Kiruna-type

**Footnotes:**

<sup>1</sup> Details of the samples from the regions of the Gibraltar, Highland Valley and Mount Polley mines, and the Woodjam deposits and prospects in south-central British Columbia can be found in Plouffe et al. (2013a) and Plouffe and Ferbey (2015a, d); for details on Madagascar and Durango reference apatites, see Thomson et al. (2012) and Young et al. (1969).  
<sup>2</sup> NAD83, UTM Zone 10 coordinates.

<sup>3</sup> Estimated apatite content (%) and total number of apatite grains (in parentheses) in the heavy mineral concentrate, i.e. 0.25–0.50 mm, >3.2 g·cm<sup>-3</sup>, >1.0 Å (non-magnetic) fraction.  
<sup>4</sup> Core samples of mineralized quartz monzonites from Gold Fields Limited's diamond-drill hole SE11-27; sample 258404 from 115.8 to 117.0 m depth below surface; sample 258405 from 117.0 to 119.0 m depth below surface. See text for details.

\* Includes 14 new LA-ICP-MS analyses of fragments in a grain mount used by Mao et al. (2015).  
 EDS = number of grains confirmed by energy dispersive X-ray spectrometry, EMPA = number of electron microprobe analyses, LA-ICP-MS = number of analyses by laser ablation - inductively coupled plasma mass spectrometry; one EMPA and LA-ICP-MS analysis each per grain, except for some large fragments of Durango and Madagascar apatites on which multiple LA-ICP-MS analyses were performed.

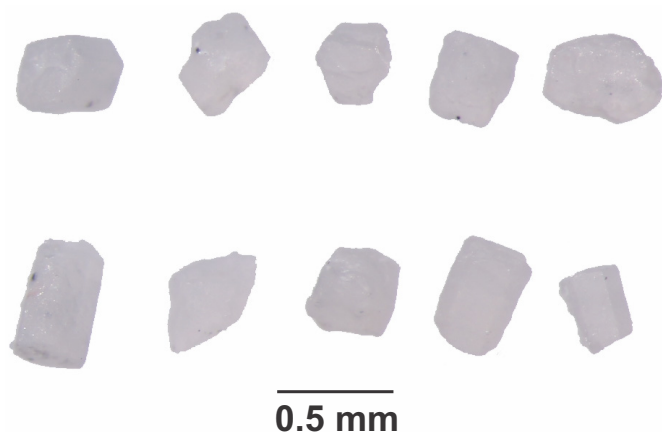


**Fig. 6.** Colourless apatite grains recovered from till in the southern part of the Highland Valley study area.

al., 2014). More than 50% of the recovered apatite grains were confirmed on a scanning electron microscope (SEM) equipped with an energy-dispersive X-ray spectrometer (EDS) (Table 1).

To evaluate the reproducibility of apatite identification in the mineral concentrates, 21 concentrates were resubmitted with new numbers. Table 2 presents results from these replicates, which demonstrate good reproducibility of apatite identification at the processing laboratory. Throughout this report, the percentage of apatite in till samples refers to the amount of apatite in the 0.25–0.50 mm,  $>3.2 \text{ g cm}^{-3}$ ,  $>1.0 \text{ A}$  fraction.

Selected apatite grains (up to 10 per sample) were mounted in epoxy mounts for electron microprobe analysis (EMPA) and laser ablation-inductively coupled plasma mass spectrometry (LA-ICP-MS). Fragments of two large natural apatite crystals from Cerro de Mercado, Durango (Young et al., 1969) and First Discovery Mine, Madagascar (Thomson et al., 2012), used as the matrix-matched standards by Mao et al. (2015), were mounted together with the apatite grains (Table 1). The grain mounts were polished by hand using BuehlerMet II lapping papers P400, P1200, P4000, and Buehler lapping powder 1  $\mu\text{m}$  and 0.3  $\mu\text{m}$ . All grain mounts were rinsed thoroughly using deionized water between polishing steps and cleaned in an ultrasonic bath for about 30 minutes before analysis. EMPA and LA-ICP-MS analyses were performed using procedures for apatite developed by Mao et al. (2015), which are summarized below.

## 5.2. EMPA analysis

All electron probe analyses (EMPA) were performed on a fully automated Cameca SX50 electron microprobe equipped with four wavelength-dispersive spectrometers at the Department of Earth, Ocean and Atmospheric Sciences, University of British Columbia (UBC). Apatite grains ( $n = 147$ ; Table 1) were analyzed using the wavelength-dispersion mode with a 15 kV excitation voltage, 10 nA beam current, and 10  $\mu\text{m}$  beam diameter. Flat surface regions, free of any inclusions or fractures, where possible, were chosen for the beam spot (one

per grain). Although some apatites display complex zoning in cathodoluminescence or back-scattered electron (BSE) imaging, reflecting magma mixing, intracrystalline diffusion or complex dissolution-precipitation (e.g., Tepper and Kuehner, 1999; Bath et al., 2006; Liaghat and Tosdal, 2008; Bouzari et al., 2011b), the examined apatite grains lacked prominent internal zonation in BSE. Peak and background counting times were 20 seconds for F, S, Cl and Fe, and 10 seconds for Na, Si, P and Ca. Fluorine was always measured on the first cycle because of migration during analysis. The background values for F were fixed and based on the first measured result. Data reduction was done using the ‘PAP’  $\Phi(\rho Z)$  method (Pouchou and Pichoir, 1985). The following standards (locations), X-ray lines, and crystals were used: topaz (Topaz Valley, UT, U.S.A.),  $\text{FK}\alpha$ , TAP; albite (Rutherford Mine, Amelia County, VA, U.S.A.),  $\text{NaK}\alpha$ , TAP; diopside (C.M. Taylor Company, locality unknown),  $\text{SiK}\alpha$ , TAP; apatite (Wilberforce, ON, Canada),  $\text{PK}\alpha$ , PET; barite (C.M. Taylor Company, locality unknown),  $\text{SK}\alpha$ , PET; scapolite (Lot 32, Con. XVII, Monmouth, ON, Canada),  $\text{ClK}\alpha$ , PET; apatite (Wilberforce, ON, Canada),  $\text{CaK}\alpha$ , PET; and synthetic fayalite (Los Alamos National Laboratory, NM, U.S.A.),  $\text{FeK}\alpha$ , LIF.

The detection limits, based on counting statistics, were 0.85 wt.% for F, 0.05 wt.% for Na, 0.04 wt.% for Si and S, 0.08 wt.% for P, 0.03 wt.% for Cl, 0.06 wt.% for Ca, and 0.07 wt.% for Fe. The relative precision ( $2\sigma$ ), based on the analyses of Durango ( $n = 7$ ) and Madagascar ( $n = 10$ ) apatites, was 1% for Ca, 4% for P, from 11% to 40% for F, Si, S, and Cl, and from 23% to  $>100\%$  for Na and Fe (Appendix 1, Rukhlov et al., 2016). Therefore, Na and Fe values close to the EMPA detection limit are semi-quantitative to qualitative.

## 5.3. LA-ICP-MS analysis

All laser ablation analyses (LA-ICP-MS) were performed using He as the carrier gas and a New Wave UP-213 coupled to a Thermo X-Series II (X7) quadrupole ICP-MS at the School of Earth and Ocean Sciences, University of Victoria (SEOS). We adopted the LA-ICP-MS analytical and data reduction procedures from Mao et al. (2015). Apatite grains ( $n = 138$ ; Table 1) were analyzed with a 30  $\mu\text{m}$  laser spot diameter, a pulse rate of 10 Hz, and measured fluence from 8.5 to 12.5  $\text{J cm}^{-2}$ . A pre-ablation warm-up of 5 seconds was used to avoid unstable laser energy at the beginning of each ablation. All LA-ICP-MS spectra were recorded for 120 s, including  $\sim 30$  s gas blank before ablation started, 60 s during ablation, and  $\sim 30$  s post ablation. At least 60 s of gas flushing was allowed between analyses. The ICP-MS was optimized to maximize sensitivity and minimize oxide formation. Forward RF was 1400 watts. The dwell time was 3 ms for all REE elements and 5 ms for all other elements.

We used  $^{43}\text{Ca}$  as the internal standard for LA-ICP-MS calibration and Ca concentrations determined directly by EMPA. NIST glasses 611, 613, and 615 (Jochum et al., 2011) were used as the external calibration standards. Madagascar and Durango apatites were analyzed 26 times each (multiple

**Table 2.** Results of apatite identification in replicate pairs of heavy mineral concentrates from till samples.

Sample	Apatite (%)	Sample	Apatite (%)
11PMA018A1	0	12PMA560A1	0
11PMA100A1	0	12PMA705A1	0
11PMA053A1	4	12PMA564A1	0
11PMA10011	4	12PMA706A1	0
11PMA010A1	<0.5	12PMA567A1	0
11PMA102A1	<0.5	12PMA707A1	0
11PMA017A1	<0.5	12PMA571A1	0
11PMA103A1	<0.5	12PMA708A1	0
11PMA003A2	<0.5	12PMA585A1	0
11PMA104A1	<0.5	12PMA709A1	0
11PMA051A1	0	12PMA586A1	0
11PMA105A1	<0.5	12PMA710A1	<0.5
12PMA515A1	<0.5	12PMA588A1	0
12PMA700A1	0	12PMA711A1	0
12PMA528A1	0	12PMA595A1	0
12PMA701A1	0	12PMA712A1	0
12PMA535A1	0	12PMA596A1	0
12PMA702A1	0	12PMA713A1	0
12PMA547A1	0	12PMA606A1	0
12PMA703A1	0	12PMA714A1	0
12PMA559A1	0		
12PMA704A1	0		

Heavy mineral concentrates (HMC) are 0.25-0.50 mm, >3.2 g·cm<sup>-3</sup>, >1 A (non-magnetic) fraction of till samples.

analyses per crystal fragment) to monitor accuracy and precision of the analyses (Appendix 1, Rukhlov et al., 2016). Appendix 3 (Rukhlov et al., 2016) provides complete analytical data for the standards. A typical session started with NIST glasses 615, 613, and 611, followed by Madagascar and Durango apatites, then 6 unknowns, and then all five standards were repeated. During offline data reduction, time-resolved count rates were carefully checked and any spectra with spikes, indicating possible inclusions, were discarded. The data reduction procedure for each element included: 1) selecting the time intervals for the background and signal region of each spectrum; 2) calculating the mean CPS (count per second) of these intervals; 3) correcting for background of the signal CPS; 4) normalizing to the internal standard; 5) correcting for drift using a linear drifting factor determined from repeat analysis

of NIST 611; 6) calibrating using sensitivities for each element determined from the initial analyses of NIST 615, 613 and 611 in each load (i.e. analytical session) to obtain the concentration value of each element.

We analyzed 30 elements by LA-ICP-MS in the apatite grains. The instrument detection limit (IDL) has been estimated as:  $IDL = 3\sigma \text{ background/Sensitivity}$  where  $3\sigma$  background is the 3 times standard deviation of the signal for a given element collected before ablation for each sample (gas blank), and Sensitivity is the slope of calibration curve (i.e. internal-standard- and drift-corrected cps versus 'true' concentration for external standards) determined from NIST 615, 613 and 611 for a given element in each session. Appendix 1 (Rukhlov et al., 2016) provides the detection limits per element, which varied between individual analyses due

to instrument background variations. The detection limits are <200 ppm for Mn, As and Ce; <75 ppm for Mg, Ti, Sr, Y, Zr, La, and Nd; <25 ppm for Cu, Zn, Mo, Ba, Pr, Sm, Gd, and Dy; <9 ppm for V, Rb, Nb, Eu, Yb, Pb, and Th; and <5 ppm for Lu, W, and U. Although Si and P were analyzed by both EMPA and LA-ICP-MS, the latter results are less precise and, therefore, will not be discussed further.

The experimental precision was determined by repeat analyses ( $n = 26$ ) of NIST glasses 611 and 613 and the Madagascar and Durango apatites. Based on NIST 613 and Durango and Madagascar apatites, the relative precision ( $2\sigma$ ) varies from 3% to 18% for elements with concentrations >10 ppm, except for As in NIST glass 613 (52%), and from 10% to 110% for elements with lower concentrations (Appendix 1, Rukhlov et al., 2016). For NIST 611, with order of magnitude higher concentrations of all elements than those in NIST 613, the precision is 2%-12% for all elements. The precision for NIST 615 (from 15% to 96%) shows that values close to the instrument detection limit are semi-quantitative to qualitative (Appendix 1, Rukhlov et al., 2016). Our results for the Madagascar and Durango apatites (Appendix 1, Rukhlov et al., 2016) are in excellent agreement with those reported by Mao et al. (2015).

## 6. Results

### 6.1. Apatite in till

Given that the abundance of apatite in till was determined in the heavy mineral fraction ( $>3.2 \text{ g}\cdot\text{cm}^{-3}$ ), our results represent only the partial abundance of apatite in till. Regardless, it demonstrates that apatite survives glacial transport and post-glacial weathering and that its composition is worth studying to fingerprint a mineralized source.

Our limited dataset from the Highland Valley area shows that most samples taken from tills overlying the Guichon Creek batholith lack apatite or contain only trace amounts (<0.5%; Fig. 2). Two samples immediately down ice from porphyry Cu-Mo mineralization in the Valley open pit and one sample in the southern part of the study area contain 3%–4% apatite. The two samples near the Valley pit also contain large numbers of chalcopyrite (2300 and 4600 grains per 10 kg of bulk material <2 mm) in the 0.25–0.50 mm,  $>3.2 \text{ g}\cdot\text{cm}^{-3}$  fraction and high Cu contents (987 and 1056 ppm) in the clay-sized fraction (<0.002 mm) of till (Plouffe et al., 2013a; Plouffe and Ferbey, 2015d).

Most till samples from the Gibraltar area (Fig. 3) lack apatite grains. However, five contain trace (<0.5%) apatite, four of which were collected northwest of the deposit, i.e. down-ice with respect to the glacial maximum ice flow. The fifth, from till overlying the Burgess Creek quartz diorite-tonalite stock, is 9 km to the northeast of the deposit. The paucity of apatite grains in the tills reflects low abundances in local bedrock (Mao et al., 2015), and makes it difficult to define down-ice dispersion from the mineralized or altered bedrock (Fig. 3). On the other hand, Cu and Mo concentrations in till clay fractions, and chalcopyrite grain abundances in till, are elevated near the Gibraltar deposit compared to tills derived from surrounding barren bedrock (Plouffe et al., 2011, 2013a; Plouffe and Ferbey,

2015a, d). The resulting amoeboid dispersion pattern may reflect the three directions of ice flow in the region (Plouffe and Ferbey, 2015d).

Hashmi et al. (2015) characterized the distribution of apatite grains in till of the Mount Polley mine area (Fig. 4). Although most of the till samples lack apatite or contain only trace amounts (<0.5%), some samples to the northwest (down-ice) of the Mount Polley deposit contain up to 3% apatite. Hashmi et al. (2015) suggested that tills with more abundant apatite were derived from the alteration zones associated with Mount Polley alkalic porphyry Cu-Au mineralization. Other indicator minerals (chalcopyrite, visible gold grains, and jarosite) are also dispersed northwest of the mineralized zones (Hashmi et al., 2015).

Tills at Woodjam contain only trace amounts (<0.5%) of apatite (Fig. 5). Similar to the Gibraltar region, the spatial distribution of apatite grains in till does not clearly define dispersion from known mineralized zones. The distribution of chalcopyrite and epidote grains in till and Cu concentrations in till clay fraction better indicate dispersion from the porphyry mineralization and alteration zones; grain counts and Cu values are elevated within 2 km of the mineralized zones compared to those farther away (Ferbey and Plouffe, 2014; Plouffe and Ferbey, 2015a, d).

### 6.2. Apatite chemistry

A total of 147 apatite grains, excluding the Durango and Madagascar apatites, were analyzed by EMPA (Table 3; see Appendix 2 in Rukhlov et al., 2016 for full analytical results). Of these grains, 138 were analyzed by LA-ICP-MS. A few grains were too small or thin for the LA-ICP-MS analysis. Results below detection limits (DL) were arbitrarily set to half of the DL value per element for plotting. Results <DL in the whole data set constitute 1% for Mg, La, Ce, Th, and U; 4% to 6% for V, As, and Ba; 8% to 9% for Zn, Rb, and Zr; 12% to 19% for Ti, Cu, and W; 45% for Mo; 59% for Nb; and 0% for the remaining elements. Results from abnormal spectra or below abnormally high detection limits for individual elements in some analyses are meaningless and therefore were discarded. Nulls (i.e. discarded values) due to poor results in the whole data set comprise 1% to 3% for Cu, Zn, Mo, Ba, Pb, and Th; 4% for Cl, 7% to 9% for Na, Si, As, and Rb; 14% to 21% for S, Fe, and Ti, and 0% for the rest of the elements.

#### 6.2.1. Major elements

Calcium, phosphorous, fluorine, and chlorine are the main constituents in calcium phosphate apatites with the general formula  $\text{Ca}_5(\text{PO}_4)_3(\text{F},\text{Cl},\text{OH})$  (Pan and Fleet, 2002; Hughes and Rakovan, 2015). Calcium occupies two distinct cation sites (M polyhedra) in the apatite structure: two 9-fold coordinated ( $\text{CaO}_9$ ) M1 and three 7-fold coordinated ( $\text{CaO}_6\text{X}_1$ ) M2 sites per half the unit cell, where  $\text{X} = \text{F}^-$ ,  $\text{Cl}^-$ ,  $\text{OH}^-$ ,  $\text{CO}_3^{2-}$ , and  $\text{O}^{2-}$  anions in columns along the edges of the unit cell. Phosphorous is in a third, tetrahedral ( $\text{PO}_4$ ) cation site (Hughes and Rakovan, 2015).

Table 3. EMPA and LA-ICP-MS data summary for apatite grains.

	Highland Valley till				Gibraltar till				Mount Polley till				Woodjam till				Woodjam SE Zone bedrock			
	Min	Max	Mean	N	Min	Max	Mean	N	Min	Max	Mean	N	Min	Max	Mean	N	Min	Max	Mean	N
<b>EMPA</b>																				
SiO <sub>2</sub> (wt%)	0.021	0.369	0.147	21	0.024	0.433	0.108	26	0.015	0.864	0.495	39	0.006	0.225	0.062	30	0.054	0.246	0.137	20
FeO (wt%)	0.007	0.261	0.069	21	0.009	0.265	0.074	27	0.001	0.204	0.066	39	0.002	0.219	0.065	39	0.010	0.142	0.072	21
CaO (wt%)	53.38	55.04	54.20	21	53.08	55.25	54.36	26	53.43	55.34	54.46	38	54.11	55.69	54.92	36	53.43	55.16	54.43	21
Na <sub>2</sub> O (wt%)	0.014	0.317	0.130	21	0.014	0.181	0.102	27	0.041	0.389	0.178	39	0.007	0.120	0.057	39	0.020	0.178	0.095	21
P <sub>2</sub> O <sub>5</sub> (wt%)	39.78	42.79	41.26	21	39.66	43.66	41.37	24	38.68	43.12	40.38	39	39.61	42.65	41.51	33	39.18	42.66	41.45	21
SO <sub>3</sub> (wt%)	0.046	0.471	0.183	21	0.020	0.318	0.127	27	0.267	1.115	0.783	39	0.005	0.215	0.075	39	0.046	0.307	0.127	21
F (wt%)	0.13	3.54	2.35	21	1.68	4.07	2.91	27	0.73	5.44	3.18	39	1.16	5.27	2.89	39	1.38	3.71	2.26	21
Cl (wt%)	0.056	1.642	0.283	18	0.010	0.156	0.050	22	0.011	1.121	0.300	38	0.003	0.905	0.176	26	0.222	0.894	0.503	21
<b>LA-ICP-MS</b>																				
Mg (ppm)	24	494	135	21	3.1	142	38	23	21	711	229	39	<3	240	67	34	41	253	168	21
Ti (ppm)	<0.2	4.8	1.2	18	0.03	15	1.2	22	0.17	7.9	1.8	36	0.04	32	2.2	28	<0.2	4.1	1.2	17
V (ppm)	1.3	93	14	21	0.06	57	8.5	23	<0.2	323	151	39	0.02	58	9.4	34	8.5	24	18	21
Mn (ppm)	518	8057	2999	21	45	6067	1973	23	275	1890	670	39	52	3332	622	34	768	1747	1392	21
Cu (ppm)	<0.2	94	5.6	20	<0.2	8.2	1.5	23	<0.2	10	1.5	38	<0.2	9.1	0.70	34	0.07	2.7	0.60	19
Zn (ppm)	0.02	3.4	0.80	20	0.03	3.2	0.55	23	<0.1	3.8	0.87	39	<0.1	21	1.4	34	<0.1	2.9	0.57	21
As (ppm)	<1	42	7.7	21	0.15	34	11	22	<1	158	30	38	0.37	1191	236	26	<1	42	18	20
Rb (ppm)	<0.01	0.26	0.079	21	0.0003	0.13	0.062	21	<0.01	0.71	0.16	34	<0.01	1.3	0.20	33	0.010	0.32	0.11	19
Sr (ppm)	179	563	335	21	158	5733	548	23	167	3640	1854	39	140	3440	485	34	139	298	258	21
Y (ppm)	270	2032	749	21	3.1	2051	899	23	129	848	550	39	12	1699	551	34	386	1617	986	21
Zr (ppm)	0.09	2.0	0.47	21	0.002	0.92	0.30	23	0.08	9.2	3.2	39	<0.02	1.1	0.13	34	<0.02	0.83	0.25	21
Nb (ppm)	<0.01	0.035	0.009	21	<0.01	0.033	0.010	23	<0.01	0.12	0.019	39	<0.01	0.14	0.014	34	<0.01	0.031	0.008	21
Mo (ppm)	0.012	0.36	0.071	21	<0.04	0.32	0.048	23	<0.04	0.62	0.15	38	<0.04	0.15	0.045	34	<0.04	0.69	0.11	19
Ba (ppm)	<0.1	5.9	1.1	20	<0.1	2.7	0.55	23	0.66	50	13	39	0.013	7.7	0.86	34	0.29	1.6	0.75	21
La (ppm)	59	1569	567	21	0.37	1084	300	23	0.77	1461	594	39	0.066	694	121	34	195	1006	551	21
Ce (ppm)	444	4524	1706	21	<1	3037	1059	23	2.9	2637	1206	39	<1	1533	296	34	533	2345	1337	21
Pr (ppm)	94	593	238	21	0.031	342	163	23	0.35	279	147	39	0.20	195	41	34	74	283	168	21
Nd (ppm)	402	2365	1012	21	0.34	1255	758	23	3.8	969	597	39	0.66	807	184	34	348	1111	691	21
Sm (ppm)	78	476	211	21	0.26	348	190	23	1.3	191	123	39	0.71	161	58	34	93	239	152	21
Eu (ppm)	8.1	44	19	21	0.084	119	20	23	0.37	48	30	39	0.13	45	10	34	9.3	18	12	21
Gd (ppm)	71	399	180	21	0.18	377	183	23	3.4	186	124	39	1.2	266	82	34	102	238	157	21

Table 3. Continued.

	Highland Valley till				Gibraltar till				Mount Polley till				Woodjam till				Woodjam SE Zone bedrock			
	Min	Max	Mean	N	Min	Max	Mean	N	Min	Max	Mean	N	Min	Max	Mean	N	Min	Max	Mean	N
Dy (ppm)	44	331	133	21	0.21	346	150	23	8.7	140	93	39	1.1	271	93	34	71	231	141	21
Yb (ppm)	16	244	57	21	0.65	147	63	23	14.3	66	34	39	0.58	158	40	34	25	155	83	21
Lu (ppm)	2.3	38	8.4	21	0.12	22	9.0	23	2.0	9.8	4.5	39	0.035	25	6.0	34	3.5	23	12	21
W (ppm)	0.007	0.36	0.12	21	0.032	1.2	0.33	23	0.0003	0.84	0.10	39	<0.02	4.5	0.47	34	<0.02	0.35	0.055	21
Pb (ppm)	0.9	2.5	1.5	21	0.14	20	5.4	23	1.1	25	2.8	39	0.20	47	8.3	34	0.37	4.6	1.8	20
Th (ppm)	1.0	80	15	21	<0.05	34	4.9	23	0.012	26	13	37	0.006	28	5.3	34	1.3	42	20	21
U (ppm)	1.9	55	11	21	0.095	23	5.8	23	0.090	16	5.5	39	0.024	26	7.4	34	2.8	25	11	21
Eu/Eu*	0.15	0.55	0.33	21	0.15	1.5	0.39	23	0.36	1.0	0.74	39	0.11	1.1	0.47	34	0.18	0.34	0.25	21
Ce/Ce*	1.0	1.5	1.2	21	0.98	1.6	1.2	23	0.89	1.4	1.0	39	0.23	3.8	1.2	34	1.0	1.2	1.1	21
(Ce/Yb) <sub>CN</sub>	1.3	27	14	21	0.027	17	5.1	23	0.024	16	10.2	39	0.006	47	5.9	34	2.6	14	5.0	21
(La/Sm) <sub>CN</sub>	0.22	3.7	1.8	21	0.031	4.0	1.0	23	0.36	5.2	3.0	39	0.058	6.0	1.3	34	1.3	3.6	2.3	21
(Gd/Yb) <sub>CN</sub>	0.85	5.2	3.5	21	0.23	13	2.7	23	0.086	4.4	3.2	39	0.014	39	3.8	34	1.2	3.5	1.7	21
∑LREE	596	6685	2511	21	1.0	4463	1522	23	4.0	4377	1947	39	1.6	2422	458	34	803	3633	2056	21
∑MREE	559	3264	1423	21	0.87	1974	1151	23	8.8	1352	874	39	2.7	1132	334	34	553	1549	1013	21
∑HREE	71	613	198	21	0.97	515	222	23	46	202	131	39	1.9	406	139	34	99	406	236	21
∑REE	1680	10322	4132	21	2.9	6052	2895	23	59	5932	2952	39	6.7	3697	932	34	1512	5519	3305	21

Footnote:

**EMPA** = electron microprobe analysis; **LA-ICP-MS** = laser ablation-inductively coupled plasma mass spectrometer analysis; **N** = total number of values; **wt.%** = weight per cent; **ppm** = parts per million.

$Ce/Ce^* = Ce_{CN}^*/(La_{CN}^*Pr_{CN}^*)^{0.5}$ ,  $Eu/Eu^* = Eu_{CN}^*/(Sm_{CN}^*Gd_{CN}^*)^{0.5}$ ; normalization (CN) values from Lodders (2010).

$\sum LREE = La + Ce + Pr$ ,  $\sum MREE = Nd + Sm + Eu + Gd$ ,  $\sum HREE = Dy + Yb + Lu$ ,  $\sum REE = Dy + Ce + Pr + Nd + Sm + Eu + Gd + Dy + Yb + Lu$ ; all totals are multivariate (i.e. all variables must be not null).

Apatite grains from till at Woodjam show slightly higher CaO contents (54.11–55.69 wt.%) than those in apatite grains from mineralized quartz monzonite at the Woodjam Southeast Zone and till at the Highland Valley, Gibraltar, and Mount Polley deposit areas, which contain 53.08–55.34 wt.% CaO (Table 3). Phosphorous contents in apatite grains from the Mount Polley area (38.68–43.12 wt.%  $P_2O_5$ ) are slightly lower than those of apatite grains from other areas (39.18–43.66 wt.%  $P_2O_5$ ) (Table 3). Bouzari et al. (2011b) attributed increased CaO contents (by ~1%) of apatites in altered rocks relative to those of pristine apatites in fresh rocks from porphyry Cu-Mo-Au deposits to the loss of minor and trace elements from apatite during hydrothermal alteration.

Accurate analysis of apatite by EMPA, particularly for F and Cl, is difficult due to anisotropy effects (Stormer et al., 1993; Raudsepp, 1995). About 14% of our apatite analyses (Appendix 2, Rukhlov et al., 2016) have F concentrations (up to 5.44 wt.%) in excess of the maximum F content of ~3.77 wt.% in end-member fluorapatite (Webster and Piccoli, 2015), indicating problematic EMPA analyses, or excess F bound to  $CO_3^{2-}$  (Piccoli and Candela, 2002). Without measured  $CO_3^{2-}$ , we made no attempt to calculate the concentration of F bound to the assumed carbonate anion. Furthermore, relatively high EMPA detection limit (0.85 wt.%) and poor precision (34–38% at 2 $\sigma$  level) render the F results largely semi-quantitative compared with more precise data for other elements. Precision for Cl (14–33% at 2 $\sigma$  level) is generally better and the detection limit is lower (~0.03 wt.%) than those for F (see Appendices 1 and 3, Rukhlov et al., 2016).

Figure 7a shows F-Cl-OH variability in the halogen-site of the examined apatite grains. The mole fractions of fluor-, chlor- and hydroxylapatite end members were calculated directly from the measured F and Cl concentrations, assuming that F<sup>-</sup>, Cl<sup>-</sup>, and OH<sup>-</sup> fill the X-site and that  $CO_3^{2-}$ ,  $O^{2-}$ , other anions, and vacancies in this site are not significant. For discussion of the methods to calculate the mole fractions in apatite, we refer the reader to Piccoli and Candela (2002). Apatite grains in this study contain between 3.4–100 mol% F, 0–73 mol% OH, and <24 mol% Cl, indicating mainly F–OH exchange (Fig. 7a), partly due to the similarity in radius for F<sup>-</sup> and OH<sup>-</sup> as compared to Cl<sup>-</sup> (Piccoli and Candela, 2002; Kusebauch et al., 2015). Most of the apatite grains show molar F/Cl ratios of >1, except for one apatite grain from till in the eastern part of the Highland Valley area (sample 12PMA515A01) with 1.64 wt.% Cl and 0.13 wt.% F (Fig. 7a; Table 3). Apatite grains from the Gibraltar deposit area and most apatite grains at Highland Valley, Woodjam and Mount Polley contain <0.32 wt.% Cl. However, some apatite grains at Woodjam (from Southeast Zone mineralized quartz monzonite and till sample 11PMA017A01) and Mount Polley (mainly from till sample 13PMA521A01) have generally higher Cl contents, ranging from 0.17 to 1.12 wt.% (Table 3; Fig. 7a).

### 6.2.2. Minor and trace elements

Calcium phosphate apatite structure can incorporate most

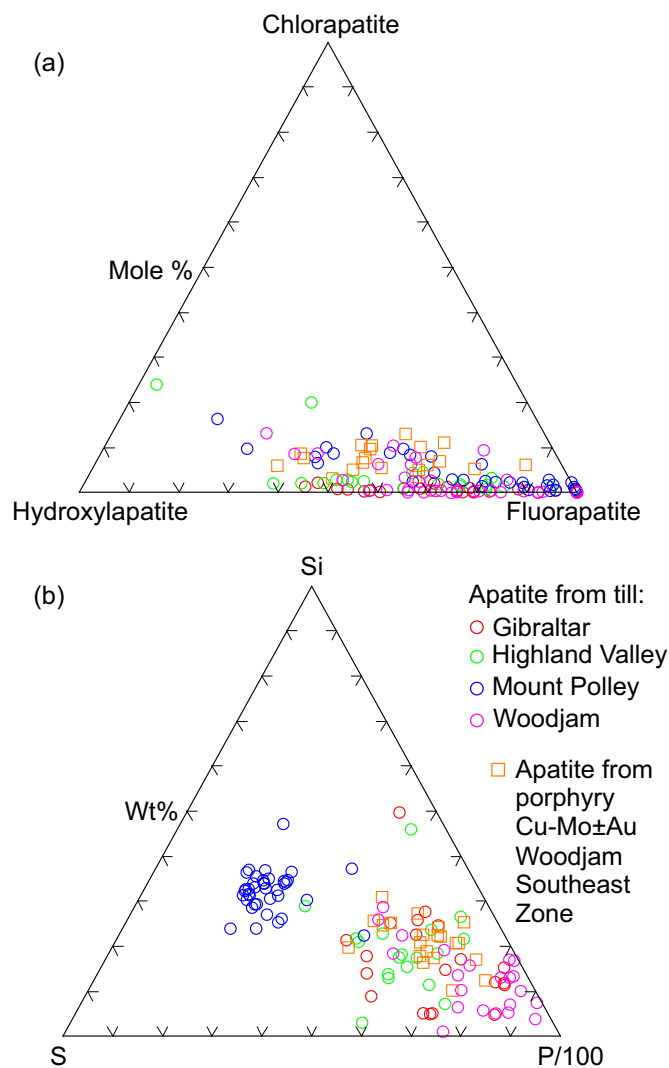


**Fig. 7.** Ternary plots for apatite. **a)** Fluorapatite-Chlorapatite-Hydroxylapatite recast as mole fractions so that F, Cl, and OH fill the halogen-site in apatite;  $X_F^{Ap}$  (fluorapatite mole fraction) =  $C_F^{Ap}/3.767$ ,  $X_{Cl}^{Ap}$  (chlorapatite mole fraction) =  $C_{Cl}^{Ap}/6.809$ ,  $X_{OH}^{Ap}$  (hydroxylapatite mole fraction) =  $1 - X_F^{Ap} - X_{Cl}^{Ap}$ , where  $C_F^{Ap}$  = F concentration in wt.% in apatite,  $C_{Cl}^{Ap}$  = Cl concentration in wt.% in apatite (after Piccoli and Candela, 2002); for a few analyses with  $(X_F^{Ap} + X_{Cl}^{Ap}) > 1$ , the fluorapatite and chlorapatite mole fractions were normalized to unity. **b)** P/100-Si-S cations (in wt.%) in the tetrahedral site.

elements in minor or trace amounts. The tetrahedral site occupied by  $P^{5+}$  can incorporate  $Si^{4+}$  and redox-sensitive  $As^{5+}$ ,  $V^{5+}$ , and  $S^{6+}$  (Pan and Fleet, 2002; Hughes and Rakovan, 2015). The M1 and M2 polyhedra in the apatite structure can accommodate substitution by many divalent cations (e.g., Mg, Mn, Fe, Cu, Zn, Sr, Ba, and Pb), with many substituents showing a strong site preference (e.g., Sr for M2 site, whereas Mn for M1 site; Pan and Fleet, 2002; Hughes and Rakovan, 2015). Because  $Mn^{2+}$  substitutes directly for  $Ca^{2+}$  due to similarities in charge and ionic radius, apatite incorporates  $Mn^{2+}$  in preference to  $Mn^{3+}$  or  $Mn^{4+}$  (Marshall, 1988; Pan and Fleet, 2002). Therefore, elevated Mn contents in apatite may reflect high  $Mn^{2+}/Mn$  in

a reduced magma, or low abundances of other Mn-bearing phases such as biotite, amphibole, and magnetite in highly fractionated, felsic magmas, which forces Mn substitution into apatite (Sha and Chappell, 1999; Belousova et al., 2002; Piccoli and Candela, 2002; Miles et al., 2014). Trivalent rare-earth elements (REE) and Y, and tetravalent U and Th substitute in the M1 and M2 sites via coupled substitution reactions to maintain charge balance (e.g.,  $\text{Na}^+ + \text{REE}^{3+} \leftrightarrow 2\text{Ca}^{2+}$  and  $\text{Si}^{4+} + \text{REE}^{3+} \leftrightarrow \text{P}^{5+} + \text{Ca}^{2+}$ ; Rønsbo, 1989; Pan and Fleet, 2002; Hughes and Rakovan, 2015). Light REEs (LREE) prefer the M2 site, whereas heavy REEs (HREE) prefer the M1 site, and the middle REEs (MREE), with ionic radii close to that of Nd, show no site preference (Hughes and Rakovan, 2015).

Unlike other REEs, Ce and Eu can exist in two valency states ( $\text{Ce}^{3+}$  and  $\text{Ce}^{4+}$  and  $\text{Eu}^{2+}$  and  $\text{Eu}^{3+}$ ) due to redox sensitivity and thus behave differently than adjacent REEs (Roeder et al., 1987; Smythe and Brenan, 2015). Because apatite structure shows strong preference for  $\text{Eu}^{3+}$  relative to  $\text{Eu}^{2+}$  (Prowatke and Klemme, 2006; Cao et al., 2012), the lack of significant depletions in Eu relative to adjacent REEs or ‘Eu anomalies’ (quantified as  $\text{Eu}/\text{Eu}^* = \text{Eu}_{\text{CN}}/(\text{Sm}_{\text{CN}} \cdot \text{Gd}_{\text{CN}})^{0.5}$  using chondrite normalization, Lodders, 2010) may indicate low  $\text{Eu}^{2+}/\text{Eu}^{3+}$  in oxidized magmas, or early crystallization of feldspars, which preferentially incorporate  $\text{Eu}^{2+}$  (Budzinski and Tischendorf, 1989; Sha and Chappell, 1999; Belousova et al., 2002; Piccoli and Candela, 2002; Tollari et al., 2008; Miles et al., 2014). Likewise, because  $\text{Ce}^{3+}$  is more compatible in apatite than  $\text{Ce}^{4+}$  (Miles et al., 2014), enrichments in Ce relative to the adjacent REEs or ‘Ce anomalies’ ( $\text{Ce}/\text{Ce}^* = \text{Ce}_{\text{CN}}/(\text{La}_{\text{CN}} \cdot \text{Pr}_{\text{CN}})^{0.5}$  using chondrite normalization, Lodders 2010) may reflect high  $\text{Ce}^{3+}/\text{Ce}^{4+}$  in reduced magmas. Unlike Eu anomalies, Ce anomalies are insensitive to feldspar fractionation. However,  $\text{Ce}/\text{Ce}^*$  variations in apatite also may result from partitioning of Ce in other accessory phases such as monazite, fluorite and zircon, that in turn partly reflects redox conditions (Ballard et al., 2002; Belousova et al., 2002; Piccoli and Candela, 2002; Colombini et al., 2011; Miles et al., 2014).

The relationships between Si, S and P, with a median atomic Si/S ratio of about 1.0, in the analyzed apatite grains (Fig. 7b) suggest the substitution  $\text{Si}^{4+} + \text{S}^{6+} \leftrightarrow 2\text{P}^{5+}$  (Harada et al., 1971; Piccoli and Candela, 2002). A weak positive correlation also exists between Na and S contents (correlation coefficient = 0.62) of the examined apatite grains, suggesting the coupled substitution reaction  $\text{S}^{6+} + \text{Na}^+ \leftrightarrow \text{P}^{5+} + \text{Ca}^{2+}$  (Kreidler and Hummel, 1970), although apparently less significant than the Si-S-P substitution. Both  $\text{SiO}_4^{4-}$  and  $\text{Na}^+$  can be incorporated in the apatite structure as charge compensators via the coupled substitutions of  $\text{REE}^{3+}$  and  $\text{Y}^{3+}$  for  $\text{Ca}^{2+}$  (Rønsbo, 1989; Sha and Chappell, 1999; Pan and Fleet, 2002; Hughes and Rakovan, 2015), and can be removed out of the apatite-fluid system in preference to REEs during metasomatic alteration of apatite by a Na- and Si-poor fluid such as  $\text{H}_2\text{O} \pm \text{CO}_2$ , HCl,  $\text{H}_2\text{SO}_4$ , or KCl brine (Harlov, 2015). Sulfur substitution for P in apatite is redox sensitive, readily incorporating  $\text{S}^{6+}$  in oxidizing conditions, unlike sulfide-bound  $\text{S}^{2-}$  in reducing conditions

(Sha and Chappell, 1999; Piccoli and Candela, 2002; Webster and Piccoli, 2015).

Spider diagrams (Fig. 8) show minor- and trace-element compositions of analyzed apatite grains normalized to the average apatite composition of Mao et al. (2015). Figure 9 provides chondrite-normalized REE profiles for these apatite grains. Figures 8 and 9 also show average apatite compositions from porphyry deposits after Mao et al. (2015). The distribution of minor and trace elements and the chondrite-normalized REE profiles, characterized by a relative enrichment in LREEs with  $(\text{Ce}/\text{Yb})_{\text{CN}} < 47$ ,  $(\text{La}/\text{Sm})_{\text{CN}} < 6.0$ , and  $(\text{Gd}/\text{Yb})_{\text{CN}} < 5.2$ , strong to weak negative Eu anomalies ( $\text{Eu}/\text{Eu}^* = 0.11\text{--}0.87$ ), and lack of significant Ce anomalies ( $\text{Ce}/\text{Ce}^* = 0.89\text{--}1.30$ ), for most of the analyzed apatite grains (Figs. 8 and 9; Table 3) are consistent with the findings of Mao et al. (2015) on apatites from porphyry deposits. Trace-element abundances of apatites at Woodjam cover much wider range of values (up to 4 orders of magnitude) than those from the Highland Valley, Gibraltar and Mount Polley (Figs. 8 and 9).

Apatite grains from mineralized bedrock at the Woodjam Southeast Zone show Si, S, Mn, V, and other trace-element abundances and the chondrite-normalized REE patterns typical of apatites from the calc-alkaline porphyry  $\text{Cu} \pm \text{Mo} \pm \text{Au}$  deposits studied by Mao et al. (2015). However, apatite grains from till at Woodjam display much wider variations in trace-element composition, ranging from concentration levels similar to those in Southeast Zone bedrock, with the LREE-enriched chondrite-normalized REE patterns, to less than detection limit for most trace elements, with LREE-depleted chondrite-normalized REE patterns (Figs. 8d and 9d; Table 3). A few apatite grains at Highland Valley, Gibraltar and Mount Polley also show similar LREE-depleted chondrite-normalized REE patterns (Figs. 9a-c), coupled with depletions in Na, Mg, Si, S, Cl, V, Mn, As, Y, Zr, Ba, Th and U (Figs. 8a-c), which are distinct from the average apatite compositions from these deposits as reported by Mao et al. (2015). These depletions probably reflect hydrothermal alteration, which is extensive near the Woodjam mineralized zones (Schiarrizza et al., 2009a; del Real et al., 2014; Vandekerckhove et al., 2014) and resulted in metasomatic removal of S, Cl and many trace elements, with LREEs in preference to HREEs and Y, from primary apatite (e.g., Harlov, 2015). The metasomatic removal of LREEs from these apatite grains also resulted in the extreme variations in their  $\text{Ce}/\text{Ce}^*$  (0.23–3.8) and elevated  $\text{Eu}/\text{Eu}^*$  (up to 1.5) (Fig. 9; Table 3). Bouzari et al. (2011b) also attributed a decrease in  $\text{Na}_2\text{O}$ ,  $\text{SiO}_2$ ,  $\text{SO}_3$ , Cl, and MnO contents and MnO/FeO of apatites in altered rocks relative to those of apatite in fresh rocks from several porphyry Cu-Mo-Au deposits to the metasomatic removal of these elements from primary apatite. Below we summarize some of the characteristic trace-element features of apatite grains from the four porphyry deposit areas.

Apatite grains from all four study areas have similar FeO contents (from <0.09 to 0.27 wt.%) and most have similar levels of Cu (<10 ppm) and Zn (<3.8 ppm), except for one grain from till sample 11PMA017A01 at Woodjam (21 ppm Zn) and one

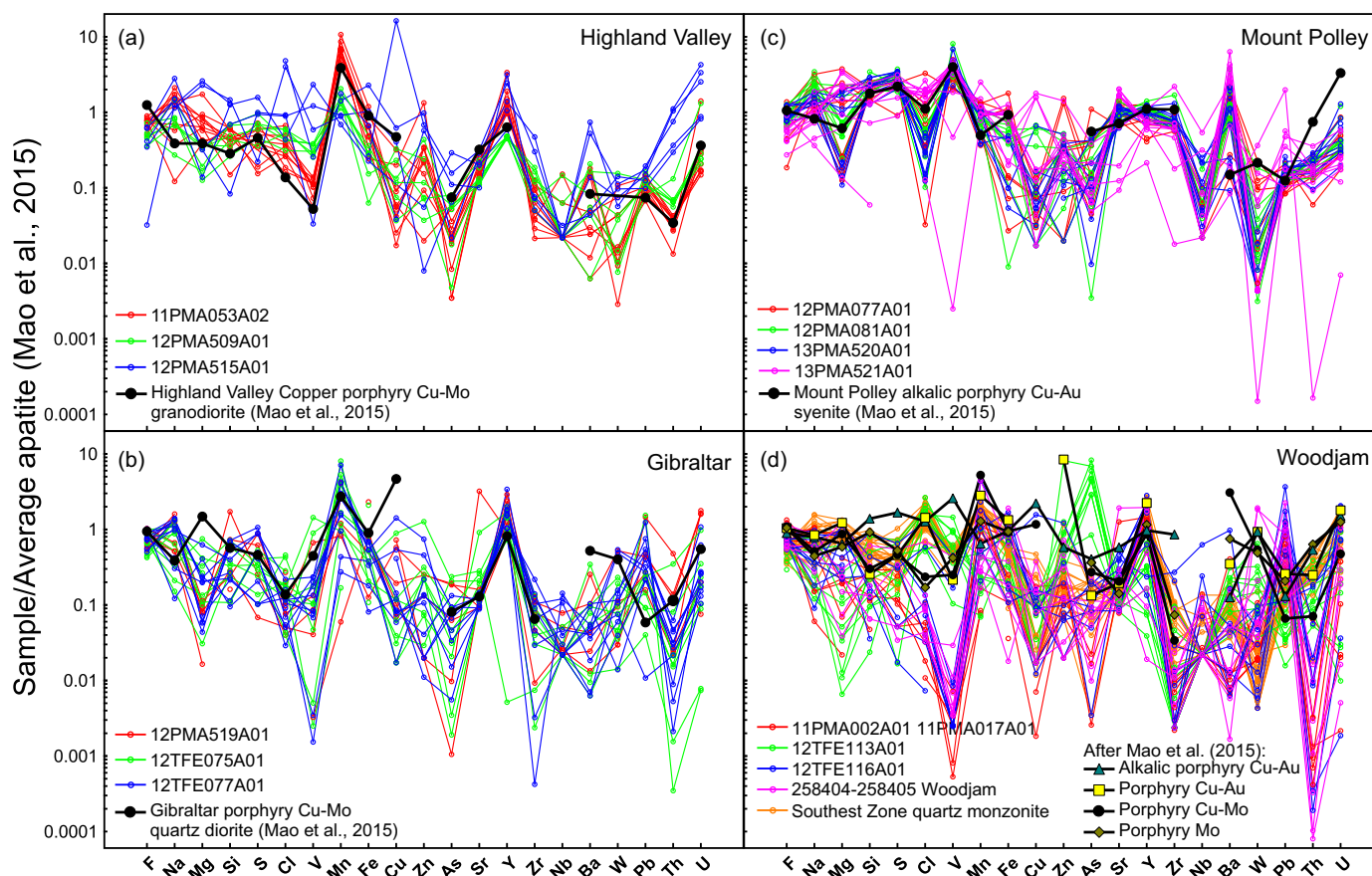


**Fig. 8.** Spider diagrams for apatite grains normalized to the average apatite of Mao et al. (2015). **a)** Highland Valley porphyry district. Average apatite from mineralized granodiorite, Highland Valley Copper calc-alkaline porphyry Cu-Mo deposit (after Mao et al., 2015) is shown for comparison. **b)** Gibraltar mine area. Average apatite from mineralized quartz diorite, Gibraltar calc-alkaline porphyry Cu-Mo deposit (after Mao et al., 2015) is shown for comparison. **c)** Mount Polley mine area. Average apatite from mineralized syenite, Mount Polley alkalic porphyry Cu-Au deposit (after Mao et al., 2015) is shown for comparison. **d)** Woodjam developed prospect area. Average apatite compositions for alkaalic porphyry Cu-Au and calc-alkaline porphyry Cu-Mo, and porphyry Mo deposits (after Mao et al., 2015) are shown for comparison.

from till sample 12PMA515A01 at Highland Valley (94 ppm Cu; Table 3). Apatite grains from Mount Polley have higher Ti contents (0.17–7.9 ppm) and those from Gibraltar have lower Ti (0.03–2.3 ppm) relative to other apatites in this study, except for one grain from Gibraltar (till sample 12TFE075A01) with 15 ppm Ti and one from Woodjam (sample 12TFE113A01) with 32 ppm Ti. Tungsten concentrations are higher in apatite grains from till at Gibraltar (up to 1.2 ppm W) and Woodjam (up to 4.5 ppm W) than those of other studied grains. Average Rb contents in apatite in till from Mount Polley (0.16 ppm) and Woodjam (0.20 ppm) are similar, and higher than those of apatite grains from bedrock at the Woodjam Southeast Zone and from till at the Highland Valley and Gibraltar deposits (Table 3). Only ~30% of the analyzed apatite grains have detectable Nb > 0.01 ppm (up to 0.14 ppm), and ~47% of the apatite grains have detectable Mo > 0.04 ppm (up to 0.69 ppm; Appendix 2, Rukhlov et al., 2016).

The trace-element chemistry of apatite grains from the Mount Polley deposit area is distinct relative to other apatite grains examined here. At Mount Polley (Fig. 7b; Table 3), apatite

grains contain much higher  $\text{SO}_3$  (mostly 0.56–1.12 wt.%) and  $\text{SiO}_2$  (mostly 0.32–0.86 wt.%) than those from other deposit areas (<0.47 wt.%  $\text{SO}_3$  and <0.43 wt.%  $\text{SiO}_2$ ), in agreement with the findings of Bouzari et al. (2011b). Most have higher  $\text{Na}_2\text{O}$  (0.04–0.39 wt.%), Sr (1107–3640 ppm), Mg (21–711 ppm), V (80–323 ppm), Ba (0.7–50 ppm), Zr (1.9–9.2 ppm), Mo (up to 0.62 ppm), Nb (up to 0.12 ppm), and low Mn (275–1890 ppm), Y (129–848 ppm), and total HREE ( $\sum\text{HREE} = \text{Dy} + \text{Yb} + \text{Lu}$ ; 46–202 ppm) contents relative to those from other areas (Table 3). Bouzari et al. (2011b) also reported MnO abundances below EMPA detection limit (~0.15 wt.% MnO) for most of apatites in rocks from the Mount Polley deposit. Their chondrite-normalized REE patterns show higher LREE/MREE, with  $(\text{La}/\text{Sm})_{\text{CN}}$  ranging mostly from 2.0 to 5.2, much higher  $\text{Eu}/\text{Eu}^*$  (mostly 0.50–0.99), and lower  $\text{Ce}/\text{Ce}^*$  (mostly 0.89–1.03; Fig. 9; Table 3). Apatite grains from the Mount Polley deposit area also have higher As contents (mostly 5.5–158 ppm) compared with others analyzed here, except for those with anomalously high As from till sample 11PMA017A01 at Woodjam (Fig. 8; Table 3). Three apatite grains at Mount Polley (all from sample

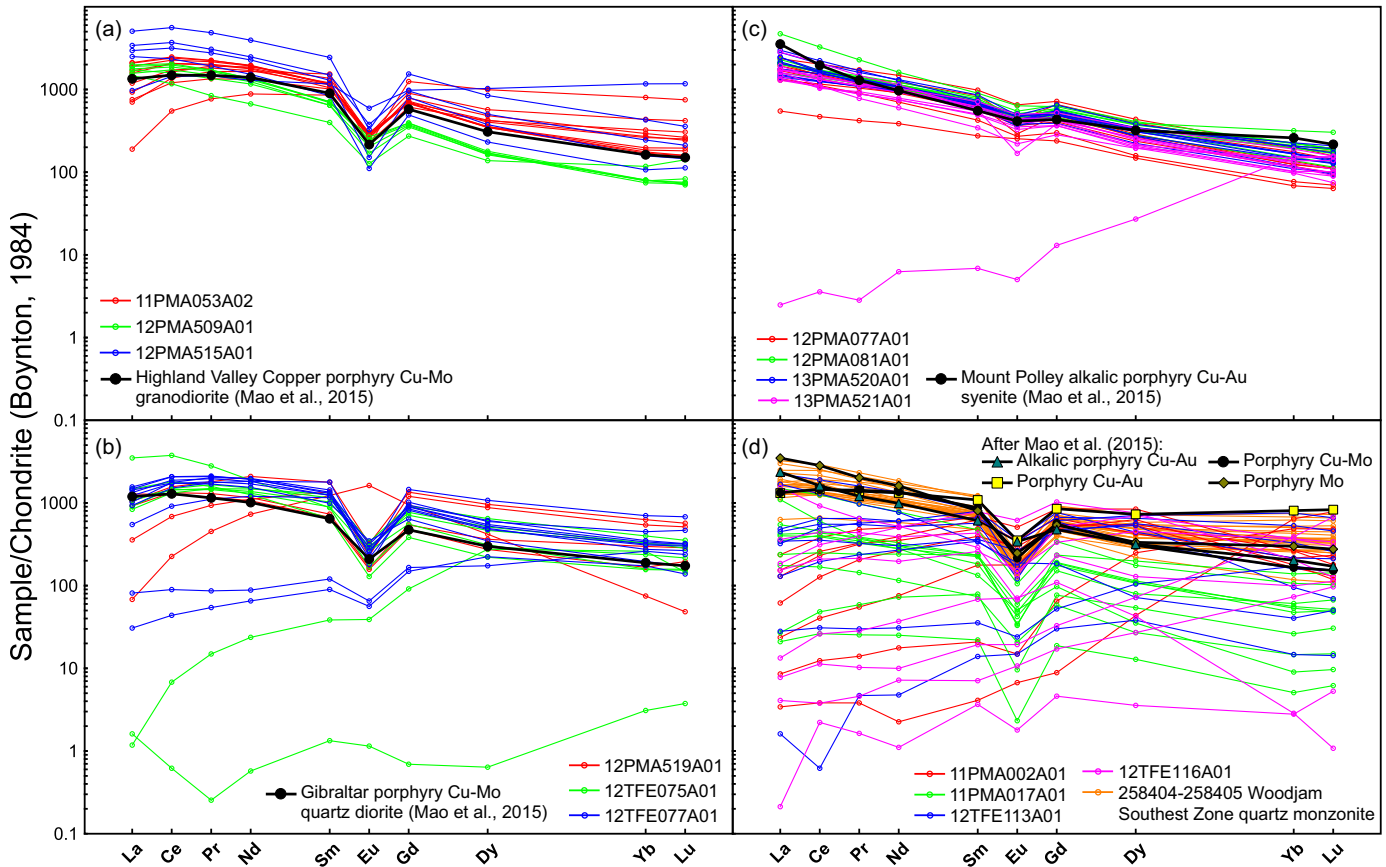


**Fig. 9.** Chondrite-normalized rare earth element plots for apatite grains, using normalization of Boynton (1984). **a)** Highland Valley porphyry district. Average apatite from mineralized granodiorite, Highland Valley Copper calc-alkaline porphyry Cu-Mo deposit (after Mao et al., 2015) is shown for comparison. **b)** Gibraltar mine area. Average apatite from mineralized quartz diorite, Gibraltar calc-alkaline porphyry Cu-Mo deposit (after Mao et al., 2015) is shown for comparison. **c)** Mount Polley mine area. Average apatite from mineralized syenite, Mount Polley alkalic porphyry Cu-Au deposit (after Mao et al., 2015) is shown for comparison. **d)** Woodjam developed prospect area. Average apatite compositions for alkalic porphyry Cu-Au and calc-alkaline porphyry Cu-Au, porphyry Cu-Mo, and porphyry Mo deposits (after Mao et al., 2015) are shown for comparison.

13PMA521A01) with much lower Sr (167–350 ppm) and V (<73.5 ppm), including two grains with low Zr (<0.75 ppm) and one grain with low LREE/HREE (e.g.,  $(\text{Ce}/\text{Yb})_{\text{CN}} = 0.02$ ;  $(\text{La}/\text{Sm})_{\text{CN}} = 0.36$ ), low Eu/Eu\* of 0.36, and high Ce/Ce\* of 1.4, were likely metasomatically altered. The lack of significant Eu anomalies, coupled with the elevated S, V, and As but low Mn contents and low Ce/Ce\* values, of apatite grains at Mount Polley relative to those from other deposit areas are indicative of the highly oxidized nature of the magmatic-hydrothermal systems that form alkalic porphyry Cu-Au deposits (e.g., Lang et al., 1995; Mao et al., 2015).

Apatite grains from till at the Highland Valley and Gibraltar calc-alkaline porphyry Cu-Mo deposits are distinguished by their much higher Mn (mostly 518–8057 ppm) and total MREE ( $\sum\text{MREE} = \text{Nd} + \text{Sm} + \text{Eu} + \text{Gd}$ ; mostly 559–3264 ppm) contents, higher Ce/Ce\* values (0.98–1.30), and by lower As contents (<1–42 ppm) relative to those from other porphyry deposit areas in this study (Figs. 8 and 9; Table 3). Notably, all apatite grains from till sample 11PMA053A02, immediately down-ice from the Highland Valley Copper deposit (Fig. 2), have the highest Mn concentrations, ranging from 3635 to 8057

ppm, in agreement with the range of values (334–10934 ppm Mn) reported by Bouzari et al. (2011b) and Mao et al. (2015) for apatites in the ore rocks at the Highland Valley porphyry Cu-Mo deposits. Compared to apatite from the Gibraltar deposit area, most grains at Highland Valley have higher  $\text{Na}_2\text{O}$  (0.01–0.32 wt.%), Mg (24–494 ppm), and  $(\text{Ce}/\text{Yb})_{\text{CN}}$  (1.3–27), and lower Nb (<0.03 ppm) and Pb (<2.5 ppm) contents. In addition, apatite grains from till near the eastern margin of the Guichon Creek batholith (sample 12PMA515A01; Fig. 2), have the highest total REE ( $\sum\text{REE} = \text{La} + \text{Ce} + \text{Pr} + \text{Nd} + \text{Sm} + \text{Eu} + \text{Gd} + \text{Dy} + \text{Yb} + \text{Lu}$ ; 3555–10322 ppm), Th (21–80 ppm), and U (10–55 ppm) contents (Table 3).

For the Woodjam deposits and prospects, apatite grains from till sample 11PMA017A01 contain the highest As concentrations (121–1191 ppm; Fig. 8d; Table 3). Mao et al. (2015) attributed high As contents in some hydrothermal ore deposits (e.g., Kiruna-type) to sedimentary sources that had accumulated As. Because the till sample with As-rich apatite grains overlies volcano-sedimentary Nicola Group rocks in contact with the Takomkane batholith, the elevated values may record precipitation from melt or hydrothermal fluid that

scavenged As from the Nicola Group. Apatite grains from till at Woodjam have generally lower Zr contents (average 0.13 ppm) than those from the Southeast Zone mineralized rocks (average 0.25 ppm Zr). Compared to grains from other areas, apatite from till at Woodjam have highly variable abundances of trace elements, with generally high Pb (0.2–47 ppm) and Rb (up to 1.3 ppm) contents, and the low  $\text{SO}_3$  (<0.22 wt.%),  $\text{SiO}_2$  (<0.23 wt.%),  $\text{Na}_2\text{O}$  (<0.17 wt.%), V (<58 ppm), and  $\Sigma\text{REE}$  (<3697 ppm) contents (Figs. 8d and 9d; Table 3). These apatites cover the widest range of  $(\text{Ce}/\text{Yb})_{\text{CN}}$  (<0.01–47),  $(\text{La}/\text{Sm})_{\text{CN}}$  (0.06–6.0),  $(\text{Gd}/\text{Yb})_{\text{CN}}$  (0.01–39),  $\text{Ce}/\text{Ce}^*$  (0.23–3.8), and  $\text{Eu}/\text{Eu}^*$  (0.11–1.11) in this study (Fig. 9d; Table 3), probably reflecting the loss of LREE in preference to HREE due to the extensive hydrothermal alteration in the Woodjam area (Schiarrizza et al., 2009a; del Real et al., 2014; Vandekerckhove et al., 2014). In contrast, concentrations of most trace elements in apatite grains from mineralized quartz monzonites at the Woodjam Southeast Zone show a more restricted range, with generally higher abundances than those from till at Woodjam, except for As, Sr, and Pb (Table 3; Figs. 8d and 9d). Compared to apatite grains from the Highland Valley and Gibraltar deposit areas, those from mineralized rocks at the Woodjam Southeast Zone show more restricted range of Mn (768–1747 ppm), V (mostly 15–24 ppm), Y (mostly 595–1617 ppm),  $(\text{Ce}/\text{Yb})_{\text{CN}}$  (2.6–14),  $(\text{Gd}/\text{Yb})_{\text{CN}}$  (1.2–3.5),  $\text{Ce}/\text{Ce}^*$  (1.00–1.18), and  $\text{Eu}/\text{Eu}^*$  (0.18–0.34) values (Table 3). These grains also have higher Mg (mostly 117–253 ppm), As (mostly 5.7–42 ppm), Mo (mostly 0.05–0.69 ppm), Th (mostly 9.6–42 ppm), U (2.8–25 ppm), and  $(\text{La}/\text{Sm})_{\text{CN}}$  (1.3–3.7), and lower W (<0.36 ppm) and MREE (559–1549 ppm) values relative to those at Highland Valley and Gibraltar (Table 3). The strong negative Eu anomalies, coupled with low S, V, As but high Mn contents and higher  $\text{Ce}/\text{Ce}^*$  values, of apatite grains from Highland Valley, Gibraltar, and Woodjam are opposite to those from Mount Polley and characterize the less oxidized magmas and fluids that form typical calc-alkaline porphyry  $\text{Cu}\pm\text{Mo}\pm\text{Au}$  deposits (Mao et al., 2015).

## 7. Discussion

### 7.1. Apatite as a proxy for fluid composition in magmatic-hydrothermal systems

Apatite in most igneous rocks is commonly F-rich, whereas high-Cl apatites are found in some magmatic-hydrothermal ore systems and may record metasomatic alteration of primary fluorapatite in mafic and mantle rocks (Roegge et al., 1974; Piccoli and Candela, 2002; Patiño Douce et al., 2011; Harlov, 2015; Webster and Piccoli, 2015). Variations in relative abundances of halogens and OH in apatite reflect the behaviour of these volatiles during magma-fluid evolution (Boyce and Hervig, 2009) and depend on many factors, including the melt and/or fluid composition, P-T conditions, and the presence of other halogen-bearing phases (Harlov, 2015; Kusebauch et al., 2015). Experimental evidence also suggests that OH is more compatible than Cl in apatite regardless of the Cl concentration in the hydrothermal fluid (Kusebauch et al., 2015). Webster and Piccoli (2015) found that Cl partitioning between apatite and

melt depends on both Cl content in coexisting fluid and pressure. For example, in rhyolitic melts at a temperature range of 850–950°C, Cl becomes more compatible in apatite as pressure decreases from 2000 to 275 bars (Webster and Piccoli, 2015). The Cl/F ratio in apatite decreases with decreasing temperature and as a result of volatile exsolution, which lowers  $\text{H}_2\text{O}/\text{F}$  and Cl/F ratios in the melt due to preferential partitioning of Cl into a fluid relative to F (Webster, 1990; Piccoli and Candela, 2002; Kusebauch et al., 2015). Assuming ideal mixing of F, Cl, and OH in apatite and that  $\text{CO}_3^{2-}$ ,  $\text{O}^{2-}$ , other anions, and vacancies in the X site are insignificant, the calculated molar Cl/OH ratios in the studied apatite grains suggest up to 0.15 m HCl in the aqueous vapour in equilibrium with these apatites and host melts at a  $T = 800^\circ\text{C}$  and a  $P = 1000$  bars, using a technique after Piccoli and Candela (2002). At a higher temperature of  $1000^\circ\text{C}$ , the vapour phase would contain up to 0.36 m HCl. However, recent studies have shown that mixing of halogens in apatite is nonideal, with anion substitutions resulting in significant changes in the apatite structure, especially in the M2 polyhedra (Hughes and Rakovan, 2015; Webster and Piccoli, 2015). Nevertheless, the calculated molar Cl/OH ratios in the examined apatite grains agree with those of apatites from some of the producing porphyry deposits elsewhere (e.g., Yerrington, Nevada; Bingham, Utah; Henderson, Colorado; Piccoli and Candela, 2002 and references therein).

### 7.2. Redox and other controls on apatite trace-element chemistry

Sulfur, vanadium, manganese, arsenic, cerium and europium exist in variable oxidation states and substitute significantly in apatite. Under oxidizing conditions, some S is present as  $\text{SO}_4^{2-}$ , which can easily substitute for  $\text{PO}_4^{3-}$  in apatite, whereas under reducing conditions, S mainly occurs as  $\text{S}^{2-}$ , which forms sulfides (Sha and Chappell, 1999; Piccoli and Candela, 2002). Similarly, under oxidizing conditions, As and V readily substitute for  $\text{PO}_4^{3-}$  as  $\text{AsO}_4^{3-}$  and  $\text{VO}_4^{3-}$  in the presence of  $\text{As}^{5+}$  and  $\text{V}^{5+}$ . In contrast, under more reducing conditions,  $\text{As}^{3+}$  crystallizes as (arseno)sulfide and  $\text{V}^{3+}$  enters Fe-Mg minerals (Kutoglu, 1974; Sha and Chappell, 1999). Experiments on S partitioning between apatite and trachyandesitic and rhyolitic melts have determined that S partitions preferentially into apatite relative to melt with increasing oxygen fugacity and with decreasing pressure and S abundances in the melt (Piccoli and Candela, 2002; Webster and Piccoli, 2015 and references therein). Peng et al. (1997) found that S concentrations of apatite in intermediate rocks increase dramatically as a function of oxygen fugacity from <0.04 wt.%  $\text{SO}_3$  in reducing conditions (quartz-fayalite-magnetite, QFM) up to 2.6 wt.%  $\text{SO}_3$  in oxidizing conditions (magnetite-hematite, MH). Therefore, the elevated  $\text{SO}_3$ , V, and As abundances in apatite grains from the Mount Polley alkalic porphyry Cu-Au deposit area suggest crystallization in an oxidizing magmatic-hydrothermal system. In contrast, the much lower concentrations of these elements in apatite grains at the Highland Valley, Gibraltar and Woodjam deposits likely reflect the somewhat less oxidizing conditions

that are typical of the calc-alkaline porphyry Cu-Mo±Au systems, consistent with the findings of Mao et al. (2015) on bedrock apatites from porphyry deposits. In addition, zoned apatites with sulfur-rich core mantled by sulfur-poor rim, documented at the Mount Polley and Galore Creek porphyry Cu-Au deposits, may indicate SO<sub>3</sub> depletion in the evolved host magma due to anhydrite precipitation (Bath et al., 2006; Liaghat and Tosdal, 2008).

Manganese exchange in apatite differs from that of S, V and As. Because Mn<sup>2+</sup> substitutes for Ca in apatite more readily than Mn<sup>3+</sup> or Mn<sup>4+</sup>, which favour Fe-Mg minerals (Marshall, 1998; Pan and Fleet, 2002), elevated Mn abundances in apatite may reflect not only the degree of magma fractionation (i.e. the lack of abundant Fe-Mg phases in highly fractionated, felsic melt) but also higher Mn<sup>2+</sup>/Mn in reducing conditions (Sha and Chappell, 1999; Belousova et al., 2002; Piccoli and Candela, 2002; Miles et al., 2014). Because Sr abundance in apatite is a function of whole-rock Sr, it reflects the degree of magma fractionation (Sha and Chappell, 1999; Belousova et al., 2002; Piccoli and Candela, 2002). Early fractionation of Fe-Mg minerals results in low Mg contents in apatite, whereas hydrothermal apatites may inherit high Mg contents from the breakdown of Mg-rich primary minerals (Mao et al., 2015). A weak positive correlation between Sr and Mg contents in the studied apatites (correlation coefficient = 0.41) suggests fractionation of both plagioclase and Fe-Mg minerals. Although apatite grains at Mount Polley contain much higher Sr and Mg than those from the other deposit areas, relatively poor negative correlation between Sr and Mn in the analyzed apatites (correlation coefficient = -0.29), therefore, suggests that variations in their Mn abundances mainly reflect redox control (Sha and Chappell, 1999; Belousova et al., 2002; Piccoli and Candela, 2002; Miles et al., 2014). The lower Mn contents of apatite grains from Mount Polley relative to those from Highland Valley, Gibraltar and Woodjam, in agreement with the findings of Bouzari et al. (2011b), are consistent with the more oxidized state of the former alkalic porphyry Cu-Au deposit relative to the calc-alkaline porphyry Cu-Mo±Au systems. Using empirical relationship between oxygen fugacity ( $f_{O_2}$ ) and Mn contents in apatite from andesitic to rhyolitic melts for a range of temperatures (920–660°C) after Miles et al. (2014), apatite grains in till at Mount Polley indicate an average  $\log f_{O_2} = -11.2 \pm 0.5$  (calibration error), in agreement with the average  $\log f_{O_2}$  of  $-10.6 \pm 0.5$  for bedrock apatites from Mount Polley (Mao et al., 2015), which is close to the magnetite-hematite (MH) buffer. For apatites from calc-alkaline porphyry Cu±Mo±Au deposits, the average  $\log f_{O_2}$  values range from  $-12.8 \pm 0.6$  (Woodjam Southeast Zone) to  $-14.1 \pm 0.7$  (Gibraltar) and  $-16.3 \pm 1.0$  (Highland Valley) in till. Apatites from mineralized rocks at the Gibraltar and Highland Valley Copper deposits (after Mao et al., 2015) yield similar average  $\log f_{O_2}$  values of  $-14.3 \pm 0.8$  and  $-16.2 \pm 1.0$ , respectively, indicating transition to relatively more reducing conditions ( $f_{O_2} < \text{NNO} + 1$ ). However, without constrained temperature of apatite crystallization, these  $\log f_{O_2}$  values, tied to a wide range of

temperatures (920–660°C), provide only relative estimates of the oxidation state for these deposits.

Cerium and europium are the only REEs with two oxidation states (Ce<sup>3+</sup> and Ce<sup>4+</sup>; Eu<sup>2+</sup> and Eu<sup>3+</sup>); both Ce<sup>3+</sup> and Eu<sup>3+</sup> are preferred in the apatite structure (Prowatke and Klemme, 2006; Cao et al., 2012). Therefore, variations in Ce and Eu abundances relative to the adjacent REEs, expressed as Ce/Ce\* and Eu/Eu\*, in apatite reflect Eu<sup>2+</sup>/Eu<sup>3+</sup> and Ce<sup>3+</sup>/Ce<sup>4+</sup> in the host magmatic-hydrothermal system as controlled by both redox state and minerals such as feldspars (concentrating Eu<sup>2+</sup>) and zircon, monazite, and fluorite (concentrating Ce; Budzinski and Tischendorf, 1989; Sha and Chappell, 1999; Ballard et al., 2002; Belousova et al., 2002; Piccoli and Candela, 2002; Tollari et al., 2008; Colombini et al., 2011; Miles et al., 2014). Residual feldspar retained in source rocks would have the same effect on Eu<sup>2+</sup>/Eu<sup>3+</sup> of the anatectic melt. Therefore, the lack of significant Eu anomalies in apatite grains from Mount Polley, in contrast to the pronounced negative Eu anomalies in those from the Highland Valley, Gibraltar and Woodjam deposits, are consistent with the more oxidized state of the former alkalic porphyry Cu-Au deposit compared to the more reduced calc-alkaline porphyry Cu±Mo±Au deposits. A positive correlation between Eu/Eu\* values and Sr contents in the studied apatites (correlation coefficient = 0.73) also suggests some control of the early feldspar fractionation on Eu<sup>2+</sup>/Eu<sup>3+</sup> of the host magmas and fluids. Thus, the low-Sr, low-Eu/Eu\* apatite grains at Highland Valley, Gibraltar and Woodjam may also imply apatite crystallization after significant plagioclase fractionation in the host melts, whereas high-Sr apatites lacking significant Eu anomalies at Mount Polley may indicate apatite crystallization before most other minerals. Unlike Eu anomalies, Ce anomalies are insensitive to feldspar fractionation. Although apatites in this study do not show significant Ce anomalies, except those with low LREE/HREE perhaps due to the metasomatic alteration (mostly apatite grains from till at Woodjam), the lower Ce/Ce\* values of apatite grains from Mount Polley relative to those from Highland Valley, Gibraltar, and Woodjam are consistent with low Ce<sup>3+</sup>/Ce<sup>4+</sup> in the oxidized alkalic porphyry system. In addition to low  $f_{O_2}$ , depolymerized melts and higher H<sub>2</sub>O contents favour stabilization of Ce<sup>3+</sup>, resulting in higher Ce<sup>3+</sup>/Ce<sup>4+</sup> relative to more polymerized or anhydrous melts (Smythe and Brenan, 2015). In summary, the systematic contrasts in abundances of redox-sensitive elements between apatite grains from the alkalic porphyry Cu-Au and the calc-alkaline porphyry Cu±Mo±Au deposits, at least in part, could be attributed to the more oxidized state of the former.

### 7.3. Apatite trace-element chemistry as a tool for mineral exploration

#### 7.3.1. Method

Here we apply the stepwise discrimination approach of Mao et al. (2015) to apatite grains recovered from tills at the Highland Valley, Gibraltar, Mount Polley and Woodjam porphyry deposits, and from mineralized rocks at the Woodjam Southeast Zone. Mao et al. (2015) subdivided apatites from barren

rocks versus different deposit types using a three-step series of discriminant-function diagrams, based on a discriminant projection analysis (DPA; Flury, 1997) of many apatite trace-element compositions from numerous deposits. For projecting into the discrimination diagrams, compositions of apatite grains are recast as scores of a series of linear discriminant functions (DP), calculated as a sum of constant and log<sub>10</sub>-transformed concentrations of up to 11 elements (Mg, V, Mn, Sr, Y, La, Ce, Eu, Dy, Yb, Pb, Th and U) in ppm, except for Mg which is in wt.%, multiplied by a coefficient for each element for a given function (Mao et al., 2015). The numbering of functions reflects the discrimination step, set (if more than one discrimination diagram is used for a given step), and DP function number. For example, DP2-1-1 represents discrimination step 2, the first set of functions, and the first discriminant function. First, the DP1-1 versus DP1-2 discrimination diagram separates apatites from ore deposits, carbonatites, and barren rocks. This discrimination is final for apatites from carbonatites and barren rocks. Second, only the apatites determined to be derived from ore systems in the first step are further subdivided into six main deposit types: undivided porphyry Cu-Au-Mo and epithermal Au-Ag; undivided iron-oxide copper-gold (IOCG) and Kiruna-type; skarn; orogenic Au; and orogenic Ni-Cu±PGE ore systems, using six discriminant functions (DP2-1-1 versus DP2-1-2, DP2-2-2 versus DP2-2-3, and DP2-3-1 versus DP2-3-2 diagrams). This step identifies apatites derived from the orogenic Au, orogenic Ni-Cu±PGE, and undivided IOCG and Kiruna-type deposits. Finally, only apatites determined to have affinities to porphyry Cu-Au-Mo or skarn deposits in the second step are subdivided into alkalic porphyry Cu-Au, porphyry Mo, porphyry Cu±Mo±Au, porphyry-related Cu-Au breccia, W skarn, and undivided Au±Co±Cu±Pb±Zn skarn types using DP3-1 versus DP3-2 and DP3-1 versus DP3-3 diagrams (Step 3a), which are different binary projections of the same 3-D discriminant space.

### 7.3.2. Discrimination of apatite grains

Equations for each DP function and their calculated scores for apatite grains analyzed in the present study are presented by Rukhlov et al. (2016). Figure 10 shows the DP1-1 versus the DP1-2 discrimination diagram for apatite grains examined here. Most of the data from each deposit area plot within the field of ore deposits, including all apatite grains from till at the Highland Valley deposit and from mineralized bedrock at the Woodjam Southeast Zone. Apatite grains from tills showing a barren-rock affinity are higher at Woodjam and Gibraltar (both ~35%) compared to Mount Polley (~14%). Two data points fall marginally in the field of carbonatites; one (sample 12PMA519A01 at Gibraltar) is at the boundary with barren rocks, the second (sample 11PMA017A01 at Woodjam) is at the boundary with ore systems (Fig. 10). Although the former apatite grain has the highest Sr in this study (5733 ppm), its low  $(La/Sm)_{CN}$  and a positive Eu anomaly (Rukhlov et al., 2016) suggest that it was derived from metasomatically altered barren rock. Likewise, despite being enriched in LREE (with

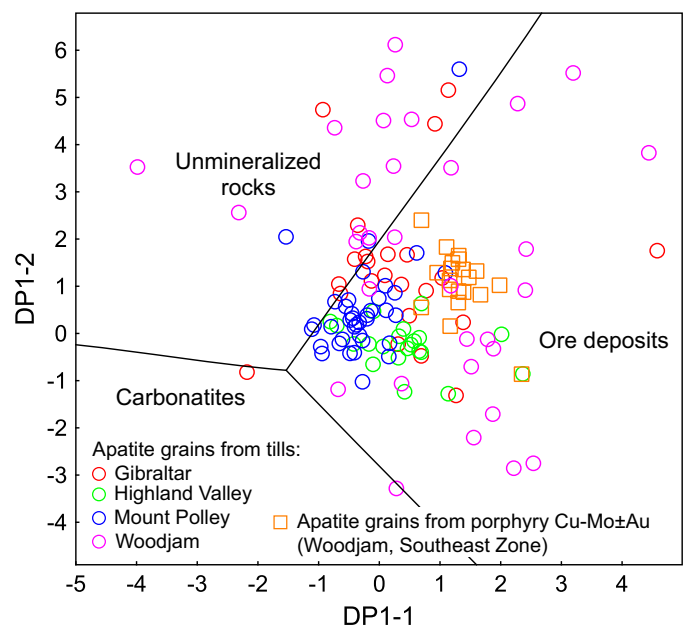


**Fig. 10.** The first discriminant function (DP1-1) versus the second discriminant function (DP1-2) discrimination diagram for apatite (Step 1) after Mao et al. (2015);  $DP1-1 = -0.06461 \cdot \text{LogMn} - 1.56 \cdot \text{LogSr} + 2.609 \cdot \text{LogY} + 0.3631 \cdot \text{LogLa} - 1.766 \cdot \text{LogCe} + 0.6243 \cdot \text{LogEu} - 3.642 \cdot \text{LogDy} + 0.7086 \cdot \text{LogYb} - 1.178 \cdot \text{LogPb} + 0.4161 \cdot \text{LogTh} + 0.963 \cdot \text{LogU} + 6.589$ ;  $DP1-2 = 0.2073 \cdot \text{LogMn} - 1.035 \cdot \text{LogSr} + 15.1 \cdot \text{LogY} + 4.995 \cdot \text{LogLa} - 5.804 \cdot \text{LogCe} + 0.1741 \cdot \text{LogEu} - 8.771 \cdot \text{LogDy} - 4.326 \cdot \text{LogYb} + 2.022 \cdot \text{LogPb} - 0.6719 \cdot \text{LogTh} + 0.02096 \cdot \text{LogU} - 10.45$ . Variables are log<sub>10</sub>-equivalents of element concentrations in parts per million (ppm).

the highest  $(Ce/Yb)_{CN}$  ratio in this study) the low absolute abundances of REEs ( $\sum \text{REE} = 713$  ppm) and Sr (339 ppm; Rukhlov et al., 2016) of the second apatite grain are atypical of apatites from carbonatites ( $>930$  ppm  $\sum \text{REE}$  and  $>1840$  ppm Sr; Mao et al., 2015).

Apatite grains that have trace-element chemistry consistent with ore systems (Fig. 10) are plotted in the discrimination diagrams for general ore deposits (Fig. 11). Excluding Woodjam, most of the data plot within the field of undivided porphyry Cu-Mo-Au and epithermal Au-Ag deposits. Data for detrital apatite grains from Woodjam spread into the adjacent fields of skarn deposits due to their highly variable trace-element compositions, which reflect extensive hydrothermal alteration (Schiarizza et al., 2009a; del Real et al., 2014; Vandekerckhove et al., 2014). Two apatite grains from till sample 11PMA017A01 overlying the contact between the Takomkane batholith and rocks of the Nicola Group (Fig. 5) plot within the field of orogenic Ni-Cu±PGE deposits (Fig. 11). Other than monzonite stocks and dikes, mafic-ultramafic intrusions suitable for this deposit-type are unknown in the Woodjam area but occur  $>20$  km to the south and southeast, up-ice from this till sample, along the contacts of the Takomkane batholith, (Schiarizza et al., 2009a; Sherlock et al., 2013; del Real et al., 2014). High As contents of these two apatite grains, similar to those of other apatite grains from this till sample, suggest a common source

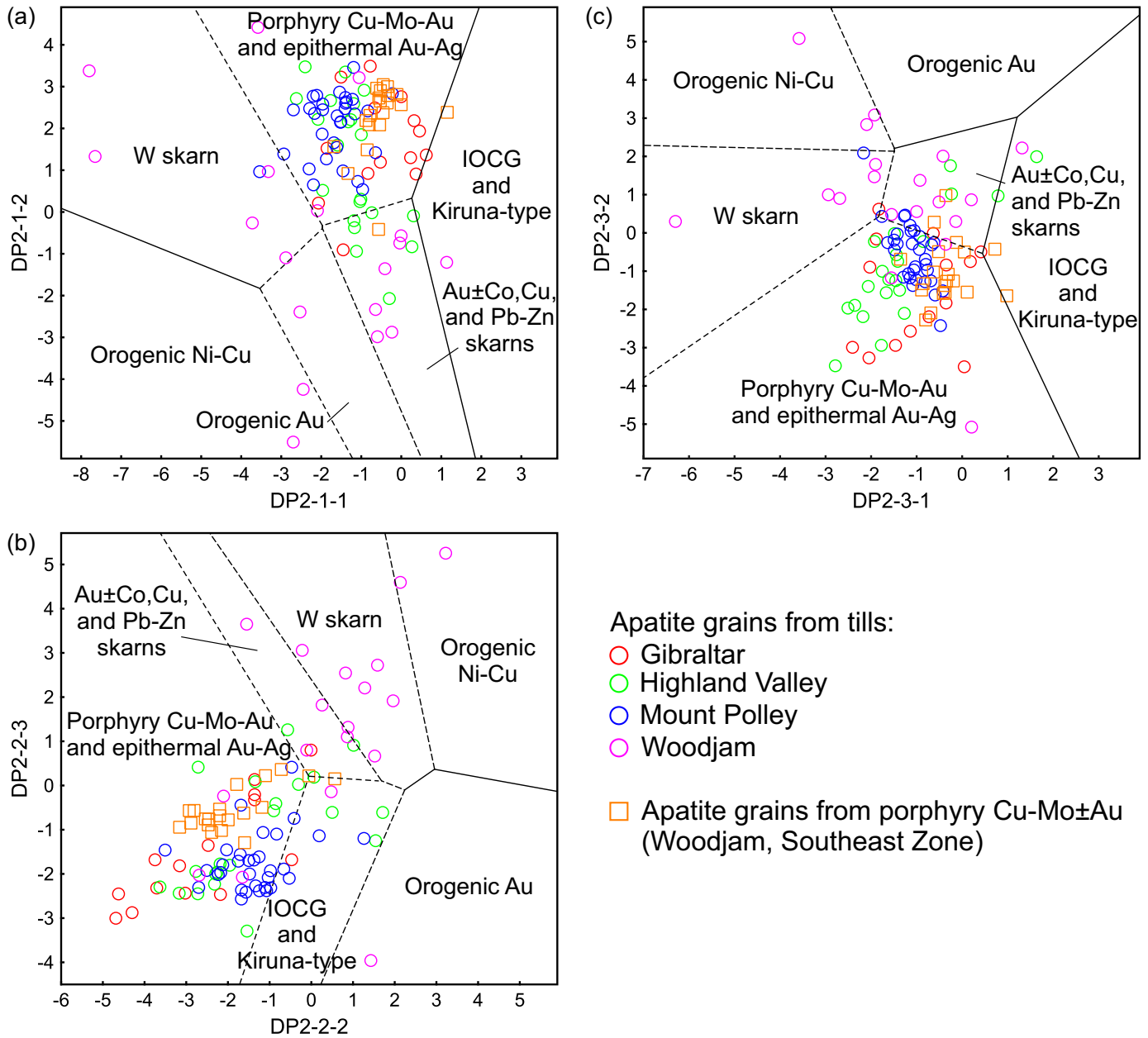


**Fig. 11.** Discrimination diagrams for apatite from ore deposits (Step 2) after Mao et al. (2015). IOCG = iron oxide copper-gold deposits; porphyry Cu-Mo-Au = undivided calc-alkaline porphyry Cu±Mo±Au and porphyry Mo, and alkalic porphyry Cu-Au deposits. **a)** The first discriminant function (DP2-1-1) versus the second discriminant function (DP2-1-2);  $DP2-1-1 = -2.275 \cdot \text{LogMn} - 1.429 \cdot \text{LogSr} + 1.504 \cdot \text{LogY} + 3.247 \cdot \text{LogCe} - 1.088 \cdot \text{LogEu} + 0.1925 \cdot \text{LogDy} + 0.7636 \cdot \text{LogYb} - 0.05301 \cdot \text{LogTh} - 1.538 \cdot \text{LogU} - 3.655$ ;  $DP2-1-2 = 1.321 \cdot \text{LogMn} + 1.576 \cdot \text{LogSr} + 14.63 \cdot \text{LogY} - 0.005804 \cdot \text{LogCe} + 1.605 \cdot \text{LogEu} - 16.53 \cdot \text{LogDy} + 3.251 \cdot \text{LogYb} - 0.2426 \cdot \text{LogTh} - 1.155 \cdot \text{LogU} - 20.3$ . **b)** The second discriminant function (DP2-2-2) versus the third discriminant function (DP2-2-3);  $DP2-2-2 = 1.882 \cdot \text{LogMg} - 1.872 \cdot \text{LogMn} - 0.8039 \cdot \text{LogSr} - 12.21 \cdot \text{LogY} - 0.6912 \cdot \text{LogCe} - 2.014 \cdot \text{LogEu} + 14.84 \cdot \text{LogDy} - 3.946 \cdot \text{LogYb} - 0.734 \cdot \text{LogTh} + 2.513 \cdot \text{LogU} + 24.20$ ;  $DP2-2-3 = -0.3009 \cdot \text{LogMg} - 0.078 \cdot \text{LogMn} - 1.591 \cdot \text{LogSr} - 6.697 \cdot \text{LogY} - 0.6125 \cdot \text{LogCe} - 0.2912 \cdot \text{LogEu} + 0.722 \cdot \text{LogDy} + 2.686 \cdot \text{LogYb} + 1.466 \cdot \text{LogTh} + 0.4239 \cdot \text{LogU} + 16.26$ . **c)** The first discriminant function (DP2-3-1) versus the second discriminant function (DP2-3-2);  $DP2-3-1 = 1.034 \cdot \text{LogMg} - 3.069 \cdot \text{LogMn} + 4.045 \cdot \text{LogY} + 3.368 \cdot \text{LogCe} - 3.127 \cdot \text{LogEu} - 0.2322 \cdot \text{LogDy} - 0.7732 \cdot \text{LogYb} - 0.1035 \cdot \text{LogPb} - 1.228 \cdot \text{LogTh} - 0.2231 \cdot \text{LogU} - 4.263$ ;  $DP2-3-2 = 1.888 \cdot \text{LogMg} - 1.839 \cdot \text{LogMn} - 4.813 \cdot \text{LogY} - 0.3218 \cdot \text{LogCe} - 3.421 \cdot \text{LogEu} + 10.67 \cdot \text{LogDy} - 5.662 \cdot \text{LogYb} + 1.706 \cdot \text{LogPb} - 1.043 \cdot \text{LogTh} + 1.803 \cdot \text{LogU} + 14.24$ . Variables are  $\log_{10}$ -equivalents of element concentrations in parts per million (ppm) for all elements, except Mg which is in weight per cent (wt.%).

of elevated As, probably in underlying sedimentary rocks of the Nicola Group.

Compositions of apatite grains shown in Figure 11, except for the two apatite grains at Woodjam indicating orogenic Ni-Cu±PGE affinity, are projected into DP3-1 versus DP3-2 and DP3-1 versus DP3-3 discrimination diagrams with fields of different sub-types of porphyry Cu-Mo-Au, porphyry-related Cu-Au breccia, and skarn deposits (Fig. 12). As expected, data for apatite grains from Mount Polley fall in the alkalic porphyry Cu-Au field (Fig. 12a). For the Highland Valley and Gibraltar deposits, apatite data straddle the porphyry Cu±Mo±Au and porphyry Mo fields in the DP3-1 versus DP3-2 projection (Fig. 12a) or the porphyry Cu±Mo±Au and alkalic porphyry Cu-Au fields in the DP3-1 versus DP3-3 projection (Fig. 12b). Note that the DP3-1 versus DP3-2 diagram better discriminates alkalic porphyry Cu-Au from other deposit types than the DP3-1 versus DP3-3 diagram, which best separates porphyry Mo deposits from others (Mao et al., 2015). However, all these deposit types are separated from each other in the 3-D discriminant space, with the apparent overlaps between some of the deposits in Figure 12 resulting from projection of their fields into 2-D diagrams (Mao et al., 2015).

In combination, the discrimination diagrams (Figs. 12a, b) reveal that most of the apatite grains at the Highland Valley and Gibraltar deposit areas have the porphyry Cu±Mo±Au affinity, as expected for these deposits. A few data points from these areas that do plot within porphyry Mo or alkalic porphyry Cu-Au fields are within the 95% confidence uncertainty of the field boundaries in these diagrams (Mao et al., 2015). Likewise, by eliminating alkalic porphyry Cu-Au plus W skarn (Fig. 12a) and porphyry Mo (Fig. 12b), apatite grains from mineralized bedrocks at the Woodjam Southeast Zone indicate porphyry Cu±Mo±Au source, consistent with their trace-element and REE features as outlined above. As we have already seen in all other diagrams, compositions of apatite grains from till at Woodjam also show the widest spread in Figure 12, scattering from porphyry Cu±Mo±Au field across porphyry-related Cu-Au breccia field to the field of undivided Au±Co-, Cu-, and Pb-Zn skarns. As discussed above, the wide variations of trace-element compositions of apatite grains from till at Woodjam likely reflect their metasomatic overprint due to the extensive hydrothermal alteration documented in this area (Schiarizza et al., 2009a; del Real et al., 2014; Vandekerkhove et al., 2014). In addition, six apatite grains from till at Woodjam and one at Gibraltar have trace-element compositions with low  $(\text{Ce}/\text{Yb})_{\text{CN}}$  ratios of  $<0.85$  (probably due to the metasomatic alteration) and fall beyond the limits of the discrimination diagrams of Mao et al. (2015). Therefore, they are not classified here (i.e. labelled “unknown” in Appendix 4; Rukhlov et al., 2016).

### 7.3.3. Spatial patterns

The abundance of chalcopyrite grains (0.25–0.50 mm,  $>3.2 \text{ g}\cdot\text{cm}^{-3}$  fraction; normalized to 10 kg of  $<2 \text{ mm}$ -size bulk sediment) in tills (after Hashmi et al., 2015; Plouffe et al., 2013a; Plouffe and Ferbey, 2015a, d) for each study area

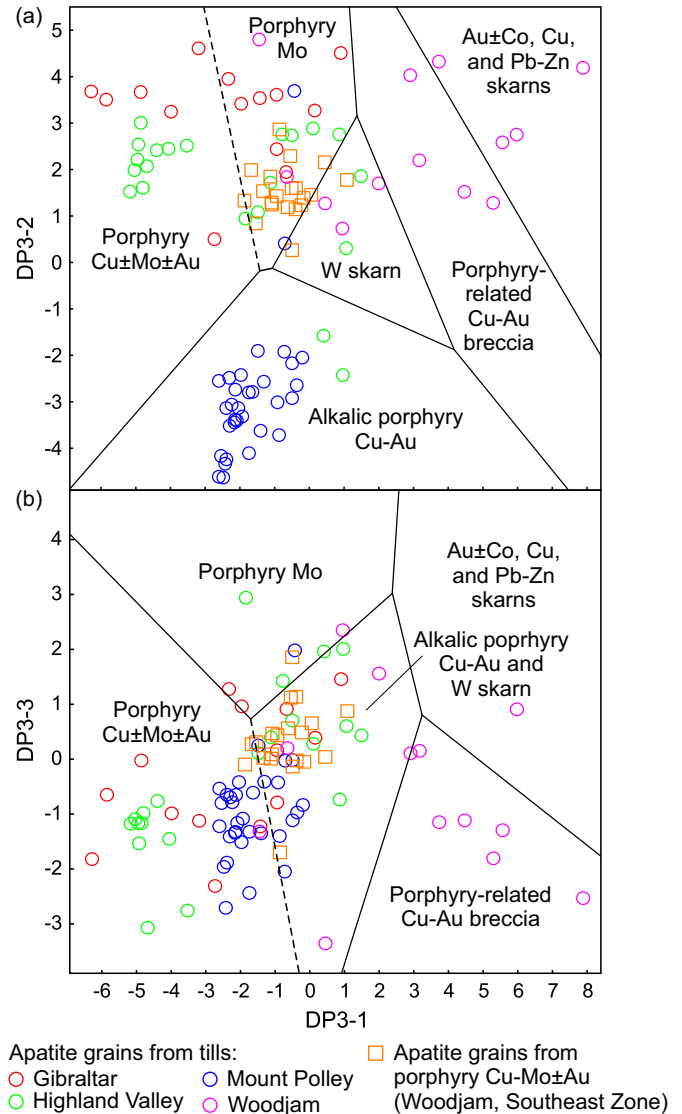


**Fig. 12.** Discrimination diagrams for apatite from porphyry and skarn deposits (Step 3) after Mao et al. (2015). **a)** The first discriminant function (DP3-1) versus the second discriminant function (DP3-2). **b)** The first discriminant function (DP3-1) versus the third discriminant function (DP3-3).  $\text{DP3-1} = 0.8718 \cdot \text{LogMg} - 4.156 \cdot \text{LogMn} - 3.065 \cdot \text{LogSr} + 6.341 \cdot \text{LogY} - 1.704 \cdot \text{LogCe} - 1.806 \cdot \text{LogEu} - 7.320 \cdot \text{LogYb} - 0.2802 \cdot \text{LogPb} + 0.6948 \cdot \text{LogTh} + 1.698 \cdot \text{LogU} + 21.07$ ;  $\text{DP3-2} = -1.473 \cdot \text{LogMg} + 2.550 \cdot \text{LogMn} - 2.981 \cdot \text{LogSr} - 5.398 \cdot \text{LogY} + 0.5600 \cdot \text{LogCe} - 2.898 \cdot \text{LogEu} + 3.780 \cdot \text{LogYb} + 2.108 \cdot \text{LogPb} - 0.4108 \cdot \text{LogTh} - 0.1375 \cdot \text{LogU} + 8.534$ ;  $\text{DP3-3} = 0.1617 \cdot \text{LogMg} - 1.173 \cdot \text{LogMn} - 4.364 \cdot \text{LogSr} + 2.634 \cdot \text{LogY} + 0.8452 \cdot \text{LogCe} + 3.378 \cdot \text{LogEu} - 3.184 \cdot \text{LogYb} + 1.619 \cdot \text{LogPb} + 1.956 \cdot \text{LogTh} - 0.6212 \cdot \text{LogU} + 4.471$ . Variables are  $\log_{10}$ -equivalents of element concentrations in parts per million (ppm) for all elements, except Mg which is in weight per cent (wt.%).

highlights glacial dispersion from known porphyry deposits (Figs. 13-16). Notably, all apatite grains in metal-rich till (with up to 2500 chalcopyrite grains), immediately down-ice from the Highland Valley Copper deposit, show consistent porphyry Cu±Mo±Au features (Fig. 13). Till with  $<51$  chalcopyrite

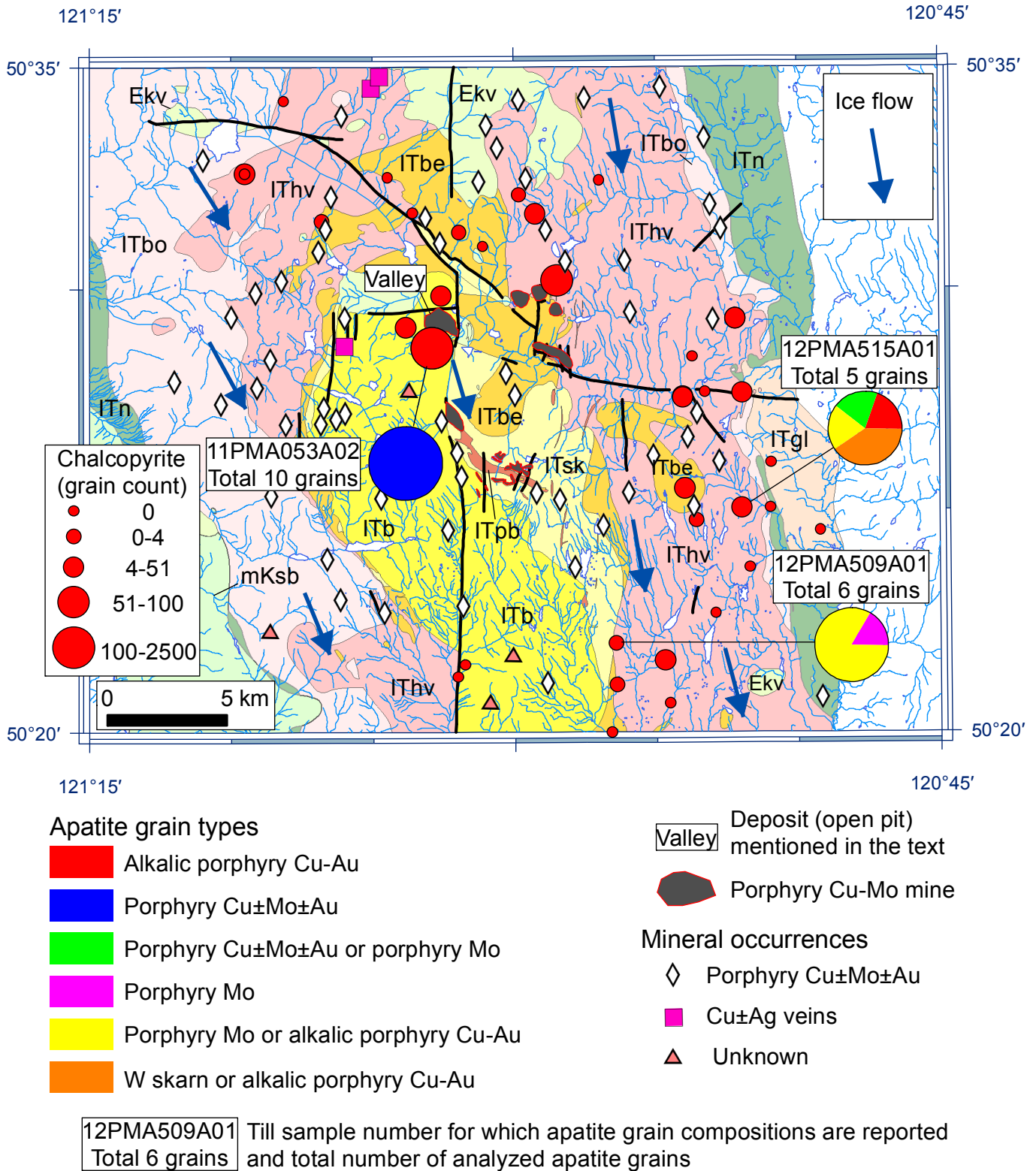


**Fig. 13.** Affinity of apatite grains (0.25–0.50 mm, >3.2 g·cm<sup>-3</sup>, >1.0 A fraction), based on the classification of Mao et al. (2015), and number of chalcopyrite grains (0.25–0.50 mm, >3.2 g·cm<sup>-3</sup> fraction; normalized to 10 kg of <2 mm-size bulk sediment; after Plouffe et al., 2013a; Plouffe and Ferbey, 2015d) from till samples, Highland Valley calc-alkaline porphyry Cu-Mo district. Bedrock legend and other symbols as in Figure 2.

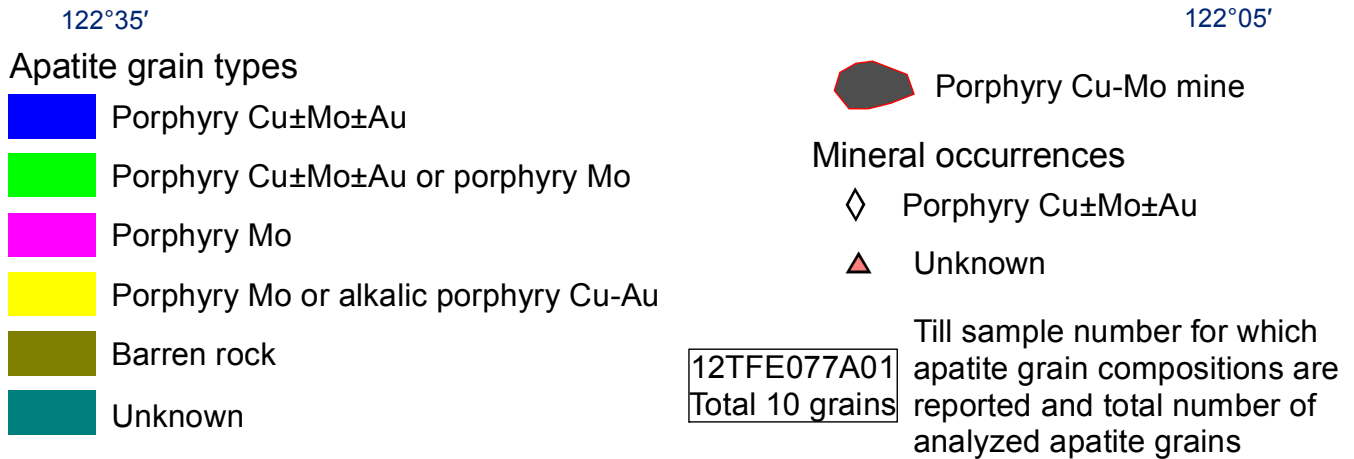
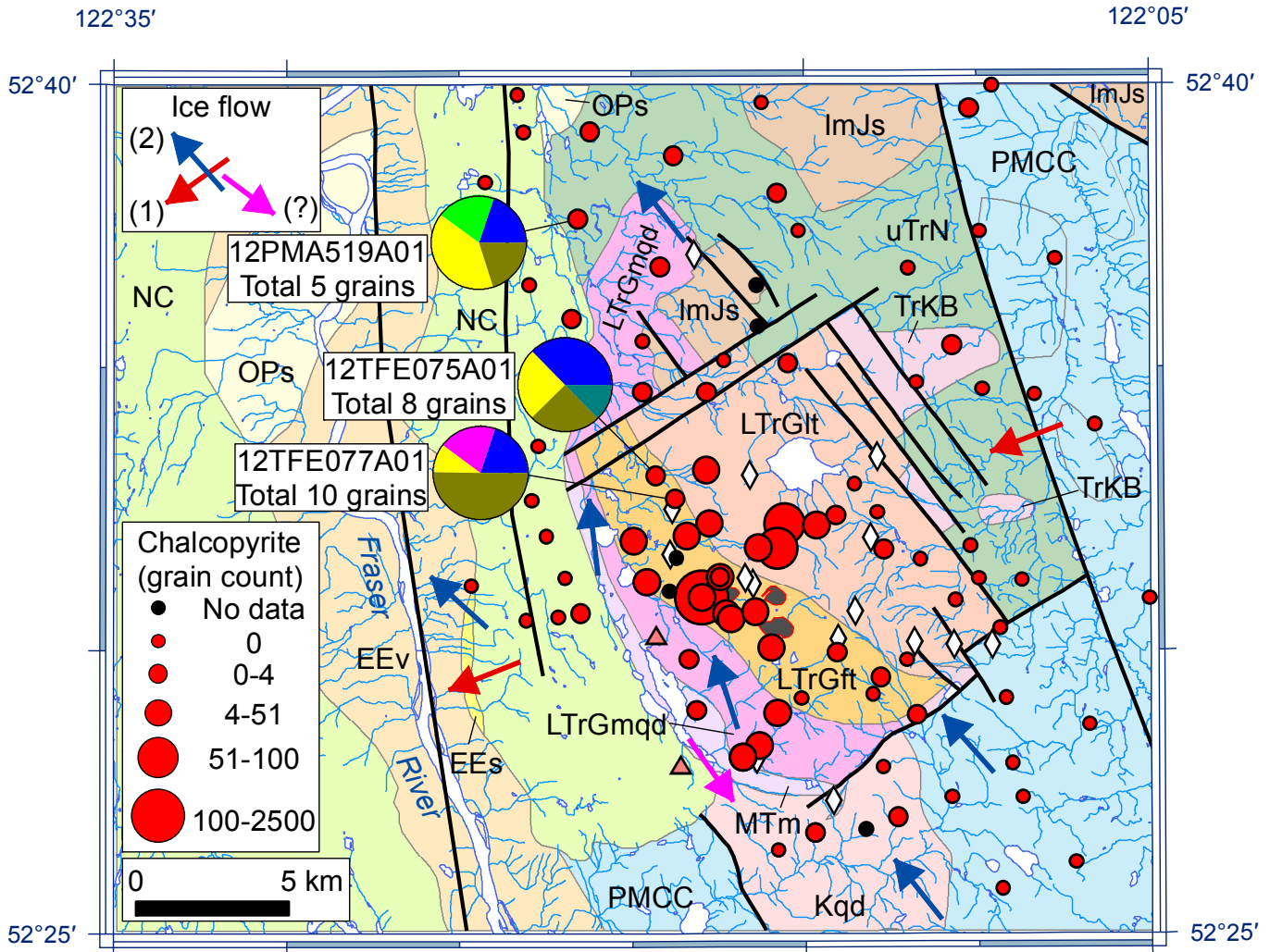
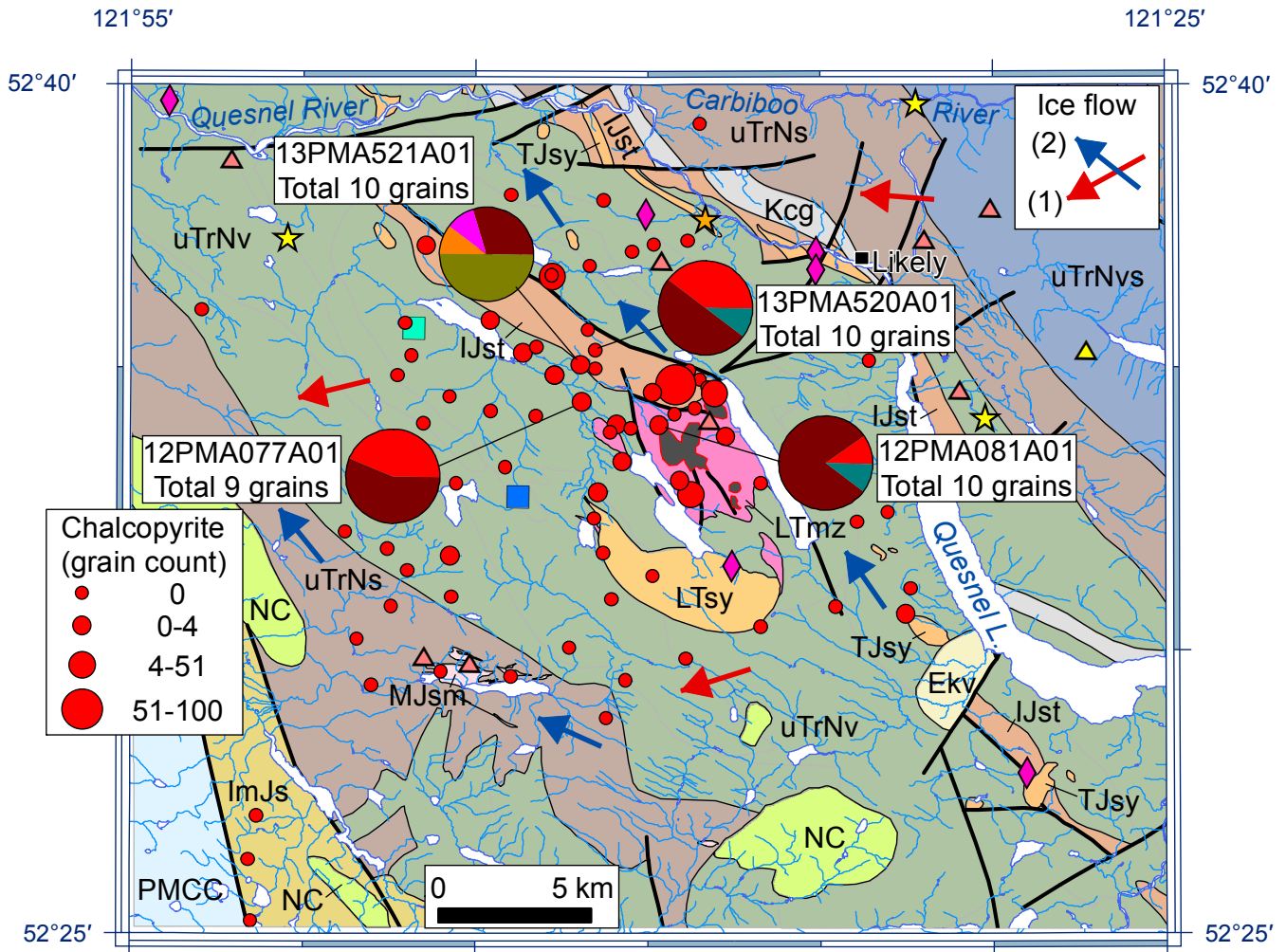


**Fig. 14.** Affinity of apatite grains (0.25–0.50 mm, >3.2 g·cm<sup>-3</sup>, >1.0 A fraction), based on the classification of Mao et al. (2015), and number of chalcopyrite grains (0.25–0.50 mm, >3.2 g·cm<sup>-3</sup> fraction; normalized to 10 kg of <2 mm-size bulk sediment; after Plouffe et al., 2013a; Plouffe and Ferbey, 2015a, d) from till samples, Gibraltar calc-alkaline porphyry Cu-Mo mine area. Bedrock legend and other symbols as in Figure 3.



**Apatite grain types**

- Alkalic porphyry Cu-Au
- Alkalic porphyry Cu-Au or porphyry Cu±Mo±Au
- Porphyry Mo
- W skarn or alkalic porphyry Cu-Au
- Barren rock
- Unknown

Alkalic porphyry Cu-Au mine

**Mineral occurrences**

- Alkalic porphyry Cu-Au
- Sediment-hosted Cu
- Au-quartz veins
- Volcanic redbed Cu
- Surficial gold placers
- Unknown
- Buried-channel gold placers

13PMA520A01 Till sample number for which apatite grain compositions are reported and total number of analyzed apatite grains  
Total 10 grains

**Fig. 15.** Affinity of apatite grains (0.25–0.50 mm, >3.2 g·cm<sup>-3</sup>, >1.0 A fraction), based on the classification of Mao et al. (2015), and number of chalcopyrite grains (0.25–0.50 mm, >3.2 g·cm<sup>-3</sup> fraction; normalized to 10 kg of <2 mm-size bulk sediment; after Hashmi et al., 2015) from till samples, Mount Polley alkalic porphyry Cu-Au mine area. Bedrock legend and other symbols as in Figure 4.

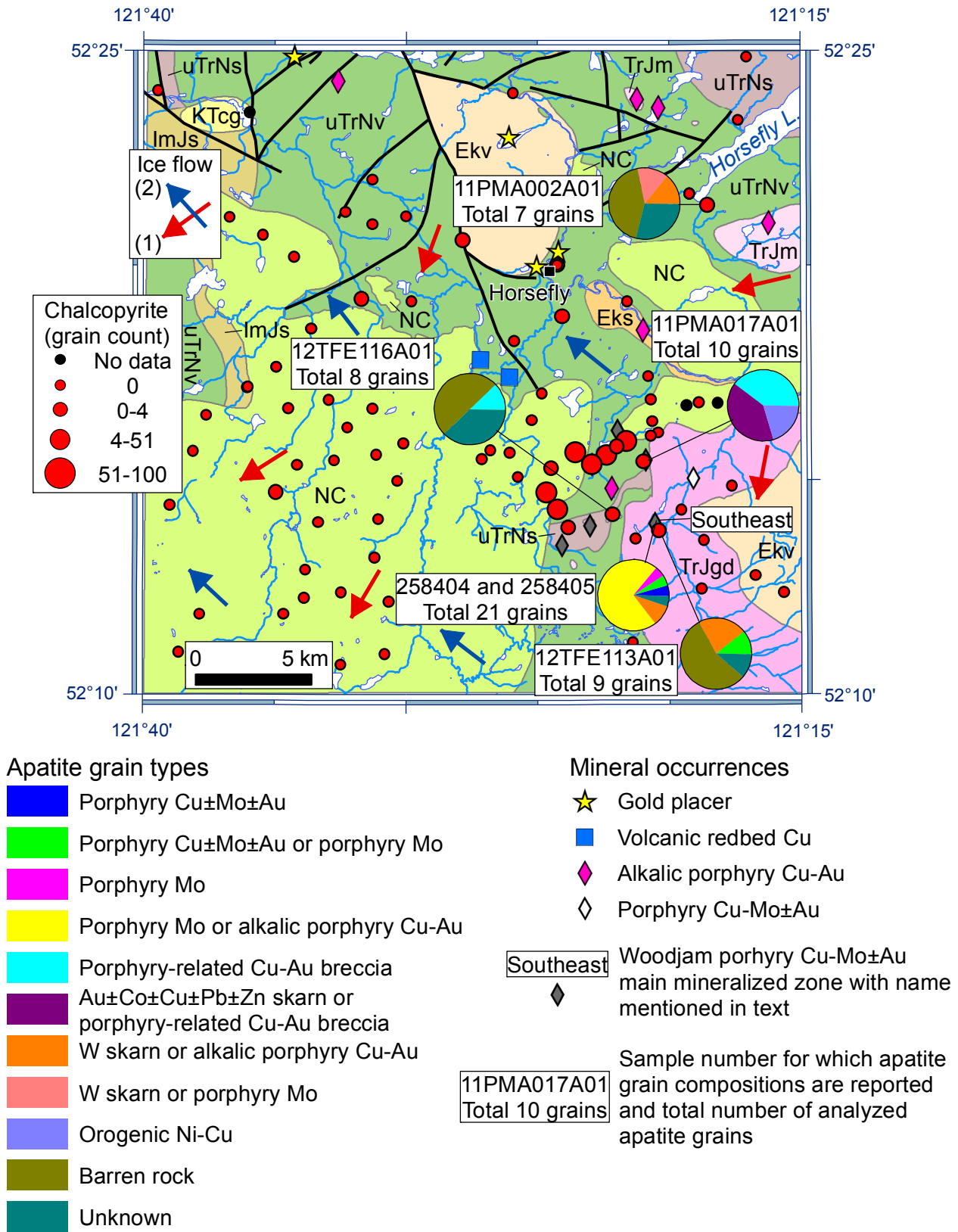


**Fig. 16.** Affinity of apatite grains (0.25–0.50 mm, >3.2 g·cm<sup>-3</sup>, >1.0 A fraction) from till and bedrock samples, based on the classification of Mao et al. (2015), and number of chalcopyrite grains from till samples (0.25–0.50 mm, >3.2 g·cm<sup>-3</sup> fraction; normalized to 10 kg of <2 mm-size bulk sediment; after Plouffe and Ferbey, 2015a, d), Woodjam high-K, calc-alkaline porphyry Cu-Mo±Au developed prospect area. Bedrock legend and other symbols as in Figure 5.

grains in the eastern part of the Highland Valley district contains less abundant apatite, with all examined grains indicating ore systems, ranging from porphyry Cu±Mo±Au to porphyry Mo or alkalic porphyry Cu-Au (Fig. 13; Table 4).

At Gibraltar, till with <4 chalcopyrite grains, deposited 5 to 15 km down-ice from the porphyry Cu-Mo deposit, contains apatite grains that mostly show the trace-element characteristics consistent with porphyry Cu±Mo±Au deposits (Fig. 14). Two apatite grains from till sample 12TFE077A01 indicate a porphyry Mo source, and one unclassified apatite grain from a nearby till sample 12TFE075A01 has the trace-element chemistry (e.g., low LREE/HREE) indicating metasomatic alteration. All till samples from Gibraltar contain apatite grains with the chemical attributes of barren rocks (20–50%; Fig. 14; Table 4). Grains of predominantly porphyry Cu±Mo±Au affinity are from till samples roughly aligned along the late-phase ice-flow direction (northwest), away from the Gibraltar deposit, and may indicate glacial transport as far as 15 km. Such dispersion is not recorded in the amounts of chalcopyrite grains in these tills, perhaps due to the limited preservation of chalcopyrite during glacial transport and postglacial weathering relative to apatite.

The chalcopyrite-poor (0–4 grains) but relatively apatite-rich (up to 3% of the HMC fraction) till samples within 0 to ~5 km down-ice (northwest) from the Mount Polley alkalic porphyry Cu-Au deposit all contain apatite grains with the trace-element signature of alkalic porphyry Cu-Au deposits (Fig. 15). The proportion of the alkalic porphyry Cu-Au-type apatite grains decreases from 90% to 40% with distance down-ice from the Mount Polley deposit, consistent with increasing dilution of tills by barren-rock material farther away from the mineralization. Half of the apatite grains (0.5% in the HMC fraction) in till sample 13PMA521A01, ~5 km down-ice from the deposit, are inferred to be from barren rocks, and one apatite grain from this sample shows chemical signature of porphyry Mo deposits.

Apatite grains from mineralized quartz monzonites at the Woodjam Southeast Zone indicate porphyry Cu±Mo±Au affinity, consistent with the high-K, calc-alkaline character of the mineralization (del Real et al., 2014; Vandekerckhove et al., 2014). Apatite grains showing barren-rock affinity or highly variable degrees of depletion in most of trace-elements with low LREE/HREE ratios, perhaps due to the extensive hydrothermal alteration of their source rocks (Schiarizza et al., 2009a; del Real et al., 2014; S.M. Vandekerckhove et al., 2014) are predominant in tills at Woodjam (Fig. 16). Three apatite grains from till sample 12TFE113A01 immediately above the Southeast Zone show porphyry Cu±Mo±Au or alkalic porphyry Cu-Au affinities. Two apatite grains from till sample 11PMA002A01, ~2.5 km down-ice from an alkalic porphyry Cu-Au occurrence, ~15 km northeast of the Southeast Zone, indicate an alkalic porphyry Cu-Au source (Fig. 16; Table 4). Apatite grains from till (sample 11PMA017A01) overlying the Takomkane batholith-Nicola Group contact show the highest As in this study and a wide range of Mg and  $\Sigma$ REE abundances, with compositions falling mostly within the

porphyry-related Cu-Au breccia field in the DP3-1 versus DP3-3 diagram (Fig. 12b), except for two apatite grains showing orogenic Ni-Cu±PGE affinity (Fig. 16). As discussed above, the trace-element chemistry of these apatite grains suggest crystallization in a hydrothermal environment with elevated As perhaps derived from sedimentary rocks of the Nicola Group. Their porphyry-related Cu-Au breccia-type affinity indicates probable derivation from breccias related to monzonite stocks and dikes at the Woodjam porphyry camp (del Real et al., 2014). The clear Cu±Mo±Au signature displayed by apatite from mineralized bedrock at the Woodjam Southeast Zone is lacking in most till grains. The latter are predominantly metasomatically altered apatites, even in tills proximal to the known mineralized zones, implying derivation from higher-level, low-temperature alteration halos related to the Takomkane batholith and its satellite intrusions.

## 8. Conclusions

Our EMPA and LA-ICP-MS examination of 147 apatite grains recovered from 14 till samples at the Highland Valley, Gibraltar, Mount Polley, and Woodjam porphyry deposits, and from two mineralized bedrock samples at the Woodjam Southeast Zone, reveals systematic trace-element patterns characteristic of both the degree of fractionation and the relative redox state of these magmatic-hydrothermal ore systems. Apatite grains from Mount Polley show higher  $\text{SO}_3$ ,  $\text{SiO}_2$ ,  $\text{Na}_2\text{O}$ , Sr, Mg, V, Ba, Zr, Mo, Nb contents,  $(\text{La}/\text{Sm})_{\text{CN}}$ , and  $\text{Eu}/\text{Eu}^*$ , and lower Mn, Y,  $\Sigma$ HREE contents and  $\text{Ce}/\text{Ce}^*$  relative to those of apatite grains from the Highland Valley, Gibraltar and Woodjam deposits. They also have systematically higher As contents, except for apatite grains from one till sample at the Woodjam porphyry camp, above the contact between the Takomkane batholith and Nicola Group volcano-sedimentary rocks, likely As sources. The lack of significant Eu anomalies, coupled with higher  $\text{SO}_3$ , V, and As, and lower Mn abundances and  $\text{Ce}/\text{Ce}^*$  values, of apatite grains at Mount Polley than those from Highland Valley, Gibraltar and Woodjam are consistent with the generally more oxidized alkalic porphyry Cu-Au deposits compared to the calc-alkaline porphyry Cu±Mo±Au systems. Average Mn abundances in primary apatite grains yield  $\log f\text{O}_2$  values of  $-11.2 \pm 0.5$  for Mount Polley,  $-12.8 \pm 0.6$  for Woodjam Southeast Zone,  $-14.1 \pm 0.7$  for Gibraltar, and  $-16.3 \pm 1.0$  for Highland Valley, using an empirical calibration for a range of temperatures (920–660 °C) and compositions (andesitic to rhyolitic) after Miles et al. (2014). These  $\log f\text{O}_2$  values provide relative estimates of the oxidation state for these porphyry deposits within a given range of temperatures. However, they will quantify the redox state (relative to mineral buffers) with an estimated temperature of apatite crystallization for a given sample. The Mn in apatite oxybarometer does not apply to metasomatically altered apatites with low minor- and trace-element abundances and low LREE/HREE. Strong negative Eu anomalies, combined with higher Mn and lower Mg and Sr contents, of apatite grains at Highland Valley, Gibraltar and Woodjam, compared to those at Mount Polley,

**Table 4.** Summary of apatite grains from till and mineralized bedrock in the Highland Valley, Gibraltar, Mount Polley, and Woodjam study areas, subdivided by barren-rock or deposit-type affinity using the apatite classification after Mao et al. (2015).

Sample	Type	Area	Total apatite grains	Alk. pry Cu-Au or pry Cu±Mo±Au	Alk. pry Cu-Au or pry Cu±Mo±Au	Pry Cu±Mo±Au or pry Mo	Pry Mo or alk. pry Cu-Au	W skarn or alk. pry Cu-Au	W skarn or pry Mo	Pry-related Cu-Au breccia	Skarn* or pry-related Cu-Au breccia	Skarn* Orogenic Ni-Cu±PGE	Unknown Barren rock
12PMA519A01	Till		5		1	1	2						1
12TFE075A01	Till	Gibraltar	8		3		2						1
12TFE077A01	Till		10		2	2	1						5
11PMA053A02	Till		10		10								
12PMA509A01	Till	Highland Valley	6			1	5						
12PMA515A01	Till		5	1		1	1	2					
12PMA077A01	Till		9	4			5						
12PMA081A01	Till	Mount	10	1			8						1
13PMA520A01	Till	Polley	10	4			5						1
13PMA521A01	Till		10			1	3	1					5
11PMA002A01	Till		7					1	1				2
11PMA017A01	Till		10							4	3	1	2
12TFE113A01	Till	Woodjam	9			1		2					1
12TFE116A01	Till		8							1			3
258404	Rock	Woodjam Southeast	11		1	1	1	8					
258405	Rock	Zone	10					7	2				1

**Alk.** = alkalic, **Pry** = porphyry.

Details of till samples can be found in Plouffe et al. (2013a) and Plouffe and Ferbey (2015a, d). We refer the reader to Mao et al. (2015) for details of the deposit types and their discrimination using apatite trace-element chemistry. The "unknown" group includes apatite grains with missing values for some elements due to poor analysis and extreme compositions falling beyond the bounds of the discrimination diagrams after Mao et al. (2015).

\* Includes Au-Co skarn, Cu skarn, and Pb-Zn skarn types (after Mao et al., 2015).

may also indicate early plagioclase and pyroxene fractionation (which lower Sr, Mg and  $\text{Eu}^{2+}/\text{Eu}^{3+}$  in the melt) and lack of significant Fe-Mg minerals (which accommodate Mn) in the evolved calc-alkaline magma. Most apatite grains from tills at Woodjam, along with a few apatite grains at Highland Valley, Gibraltar, and Mount Polley, show variable degrees of depletion in most of minor and trace elements and LREEs, yielding extreme ranges in  $(\text{Ce}/\text{Yb})_{\text{CN}}$  ( $<0.01$ – $47$ ),  $(\text{La}/\text{Sm})_{\text{CN}}$  ( $0.06$ – $6.0$ ),  $(\text{Gd}/\text{Yb})_{\text{CN}}$  ( $0.01$ – $39$ ),  $\text{Ce}/\text{Ce}^*$  ( $0.23$ – $3.8$ ) and elevated  $\text{Eu}/\text{Eu}^*$  (up to  $1.5$ ). The trace-element and REE patterns of these grains, distinct from those in mineralized rocks at Woodjam and other porphyry deposits (Mao et al., 2015), probably reflect metasomatic alteration, which is extensive at the Woodjam high-K, calc-alkaline Cu-Mo±Au porphyry camp (Schiarrizza et al., 2009a; del Real et al., 2014; Vandekerckhove et al., 2014). Calculated molar Cl/F and Cl/OH ratios in the examined apatite grains, assuming molar  $(\text{F} + \text{OH} + \text{Cl}) = 1$ , agree with those of apatites from some producing porphyry deposits elsewhere (Piccoli and Candela, 2002). The trace-element chemistry of apatite grains correctly identifies the porphyry systems in all four study areas. Paucity of porphyry Cu±Mo±Au-type apatite grains in Woodjam tills implies protection of the mineralized zones from erosion during the most recent glaciation by a cover of pre-glacial sediment or unmineralized rock (Bissig et al., 2013; del Real et al., 2014; Vandekerckhove et al., 2014; J.W. Morton, pers. comm. 2014).

Our study indicates that apatite can survive glacial transport and post-glacial weathering. It presents the first test of the apatite classification by Mao et al. (2015) on grains from till, and demonstrates that apatite trace-element chemistry can be an effective mineral exploration tool. Future research should test the effectiveness of the method on apatite from other deposit types, including carbonatites, orogenic Au, IOCG, porphyry Mo, orogenic Ni-Cu±PGE, and barren rocks. Our study was limited to the heavy ( $>3.2 \text{ g}\cdot\text{cm}^{-3}$ ) apatite fraction; separation and identification methods need to be further developed to incorporate less dense fractions.

### Acknowledgments

We thank Overburden Drilling Management Limited for help with recovering and identifying apatite grains from heavy mineral concentrates. Edith Czech (University of British Columbia) and Mati Raudsepp (University of British Columbia) are acknowledged for their assistance with the electron microprobe analysis (EMPA). We are grateful to Beth McClenaghan (Geological Survey of Canada), Stephen Rowins (British Columbia Geological Survey), and Larry Aspler (British Columbia Geological Survey) for thorough reviews of the paper. ESS contribution # 20150382.

### References cited

Anderson, R.G., Plouffe, A., Ferbey, T., and Dunn, C.E., 2012a. The search for surficial expressions of buried Cordilleran porphyry deposits; a new TGI4 activity in the southern Canadian Cordillera. Geological Survey of Canada Open File 7081, poster.  
Anderson, R.G., Plouffe, A., Ferbey, T., and Dunn, C.E., 2012b. The

search for surficial expressions of buried Cordilleran porphyry deposits: background and progress in a new TGI-4 activity in the southern Canadian Cordillera. In: Current Research 2012-7, Geological Survey of Canada, 15p.  
Anderson, R.G., Plouffe, A., Ferbey, T., and Dunn, C.E., 2012c. The search for surficial expressions of buried Cordilleran porphyry deposits: preliminary findings in a new TGI4 activity in the southern Canadian Cordillera. Geological Survey of Canada Open File 7266, 82p.  
Ash, C.H. and Riveros, C.P., 2001. Geology of the Gibraltar copper-molybdenite deposit, east-central British Columbia (93B/9). In: Geological Fieldwork 2000, British Columbia Ministry of Energy and Mines, British Columbia Geological Survey Paper 2001-1, pp. 119–134.  
Ash, C.H., Panteleyev, A., MacLellan, K.L., Payne, C.W., and Rydman, M.O., 1999a. Geology of the Gibraltar Mine area (93B/6&9). British Columbia Ministry of Energy and Mines, British Columbia Geological Survey Open File 1999-7, 1:50,000 scale.  
Ash, C.H., Rydman, M.O., Payne, C.W., and Panteleyev, A., 1999b. Geological setting of the Gibraltar mine south central British Columbia (93B/8, 9). In: Exploration and Mining in British Columbia - 1998, Part B - Geological Descriptions of Selected Properties, British Columbia Ministry of Energy and Mines, pp. A1–A15.  
Ballard, J.R., Palin, J.M., and Campbell, I.H., 2002. Relative oxidation states of magmas inferred from Ce(IV)/Ce(III) in zircon: application to porphyry copper deposits of northern Chile. Contributions to Mineralogy and Petrology, 144, 347–364.  
Bath, A.B., Logan, J.M., and Kamenetsky, V.S., 2006. Apatite in Cu-sulfide ore from Mount Polley alkalic porphyry, BC Canada. Geochimica et Cosmochimica Acta, 70, A40.  
Belousova, E.A., Griffin, W.L., O'Reilly, S., and Fisher, N.I., 2002. Apatite as an indicator mineral for mineral exploration: trace element compositions and their relationship to host rock type. Journal of Geochemical Exploration, 76, 45–69.  
Berry, L.G., Mason, B., and Dietrich, R.V., 1983. Mineralogy. W.H. Freeman and Company, San Francisco, 561p.  
Bissig, T., Heberlein, D.R., and Dunn, C.E., 2013. Geochemical techniques for detection of blind porphyry copper-gold mineralization under basalt cover, Woodjam prospect, south-central British Columbia (NTS93A/03, /06). In: Summary of Activities 2012, Geoscience BC Report 2013-1, pp. 63–78.  
Bouzari, F., Hart, C.J.R., Barker, S., and Bissig, T., 2010. Porphyry indicator minerals (PIMs): exploration for concealed deposits in south central British Columbia (NTS 092I/06, 093A/12, 093N/01, /14). In: Summary of Activities 2009, Geoscience BC Report 2010-1, pp. 25–32.  
Bouzari, F., Hart, C.J.R., Barker, S., and Bissig, T., 2011a. Exploration for concealed deposits using porphyry indicator minerals (PIMs): Application of apatite texture and chemistry. In: 25th International Applied Geochemistry Symposium, Series B 92-1, Rovaniemi, Finland, Vuorimiesyhdistys-Finnish Association of Mining and Metallurgical Engineers, pp. 89–90.  
Bouzari, F., Hart, C.J.R., Barker, S., and Bissig, T., 2011b. Porphyry indicator minerals (PIMs): a new exploration tool for concealed deposits in south-central British Columbia. Geoscience BC Report 2011-17, 31p.  
Bouzari, F., Hart, C.J.R., and Bissig, T., 2015. Mineralogical characteristics of porphyry-fertile plutons: Guichon Creek, Takomkane, and Granite Mountain batholiths, south central British Columbia. In: Summary of Activities 2014, Geoscience BC Report 2015-1, pp. 63–68.  
Boyce, J.W. and Hervig, R.L., 2009. Apatite as a monitor of late-stage magmatic processes at Volcán Irazú, Costa Rica. Contributions to Mineralogy and Petrology, 157, 135–145.  
Boynton, W.V., 1984. Geochemistry of the rare earth elements:

- Meteorite studies. In: Henderson, P., (Ed.), *Rare Earth Element Geochemistry*, Elsevier, New York, pp. 63–114.
- Budzinski, H. and Tischendorf, G., 1989. Distribution of REE among minerals in the Hercynian postkinematic granites of Westergebirge-Vogtland, GDR. *Zeitschrift für Geologische Wissenschaften*, 17, 1019–1031.
- Byrne, K., Stock, E., Ryan, J., Johnson, C., Nisenson, J., Alva Jimenez, T., Lapointe, M., Stewart, H., Grubisa, G., and Syroka, S., 2013. Porphyry Cu-(Mo) deposits in the Highland Valley district, south-central British Columbia. In: Logan, J.M. and Schroeter, T.G., (Eds.), *Porphyry Systems of Central and Southern British Columbia: Tour of Central British Columbia Porphyry Deposits from Prince George to Princeton*. Society of Economic Geologists Field Trip Guidebook Series 43, pp. 99–116.
- Byssouth, G.D., Campbell, K.V., Barker, G.E., and Gagnier, G.K., 1995. Tonalite-trondhjemite fractionation of peraluminous magma and the formation of syntectonic porphyry copper mineralization, Gibraltar mine, central British Columbia. In: Schroeter, T.G., (Ed.), *Porphyry Deposits of the Northwestern Cordillera of North America*. Canadian Institute of Mining, Metallurgy and Petroleum Special Volume 46, pp. 201–213.
- Cao, M., Li, G., Qin, K., Seitmuratova, E.Y., and Liu, Y., 2012. Major and trace element characteristics of apatite in granitoids from central Kazakhstan: implications for petrogenesis and mineralization. *Resource Geology*, 62, 63–83.
- Carson, D.J.T. and Jambor, J.L., 1974. Mineralogy, zonal relationships and economic significance of hydrothermal alteration at porphyry copper deposits, Babine Lake area, British Columbia. *Canadian Institute of Mining and Metallurgy Bulletin*, 67, 110–133.
- Casselman, M.J., McMillan, W.J., and Newman, K.M., 1995. Highland Valley porphyry copper deposits near Kamloops, British Columbia: A review and update with emphasis on the Valley deposit. In: Schroeter, T.G., (Ed.), *Porphyry Deposits of the Northwestern Cordillera of North America*. Canadian Institute of Mining, Metallurgy and Petroleum Special Volume 46, pp. 161–191.
- Celis, M.A., Bouzari, F., Bissig, T., Hart, C.J.R., and Ferbey, T., 2014. Petrographic characteristics of porphyry indicator minerals from alkalic porphyry copper-gold deposits in south-central British Columbia (NTS 092, 093). In: *Summary of Activities 2013*, Geoscience BC Report 2014-1, pp. 53–62.
- Celis, M.A., Hart, C.J.R., Bouzari, F., Bissig, T., and Ferbey, T., 2013. Porphyry indicator minerals (PIMs) from alkalic porphyry copper-gold deposits in south-central British Columbia (NTS 092, 093). In: *Summary of Activities 2012*, Geoscience BC Report 2013-1, pp. 37–46.
- Clague, J.J., compiler, 1989. Chapter 1. Quaternary geology of the Canadian Cordillera. In: Fulton, R.J., (Ed.), *Quaternary Geology of Canada and Greenland*. Geological Survey of Canada, *Geology of Canada Series 1*, pp. 15–96.
- Colombini, L.L., Miller, C.F., Gualda, G.A.R., Wooden, J.L., and Miller, J.S., 2011. Sphene and zircon in the Highland Range volcanic sequence (Miocene, southern Nevada, USA): elemental partitioning, phase relations, and influence on evolution of silicic magma. In: Broska, I., Finger, F., and Harlov, D., (Eds.), *Accessory Minerals in Igneous and Metamorphic Rocks*. *Mineralogy and Petrology*, 102, pp. 29–50.
- Dawson, K.M., Panteleyev, A., Sutherland Brown, A., and Woodsworth, G.J., 1991. Regional metallogeny. In: Gabrielse, H. and Yorath, C.J., (Eds.), *Geology of the Cordilleran Orogen in Canada*. Geological Survey of Canada, *Geology of Canada Series 4*, pp. 709–768.
- del Real, I., Hart, C.J.R., Bouzari, F., Blackwell, J.L., Rainbow, A., and Sherlock, R., 2014. Relationships between calcalkalic and alkalic mineralization styles at the copper-molybdenum Southeast Zone and copper-gold Deerhorn porphyry deposits, Woodjam property, central British Columbia (NTS 093A). In: *Summary of Activities 2013*, Geoscience BC Report 2014-1, pp. 63–82.
- Drummond, A.D., Sutherland Brown, A., Young, R.J., and Tennant, S.J., 1976. Gibraltar - regional metamorphism, mineralization, hydrothermal alteration and structural development. In: Sutherland Brown, A., (Ed.), *Porphyry Deposits of the Canadian Cordillera*. Canadian Institute of Mining and Metallurgy Special Volume 15, pp. 195–205.
- Drummond, A.D., Tennant, S.J., and Young, R.J., 1973. The interrelationship of regional metamorphism, hydrothermal alteration and mineralization at the Gibraltar mines copper deposit in B.C. *Canadian Mining and Metallurgical Bulletin*, 66, 48–55.
- Duuring, P., Rowins, S.M., McKinley, B.S.M., Dickinson, J.M., Diakow, L.J., Young-Seog, K., and Creaser, R.A., 2009. Magmatic and structural controls on porphyry-style Cu-Au-Mo mineralization at Kemess South, Toodoggone District of British Columbia, Canada. *Mineralium Deposita*, 44, 435–462.
- Ferbey, T. and Plouffe, A., 2014. Lifting the burden of overburden in British Columbia: recent advances in till geochemical surveys. In: *Mineral Exploration Roundup 2014 Conference, Abstract Volume*, Association for Mineral Exploration British Columbia, Vancouver, B.C., pp. 26–28.
- Ferbey, T., Arnold, H., and Hickin, A.S., 2013. Ice-flow indicator compilation, British Columbia. British Columbia Ministry of Energy and Mines, British Columbia Geological Survey Open File 2013-06, 1:1,650,000 scale.
- Ferbey, T., Plouffe, A., and Anderson, R.G., 2014. An integrated approach to search for buried porphyry-style mineralization in central British Columbia using geochemistry and mineralogy: a TGI-4 project. In: *Current Research 2014-2*, Geological Survey of Canada, 12p.
- Flury, B., 1997. *A First Course in Multivariate Statistics*. Springer-Verlag, New York, 715p.
- Fraser, T.M., Stanley, C.R., Nikic, Z.T., Pesalj, R., and Gorc, D., 1995. The Mount Polley alkalic porphyry copper-gold deposit, south-central British Columbia. In: Schroeter, T.G., (Ed.), *Porphyry Deposits of the Northwestern Cordillera of North America*. Canadian Institute of Mining and Metallurgy Special Volume 46, pp. 609–622.
- Harada, K., Nagashima, K., Nakao, K., and Kato, A., 1971. Hydroxyllellestadite, a new apatite from Chichibu Mine, Saitama prefecture, Japan. *American Mineralogist*, 56, 1507–1518.
- Harlov, D.E., 2015. Apatite: a fingerprint for metasomatic processes. *Elements*, 11, 171–176.
- Hashmi, S., Ward, B.C., Plouffe, A., Ferbey, T., and Leybourne, M.I., 2014. Geochemical and mineralogical dispersal in till from the Mount Polley Cu-Au porphyry deposit, central British Columbia, Canada. Geological Survey of Canada Open File 7589, poster.
- Hashmi, S., Ward, B.C., Plouffe, A., Leybourne, M.I., and Ferbey, T., 2015. Geochemical and mineralogical dispersal in till from the Mount Polley Cu-Au porphyry deposit, central British Columbia, Canada. *Geochemistry: Exploration, Environment, Analysis*, 15, 234–249.
- Hodgson, C.J., Balles, R.J. and Verzosa, R.S., 1976. Cariboo-Bell. In: Sutherland Brown, A., (Ed.), *Porphyry Deposits of the Canadian Cordillera*. Canadian Institute of Mining and Metallurgy Special Volume 15, pp. 388–396.
- Holland, S.S., 1976. Landforms of British Columbia, a physiographic outline. *British Columbia Department of Mines and Petroleum Resources Bulletin* 48, 138p.
- Hughes, J.M. and Rakovan, J.F., 2015. Structurally robust, chemically diverse: apatite and apatite supergroup minerals. *Elements*, 11, 165–170.
- Jochum, K.P., Weis, U., Stoll, B., Kuzmin, D., Yang, Q., Raczek, I., Jacob, D.E., Stracke, A., Birbaum, K., Frick, D.A., Günther, D., and Enzweiler, J., 2011. Determination of reference values for NIST SRM 610–617 glasses following ISO guidelines.

- Geostandards and Geoanalytical Research, 35, 397–429.
- Kelley, K.D., Eppinger, R.G., Lang, J., Smith, S.M., and Fey, D.L., 2011. Porphyry Cu indicator minerals in till as an exploration tool: example from the giant Pebble porphyry Cu-Au-Mo deposit, Alaska, USA. *Geochemistry: Exploration, Environment, Analysis*, 11, 321–334.
- Kreidler, E.R. and Hummel, F.A., 1970. The crystal chemistry of apatite: structure fields of fluor- and chlorapatite. *American Mineralogist*, 55, 170–184.
- Kusebauch, C., John, T., Whitehouse, M.J., Klemme, S., and Putnis, A., 2015. Distribution of halogens between fluid and apatite during fluid-mediated replacement processes. *Geochimica et Cosmochimica Acta*, 170, 225–246.
- Kutoglu, A., von, 1974. Structure refinement of the apatite  $\text{Ca}_5(\text{VO}_4)_3(\text{OH})$ . *Neues Jahrbuch für Mineralogie – Monatshefte*, 5, 210–218.
- Lang, J.R., Stanley, C.R., and Thompson, J.F.H., 1995. Porphyry copper-gold deposits related to alkalic igneous rocks in the Triassic-Jurassic arc terranes of British Columbia. In: Wahl Pierce, F., and Bolm, J.G., (Eds.), *Porphyry Copper Deposits of the American Cordillera*, Arizona Geological Society, Digest 20, p. 219–236.
- Liaghat, S. and Tosdal, R., 2008. Apatite chemical composition and textures as a probe into magmatic conditions at Galore Creek porphyry copper-gold deposit, British Columbia. *Geochimica et Cosmochimica Acta*, 72, A550.
- Lodders, K., 2010. Solar system abundances of the elements: Principles and Perspectives in Cosmochemistry. In: *Astrophysics and Space Science Proceedings*, Springer-Verlag, Berlin, Heidelberg, pp. 379–417.
- Logan, J.M., 2013. Porphyry systems of central and southern BC: Overview and field trip road log. In: Logan, J.M. and Schroeter, T.G., (Eds.), *Porphyry Systems of Central and Southern British Columbia: Tour of central British Columbia Porphyry Deposits from Prince George to Princeton*. Society of Economic Geologists Field Trip Guidebook Series 43, pp. 1–45.
- Logan, J.M., Bath, A.B., Mihalynuk, M.G., and Rees, C.J., 2007a. Regional geology of the Mount Polley area, central British Columbia. British Columbia Ministry of Energy and Mines, British Columbia Geological Survey Geoscience Map 2007-1, 1:50,000 scale.
- Logan, J.M., Mihalynuk, M.G., Ullrich, T., and Friedman, R.M., 2007b. U-Pb ages of intrusive rocks and  $^{40}\text{Ar}/^{39}\text{Ar}$  plateau ages of copper-gold-silver mineralization associated with alkaline intrusive centres at Mount Polley and the Iron Mask batholith, southern and central British Columbia. In: *Geological Fieldwork 2006*, British Columbia Ministry of Energy, Mines and Petroleum Resources, British Columbia Geological Survey Paper 2007-1, pp. 93–116.
- Logan, J.M., Schiarizza, P., Struik, L.C., Barnett, C., Nelson, J.L., Kowalczyk, P., Ferri, F., Mihalynuk, M.G., Thomas, M.D., Gammon, P., Lett, R., Jackaman, W., and Ferbey, T., compilers, 2010. Bedrock geology of the QUEST map area, central British Columbia. Geoscience BC Report 2010-5, British Columbia Ministry of Forests, Mines and Lands, British Columbia Geological Survey Geoscience Map 2010-1, Geological Survey of Canada Open File 6476, 1:500,000 scale.
- Mao, M., Rukhlov, A.S., Rowins, S.M., Spence, J., and Coogan, L.A., 2015. Detrital apatite trace-element compositions: a robust new tool for mineral exploration. British Columbia Ministry of Energy and Mines, British Columbia Geological Survey GeoFile 2015-9 (poster).
- Marshall, O.J., 1988. Cathodoluminescence of Geological Materials. Unwin Hyman, Boston, 146p.
- Massey, N.W.D., MacIntyre, D.G., Desjardins, P.J., and Cooney, R.T., 2005. Geology of British Columbia. British Columbia Ministry of Energy, Mines and Petroleum Resources, British Columbia Geological Survey Geoscience Map 2005-3, 1:1,000,000 scale.
- McMillan, W.J., 1985. Geology and ore deposits of the Highland Valley camp. Geological Association of Canada, Mineral Deposits Division, Field Guide and Reference Manual Series 1, 121p.
- McMillan, W.J., 2005. Porphyry Cu-Mo deposits of the Highland Valley district, Guichon Creek batholith, British Columbia, Canada. In: Porter, T.M. (Ed.), *Super Porphyry Copper & Gold Deposits: A Global Perspective*, PGC Publishing, Adelaide, 1, p. 259–274.
- McMillan, W.J., Anderson, R.G., Chan, R., and Chow, W., 2009. Geology and mineral occurrences (Minfile), Guichon Creek Batholith and Highland Valley porphyry copper district, British Columbia. Geological Survey of Canada Open File 6079, 2 sheets, 1:100,000 and 1:150,000 scale.
- Miles, A.J., Graham, C.M., Hawkesworth, C.J., Gillespie, M.R., Hinton, R.W., Bromiley, G.D., and EMMAC, 2014. Apatite: a new redox proxy for silicic magmas? *Geochimica et Cosmochimica Acta*, 132, 101–119.
- Nelson, J.L., Colpron, M., Israel, S., 2013. The Cordillera of British Columbia, Yukon and Alaska: tectonics and metallogeny. In: Colpron, M., Bissig, T., Rusk, B.G., and Thompson, F.H., (Eds.), *Tectonics, Metallogeny, and Discovery: The North American Cordillera and Similar Accretionary Settings*. Society of Economic Geologists, Inc. Special Publication 17, pp. 53–109.
- Normandeau, P.X., Corriveau, L., Paquette, J., and McMartin, I., 2014. Apatite as an indicator mineral to IOCG deposits in the Great Bear magmatic zone, Northwest Territories, Canada. In: 42nd Annual Yellowknife Geoscience Forum, Yellowknife, November 25–27, 2014. Northwest Territories Geoscience Office, Yellowknife Geoscience Forum Abstracts 2014, p. 53–54.
- Pan, Y. and Fleet, M.E., 2002. Compositions of the apatite-group minerals: substitutions mechanisms and controlling factors. *Reviews in Mineralogy and Geochemistry*, 48, 13–49.
- Pass, H.E., 2010. Breccia-hosted chemical and mineralogical zonation patterns of the Northeast Zone, Mt. Polley Cu-Ag-Au alkalic porphyry deposit, British Columbia, Canada. Unpublished Ph.D. thesis, The University of Tasmania, Hobart, Tasmania, Australia, 276p.
- Patiño Douce, A.E., Roden, M.F., Chaumba, J., Fleisher, C., and Yogodzinski, G., 2011. Compositional variability of terrestrial mantle apatites, thermodynamic modeling of apatite volatile contents, and the halogen and water budgets of planetary mantles. *Chemical Geology*, 288, 14–31.
- Peng, G., Luhr, J.F., and McGee, J.J., 1997. Factors controlling sulfur concentrations in volcanic apatite. *American Mineralogist*, 82, 1210–1224.
- Piccoli, P.M. and Candela, P.A., 2002. Apatite in igneous systems. *Reviews in Mineralogy and Geochemistry*, 48, 255–292.
- Plouffe, A., 2000. Quaternary geology of the Fort Fraser and Manson River map areas, central British Columbia. Geological Survey of Canada Bulletin 554, 62p.
- Plouffe, A. and Ferbey, T., 2015a. Discovering buried copper porphyry mineralization: geochemistry and indicator minerals in till. Geological Survey of Canada Open File 7680, 45p.
- Plouffe, A. and Ferbey, T., 2015b. Surficial geology, Gnawed Mountain area, British Columbia, parts of NTS 921/6, 1/7, 1/10 and 1/11. Geological Survey of Canada Canadian Geoscience Map 214 (preliminary), British Columbia Geological Survey Geoscience Map 2015-3, 1:50,000 scale.
- Plouffe, A. and Ferbey, T., 2015c. Surficial geology, Granite Mountain area, British Columbia, parts of NTS 93-B/8 and 93-B/9. Geological Survey of Canada Canadian Geoscience Map 223 (preliminary), British Columbia Geological Survey Geoscience Map 2015-4, 1:50,000 scale.
- Plouffe, A. and Ferbey, T., 2015d. Till composition near Cu-porphyry deposits in British Columbia: Highlights for mineral exploration. In: Rogers, N., (Ed.), *TGI 4 - Intrusion Related Mineralisation*

- Project: New Vectors to Buried Porphyry-Style Mineralisation. Geological Survey of Canada Open File 7843, pp. 15–37.
- Plouffe, A., Anderson, R.G., and Dunn, C.E., 2011. Till composition and biogeochemistry near a porphyry Cu-Mo deposit: Gibraltar Mine, British Columbia. Geological Survey of Canada Open File 6755, 25p.
- Plouffe, A., Bednarski, J.M., Huscroft, C.A., Anderson, R.G., and McCuaig, S.J., 2011c. Late Wisconsinan glacial history in the Bonaparte Lake map area, south central British Columbia: implications for glacial transport and mineral exploration. *Canadian Journal of Earth Sciences*, 48, 1091–1111.
- Plouffe, A., Ferbey, T., and Anderson, R.G., 2014. Till composition and ice-flow history in the region of the Gibraltar Mine: developing indicators for the search of buried mineralization. Geological Survey of Canada Open File 7592, poster.
- Plouffe, A., Ferbey, T., Anderson, R.G., Hashmi, S., and Ward, B.C., 2013a. New TGI-4 till geochemistry and mineralogy results near the Highland Valley, Gibraltar, and Mount Polley mines, and Woodjam District: An aid to search for buried porphyry deposits. Geological Survey of Canada Open File 7473, 58p.
- Plouffe, A., Ferbey, T., Anderson, R.G., Hashmi, S., Ward, B.C., and Sacco, D.A., 2013b. The use of till geochemistry and mineralogy to explore for buried porphyry deposits in the Cordillera - preliminary results from a TGI-4 intrusion-related ore systems project. Geological Survey of Canada Open File 7367, poster.
- Plouffe, A., Ferbey, T., Levson, V.M., and Bond, J.D., 2012. Glacial history and drift prospecting in the Canadian Cordillera: recent developments. Geological Survey of Canada Open File 7261, 51p.
- Plouffe, A., McClenaghan, M.B., Paulen, R.C., McMartin, I., Campbell, J.E., and Spirito, W.A., 2013c. Processing of glacial sediments for the recovery of indicator minerals: protocols used at the Geological Survey of Canada. *Geochemistry: Exploration, Environment, Analysis*, 13, 303–316.
- Pouchou, J.L. and Pichoir, F., 1985. “PAP”  $\Phi(\rho Z)$  procedure for improved quantitative microanalysis. In: Armstrong, J.T., (Ed.), *Microbeam Analysis*. San Francisco Press, San Francisco, USA, pp. 104–106.
- Prowatke, S. and Klemme, S., 2006. Trace element partitioning between apatite and silicate melts. *Geochimica et Cosmochimica Acta*, 70, 4513–4527.
- Raudsepp, M., 1995. Recent advances in the electron-probe microanalysis of minerals for the light elements. *The Canadian Mineralogist*, 33, 203–218.
- Rees, C., 2013. The Mount Polley Cu-Au deposit, south-central British Columbia, Canada. In: Logan, J.M. and Schroeter, T.G., (Eds.), *Porphyry Systems of Central and Southern British Columbia: Tour of Central British Columbia Porphyry Deposits from Prince George to Princeton*. Society of Economic Geologists Field Trip Guidebook Series 43, pp. 67–98.
- Rees, C., Riedell, K.B., Proffett, J.M., MacPherson, J., and Robertson, S., 2015. The Red Chris copper-gold deposit, northern British Columbia, Canada: Igneous phases, alteration, and controls of mineralization. *Economic Geology*, 110, 857–888.
- Roeder, P.L., MacArthur, D., Ma, X.-P., Palmer, G.R., and Mariano, A.N., 1987. Cathodoluminescence and microprobe study of rare-earth elements in apatite. *American Mineralogist*, 72, 801–811.
- Roegge, J.S., Logsdon, M.J., Young, H.S., Barr, H.B., Borcsik, M., and Holland, H.D., 1974. Halogens in apatite from the Providencia area, Mexico. *Economic Geology*, 69, 229–240.
- Rønso, J.G., 1989. Coupled substitution involving REEs and Na and Si in apatite in alkaline rocks from the Ilímaussaq intrusion, South Greenland, and the petrological implications. *American Mineralogist*, 74, 896–901.
- Rotherham, D.C., Drummond, A.D., and Tennant, S.J., 1972. Exploration of Gibraltar. *Western Miner*, 45, 25–28.
- Rukhlov, A.S., Plouffe, A., Ferbey, T., Mao, M., and Spence, J., 2016. Supplementary data for application of trace-element compositions of detrital apatite to explore for porphyry deposits in central British Columbia. British Columbia Ministry of Energy and Mines, British Columbia Geological Survey GeoFile 2016-1.
- Schiarizza, P., 2014. Geological setting of the Granite Mountain batholith, host to the Gibraltar porphyry Cu-Mo deposit, south-central British Columbia. In: *Geological Fieldwork 2013*, British Columbia Ministry of Energy and Mines, British Columbia Geological Survey Paper 2014-1, pp. 95–110.
- Schiarizza, P., 2015. Geological setting of the Granite Mountain batholith, south-central British Columbia. In: *Geological Fieldwork 2014*, British Columbia Ministry of Energy and Mines, British Columbia Geological Survey Paper 2015-1, pp. 19–39.
- Schiarizza, P., Bell, K., and Bayliss, S., 2009a. Geology and mineral occurrences of the Murphy Lake area, south-central British Columbia (NTS 093A/03). In: *Geological Fieldwork 2008*, British Columbia Ministry of Energy, Mines and Petroleum Resources, British Columbia Geological Survey Paper 2009-1, pp. 169–187.
- Schiarizza, P., Bell, K., and Bayliss, S., 2009b. Geology of the Murphy Lake area, NTS 93A/03. British Columbia Ministry of Energy, Mines and Petroleum Resources, British Columbia Geological Survey Open File 2009-03, 1:50,000 scale.
- Schroeter, T.G., 2009. Woodjam copper-molybdenum-gold porphyry project: the exciting South East Zone discovery and beyond. In: *Mineral Exploration Roundup 2009 Conference*, Abstract volume, Association for Mineral Exploration British Columbia, Vancouver, B.C., pp. 37–38.
- Schroeter, T.G., editor, 1995. *Porphyry deposits of the northwestern Cordillera of North America*. Canadian Institute of Mining, Metallurgy and Petroleum Special Volume 46, 888p.
- Sha, L.-K. and Chappell, B.W., 1999. Apatite chemical composition, determined by electron microprobe and laser-ablation inductively coupled plasma mass spectrometry, as a probe into granite petrogenesis. *Geochimica et Cosmochimica Acta*, 63, 3861–3881.
- Sherlock, R. and Trueman, A., 2013. NI 43-101 technical report for 2012 activities on the Woodjam South property. Gold Fields Horsefly Exploration Group and Consolidated Woodjam Copper Corporation, Cariboo Mining Division, British Columbia, 158p.
- Sherlock, R., Blackwell, J., and Skinner, T., 2013. NI 43-101 technical report for 2012 activities on the Woodjam North property. Gold Fields Horsefly Exploration Group and Consolidated Woodjam Copper Corporation, Cariboo Mining Division, British Columbia, 275p.
- Smythe, D.J. and Brenan, J.M., 2015. Cerium oxidation state in silicate melts: Combined  $fO_2$ , temperature and compositional effects. *Geochimica et Cosmochimica Acta*, 170, 173–187.
- Stormer, J.C., Jr., Pierson, M.L., and Tacker, R.C., 1993. Variation of F and Cl X-ray intensity due to anisotropic diffusion in apatite during electron microprobe analysis. *American Mineralogist*, 78, 641–648.
- Sutherland Brown, A.E., 1974. Gibraltar Mine (93B-12, 13). In: *Geology, Exploration and Mining in British Columbia 1973*, British Columbia Ministry of Mines and Petroleum Resources, pp. 299–318.
- Sutherland Brown, A.E., editor, 1976. *Porphyry deposits of the Canadian Cordillera*. Canadian Institute of Mining and Metallurgy Special Volume 15, 510p.
- Tepper, J.H. and Kuehner, S.M., 1999. Complex zoning in apatite from the Idaho batholith: a record of magma mixing and intracrystalline trace element diffusion. *American Mineralogist*, 84, 581–595.
- Thomson, S.N., Gehrels, G.E., Ruiz, J., and Buchwaldt, R., 2012. Routine low-damage apatite U-Pb dating using laser ablation-multicollector-ICPMS. *Geochemistry, Geophysics, Geosystems*, 13, doi:10.1029/2011GC003928.
- Tipper, H.W., 1971a. Glacial geomorphology and Pleistocene history of central British Columbia. *Geological Survey of Canada Bulletin* 196, 89p.

- Tipper, H.W., 1971b. Multiple glaciations in central British Columbia. *Canadian Journal of Earth Sciences*, 8, 743–752.
- Tollari, N., Barnes, S.-J., Cox, R.A., and Nabil, H., 2008. Trace element concentrations in apatite from the Sept-Îles Intrusive Suite, Canada — Implications for the genesis of nelsonites. *Chemical Geology*, 252, 180–190.
- Vandekerkhove, S., Rowins, S.M., and Johnston, S.T., 2014. Geology and physicochemical conditions of copper-gold mineralization at the Three Firs porphyry prospect, Woodjam district, south-central British Columbia. In: *Geological Fieldwork 2013*, British Columbia Ministry of Energy and Mines, British Columbia Geological Survey Paper 2014-1, pp. 67-94.
- van Straaten, B.I., Oliver, J., Crozier, J., and Goodhue, L., 2013. A summary of the Gibraltar porphyry copper-molybdenum deposit, south-central British Columbia, Canada. In: Logan, J.M. and Schroeter, T.G., (Eds.), *Porphyry Systems of Central and Southern British Columbia: Tour of Central British Columbia Porphyry Deposits from Prince George to Princeton*. Society of Economic Geologists Field Trip Guidebook Series 43, pp. 55–66.
- Ward, B., Maynard, D., Geertsema, M., and Rabb, T., 2009. Iceflow history, drift thickness and drift prospecting for a portion of the QUEST Project area, central British Columbia (NTS 093G, H[west half], J). In: *Summary of Activities 2008*, Geoscience BC Report 2009-1, pp. 25-32.
- Webster, J.D., 1990. Partitioning of F between H<sub>2</sub>O and CO<sub>2</sub> fluids and topaz rhyolite melt: Implications for mineralizing hydrothermal fluids in F-rich granitic systems. *Contributions to Mineralogy and Petrology*, 104, 424–438.
- Webster, J.D. and Piccoli, P.M., 2015. Magmatic apatite: a powerful, yet deceptive, mineral. *Elements*, 11, 177–182.
- Williams, S.A. and Cesbron, F.P., 1977. Rutile and apatite: useful prospecting guides for porphyry copper deposits. *Mineralogical Magazine*, 41, 288–292.
- Young, E.J., Myers, A.T., Munson, E.L., and Conklin, N.M., 1969. Mineralogy and geochemistry of fluorapatite from Cerro de Mercado, Durango, Mexico. In: *US Geological Survey Paper 650D*, pp. 84–93.

